3.3.0 Task 4. Catalyst Testing

3.3.1 Deactivation of Iron-based Catalysts for Slurry-Phase Fischer-Tropsch Synthesis

ABSTRACT

Deactivation rates and aged catalyst properties have been investigated as a function of time on stream for iron-based Fischer-Tropsch catalysts in the presence/absence of potassium and/or silicon. There is a synergism in activity maintenance with the addition of both potassium and silicon to an iron catalyst. The addition of silicon appears to stabilize the surface area of the catalyst. Catalysts containing only iron or added silicon with or without potassium consist mainly of iron oxide at the end of the run. However, iron carbides are the dominant phase of the iron catalyst with added potassium alone. Catalyst surface areas increase slightly during synthesis. The bulk phase of the catalyst does not correlate to the catalyst activity. The partial pressure of water in the reactor is lower for potassium-containing catalysts and is not a reliable predictor of catalyst deactivation rate.

INTRODUCTION

The Fischer-Tropsch Synthesis (FTS) converts synthesis gas (a mixture of CO and H_2) to hydrocarbons. Iron-based catalysts lose activity with time on stream (TOS). The rate of deactivation is dependent on the presence/absence of promoters such as potassium and/or binders such as silica [1,2]. Several possible causes of catalyst deactivation have been postulated [3]: (i) Sintering, (ii) Carbon deposition, and, (iii) Phase transformations. With respect to phase transformations, there is considerable disagreement whether the active phase for the FTS is iron oxide or carbide [4,5]. In

addition, certain reactor conditions, such as a high partial pressure of water, are known to cause a decline in activity [6].

There were two major objectives of this study. Firstly, the effects of the addition of potassium and/or silicon on catalyst deactivation rates and changes in catalyst properties with TOS were investigated. Secondly, the possible causes of catalyst deactivation were examined by following aged catalyst properties and reactor conditions as a function of TOS for each catalyst. The FTS was carried out in a continuous-flow stirred slurry reactor to ensure uniformity in catalyst aging and reactor conditions throughout the reactor. The aged catalyst properties examined as a function of TOS were total surface areas, carbon deposits and phase transformations.

EXPERIMENTAL

Four precipitated iron-based catalysts were used. The first catalyst consisted of only iron. The other catalysts contained either added potassium, added silicon or both. The catalysts were designated in terms of the atomic ratios as: 100Fe, 100Fe/3.6Si, 100Fe/0.71K and 100Fe/3.6Si/0.71K. The catalysts were prepared by continuous precipitation from iron (III) nitrate and concentrated ammonium hydroxide. For silica-containing catalysts, a colloidal suspension of tetraethyl ortho silicate was mixed with the iron nitrate solution prior to precipitation. Potassium was added to the catalysts in the form of potassium tertiary butoxide during the loading of the FTS reactor.

The FTS was carried out in a 1 liter continuous flow stirred tank slurry reactor. The vapor phase products exiting the reactor passed through two traps in series. The first trap was maintained at 100^{o}C while the second was maintained at 0^{o}C. The second trap served to condense almost all of the water present in the product stream. Further

details of the reaction system and product analysis (both on- and off-line) have been reported previously [7]. A known amount (~ 70 g) of the catalyst was charged to the reactor along with 300 g of a hydrocarbon oil supplied by Ethyl Corp. (carbon number range of about C_{25} - C_{30}). The catalyst was pretreated with a continuous flow of CO at 2.0 NL/hr-gFe at 270^{o}C, 175 psig for 24 hours. Subsequently, the FTS was carried out at 270^{o}C, 175 psig with a synthesis gas having an H_2/CO ratio of 0.7 at a flowrate of 3.4 NL/hr-gFe. Both during pretreatment and synthesis, small amounts of catalysts (0.1 to 0.2 g per sample) were removed from the reactor at various TOS. The aged catalyst samples were Soxhlet-extracted with xylene prior to analysis. These aged catalyst samples were examined to determine BET surface areas, elemental carbon and hydrogen contents and bulk catalytic phases.

Elemental carbon and hydrogen contents were determined using a Leco CHN analyzer wherein the catalyst sample was placed in a furnace at 1350^{o}C under flowing oxygen. All of the carbon and hydrogen in the sample was converted to CO_2 and water repectively which were then measured. Bulk catalyst phases were determined by two methods: X-ray diffraction (XRD) and Mossbauer spectroscopy (MS). X-ray diffraction patterns were obtained using a Phillips APD X-ray diffraction spectrometer equipped with a Cu anode and a Ni filter operated at 40 kV and 20 mA (CuKa=1.5418 Å).Mossbauer spectra of the catalyst samples were obtained with a constant acceleration spectrometer using a radioactive source consisting of 50 to 100 mCi of ^{57}Co in a Pd matrix.

RESULTS AND DISCUSSION

The conversion of synthesis gas is a measure of the FTS activity of a catalyst. The catalysts studied show varying rates of decline in synthesis gas conversion with TOS (Figure 1). Note that the conversions for different catalysts are compared at the same synthesis gas space velocity which is defined as normal liters of synthesis gas per gram of iron in the reactor. The addition of silica alone (100Fe/3.6Si) slows the decline in FTS activity as compared to a catalyst containing only iron (100Fe). In contrast, the addition of potassium alone increases the deactivation rate as compared to a catalyst containing only iron (100Fe). The catalyst containing both silica and potassium (100Fe/3.6Si/0.71K) exhibits the lowest deactivation rate. Hence, there is a synergism in the maintenance of FTS activity with the addition of both silica and potassium.

The surface areas of the catalysts are substantially decreased during pretreatment (Figure 2). During synthesis, however, the surface area of the catalysts increases slightly. It is postulated that this slight increase may be due to the deposition of porous carbon on the catalyst surface. Catalysts containing silica exhibit higher surface areas on preparation, and during pretreatment and synthesis. Hence, silica appears to stabilize the surface area of the catalysts. Since the total surface area increases during synthesis, the presence/absence of sintering during FTS cannot be deduced from BET surface area measurements.

The catalyst sample is exposed to air for a short time during XRD and MS. However, using similar procedures Mossbauer spectra have been previously obtained showing 97% of the iron in a catalyst as iron carbide and substantial (36%) amounts of

metallic iron in another catalyst [8]. Hence, re-oxidation of catalyst phases during XRD and MS is negligible. The results from XRD indicate the following events occurring during pretreatment and synthesis: The catalyst as charged into the reactor is in the form of an oxide and/or an oxyhydroxide. During pretreatment in CO, the catalyst is rapidly converted to Fe_3O_4 which is subsequently partially converted in a slow step to a mixture of carbides (Fe_5C_2 and $Fe_{2.2}C$) as shown in Figure 3. During synthesis, the relative amounts of carbide and oxide change dependent on the catalyst composition. For the catalyst containing only potassium, the catalyst at the end of the run consists of mainly carbides (Figure 3) while for the other catalysts the oxide is the dominant phase at the end of the run (example of 100Fe given in Figure 3). These qualitative observations are consistent with quantitative results obtained by MS. Since the catalyst containing potassium alone has the highest deactivation rate, it is tempting to conclude that the iron oxide is the active phase, or at least more active than the carbide, for the FTS. However this is not true as the bulk composition of the catalyst, as shown below, does not correlate to the catalyst activity. Figure 4 shows quantitative results of the bulk composition of the catalyst obtained by MS as a function of TOS for the catalyst with the lowest deactivation rate (100Fe/3.6Si/0.71K). The results are similar to those for the catalyst containing only iron but are different from those obtained for the catalyst containing iron and potassium but no silicon. The bulk composition of the catalyst changes greatly with TOS. At small TOS, iron carbide is the dominant phase while at long TOS the catalyst consists predominantly (80%) of iron oxide. Note, however, that synthesis gas conversion for this catalyst varied only slightly (between 80 and 90%)

with TOS. Hence, the particular active phase of the catalyst (oxide or carbide) cannot be deduced from bulk catalyst compositions.

The carbon measured as a result of high temperature oxidation can be due to either CH_x species on the catalyst surface, or the oxidation of iron carbides, or the oxidation of carbon deposits. The contribution of CH_x species can be estimated by elemental analysis of hydrogen and assuming the value of x to be 2. The remaining carbon measured on the catalysts (Figure 5) ranged from 10 to 30 wt.%. Note that if all the iron in the catalyst were converted to carbide the carbon amount would be 8 to 9 wt.% assuming the iron carbides are Fe_5C_2 and $Fe_{2.2}C$ as shown by XRD and MS. Hence, substantial amounts of carbon deposits were present on the catalyst surface. The addition of potassium to the catalyst containing only iron (100Fe/0.71K) increased the amount of carbon measured as well as its rate of increase. However, this may have been due to the high amount of carbide formed on this catalyst during synthesis as shown by XRD and MS. The catalyst with the lowest deactivation rate (100Fe/3.6Si/0.71K) contained substantial amounts of carbon at the end of the run even though its activity was quite stable. Recall that this catalyst consisted mainly of iron oxide so that the carbon measured consisted mainly of carbon deposits. Hence, the amount of carbon deposits on the catalysts does not correlate with the rate of deactivation.

As stated previously, almost all of the water present in the product stream is condensed in a trap downstream of the reactor maintained at 0^oC. It is further assumed that the uncondensed gases leaving the trap are saturated with water. The partial pressure of water is then calculated by measuring the total flow rate of the

uncondensed gases and the composition of the other products and unconverted reactants. This procedure yields oxygen component balances of greater than 96%. The value of the partial pressure of water in the reactor depends on the presence/absence of potassium promoter (Figure 6). The partial pressure of water is low for catalysts containing potassium and decreases slightly with TOS. In contrast, the partial pressure of water is higher for catalysts without potassium and increases with TOS. Low water partial pressures for potassium-containing catalysts may be due to the higher rates of the water gas shift (WGS) reaction observed over these catalysts. A high partial pressure of water is known to deactivate the catalyst [6]. However, the results shown in Figure 6 indicate that the value of the partial pressure of water does not correlate to the rate of catalyst deactivation. For instance, both the catalyst with the highest and lowest deactivation rates (100Fe/0.71K and 100Fe/3.6Si/0.71K respectively) exhibit similar partial pressures of water.

It has been postulated that changes in the amount of iron oxide on the catalyst surface (as opposed to the bulk followed by XRD and MS) can be followed by a comparison of the ratios of the rates of the FTS to that of the WGS with TOS [9]. It is postulated [9] that iron oxide is more active than iron carbides for the WGS than for the FTS and hence, a decrease in the ratio of the rate of the FTS to the rate of the WGS indicates an increase in the amount of iron oxide on the catalyst surface. However, none of the catalysts examined in this study show a decline in the reaction rate ratio with TOS (Figure 7). For catalysts containing potassium, the reaction rate ratio changes negligibly with TOS, while the reaction rate ratio actually increases with TOS for the catalysts without potassium. Further, the increase in the reaction rate ratio with

TOS for catalysts without potassium may not be due to changes in surface phases. We have earlier shown [10] during kinetic studies that the ratio of the reaction rate of the FTS to that of the WGS increases with residence time (not TOS) or synthesis gas conversion for iron-based catalysts. Hence, the increase in the reaction rate ratio observed for two of the catalysts studied may be a consequence of decreasing synthesis gas conversion (due to deactivation) rather than a change in surface catalyst phases.

CONCLUSION

Increasing and decreasing deactivation rates of iron FTS catalysts are observed upon the addition of potassium and/or silicon respectively. There is a synergism in the maintenance of activity with the addition of both potassium and silicon leading to a low deactivation rate.

Changes in catalyst properties and reactor conditions with TOS depend upon the presence/absence of potassium and silicon. The addition of silicon appears to stabilize the surface area of the catalyst both on preparation and during pretreatment and synthesis. At the end of pretreatment, all of the catalysts studied consist of a mixture of iron oxide (Fe_3O_4) and iron carbides (Fe_5C_2 and $Fe_{2.2}C$). During synthesis, the catalyst containing potassium alone is converted predominantly to iron carbides at the end of the run. The other catalysts, however, decline in the amount of iron carbide and increase in the amount of iron oxide during synthesis. The addition of potassium alone to an iron catalyst substantially increases the amount of carbon (from carbon deposits and carbides) measured by high temperature oxidation of aged catalyst

samples. The partial pressure of water in the reactor is low and decreases with TOS for potassium-containing catalysts while it is higher and increases with TOS for the catalysts without potassium.

Possible causes of catalyst deactivation have been investigated in this study. The surface areas of aged catalyst samples increase with TOS during synthesis possibly due to porous carbon deposits. Hence, information from total surface area on sintering as a possible mechanism of deactivation is inconclusive. Measurement of the amount of carbon deposits on the catalysts by high temperature oxidation is complicated due to the contribution from iron carbides. The bulk composition of the catalyst having the lowest deactivation rate changes greatly during synthesis whereas the synthesis gas conversion changes negligibly. This implies that the catalyst bulk composition does not correlate to the rate of activity decline. The value of the partial of water as well as its variation with TOS are similar for the catalysts with the highest and lowest deactivation rates. Hence, water partial pressure is not a reliable predictor of the catalyst deactivation rate.

REFERENCES

1. D.B. Bukur, D. Mukesh and S.A. Patel, Ind. Eng. Chem. Res., 29, 194 (1990).
2. D.B. Bukur, X. Lang, D. Mukesh, W.H. Zimmerman, M.P. Rosynek and C. Li, Ind. Eng. Chem. Res., 29, 1588 (1990).
3. M.E. Dry, in J.R. Anderson and M. Boudart (Eds.), Catalysis-Science and Technology, Vol. 1, 159-255, Springer, Berlin (1981).
4. J.P. Reymond, P. Meriaudeau and S.J. Teichner, J. Catal., 75, 39 (1982).
5. G.B. Raupp and W.N. Delgass, J. Catal., 58, 361 (1979).
6. C.N. Satterfield, R.T. Hanlon, S.E. Tung, Z. Zou, G.C. Papaefthymiou, Ind. Eng. Chem. Prod. Res. Dev., 25, 407 (1986).
7. L. Xu, S. Bao, R.J. O'Brien, D.J. Houpt and B.H. Davis, Fuel Sci. Tech. Int., 12, 1323 (1994).
8. C.-S. Huang, B. Ganguly, G.P. Huffman, F.E. Huggins and B.H. Davis, Fuel Sci. Tech. Int., 11, 1289 (1993).
9. B. Jager and R. Espinoza, Catalysis Today, 23, 17 (1995).
10. A.P. Raje and B.H. Davis, Catalysis Today, (accepted for publication).

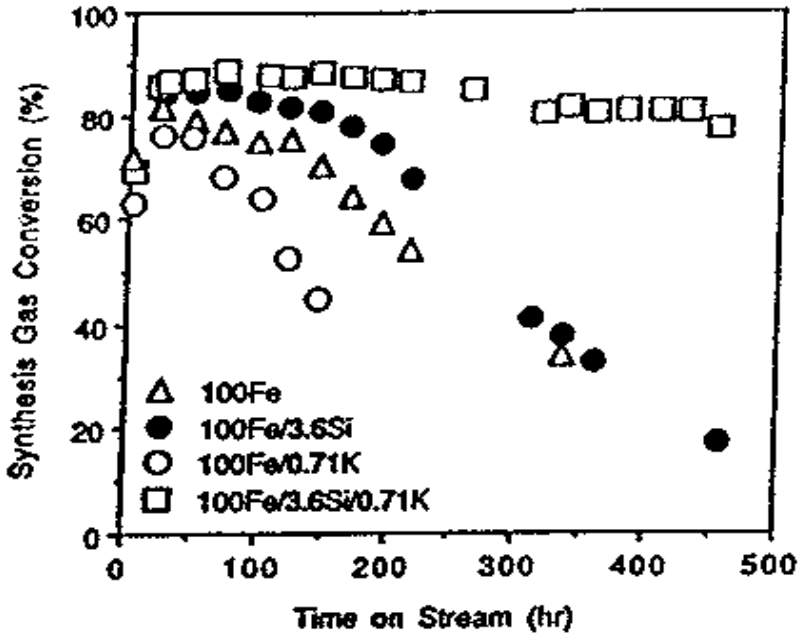

Figure 1. Synthesis gas conversion as a function of time-on-stream.

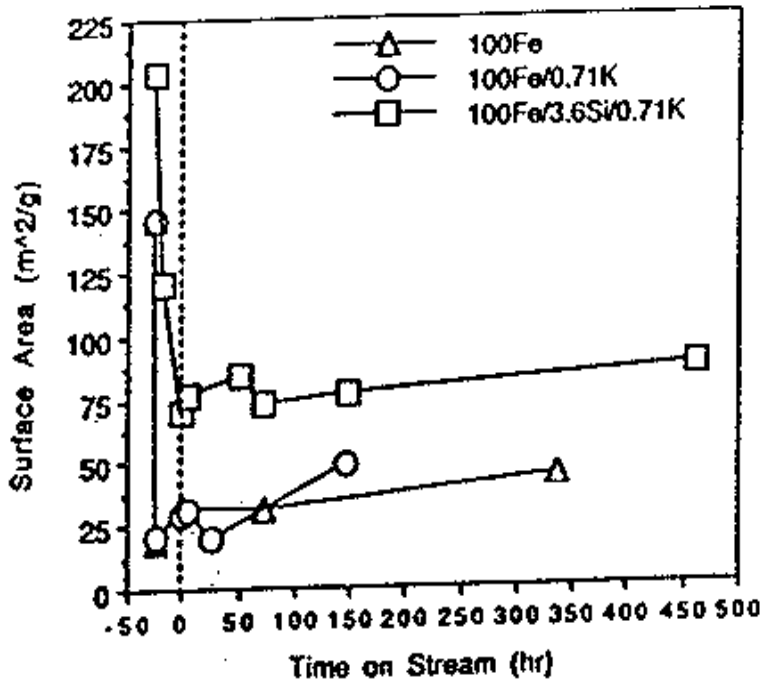

Figure 2. Catalyst surface areas as a function of time-on-stream (TOS). Negative TOS denote catalyst pretreatment; positive TOS denote Fischer-Tropsch synthesis.

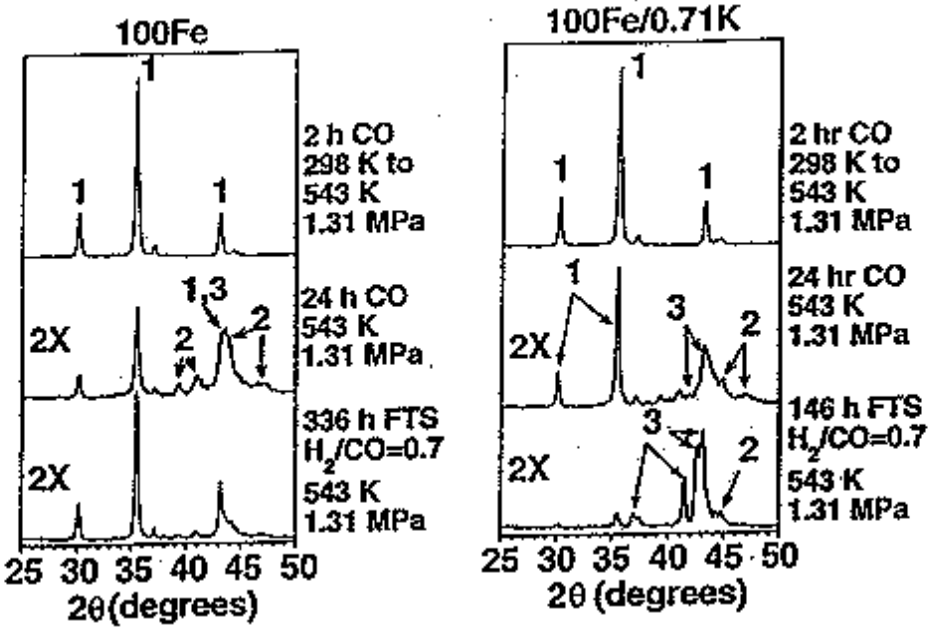

Figure 3. X-ray diffraction results for two catalysts (100Fe and 100Fe/0.71K) during pretreatment and at the end of synthesis ((1) Fe_3O_4, (2) ?-Fe_5C_2, (3) ?-$Fe_{2.2}C$).

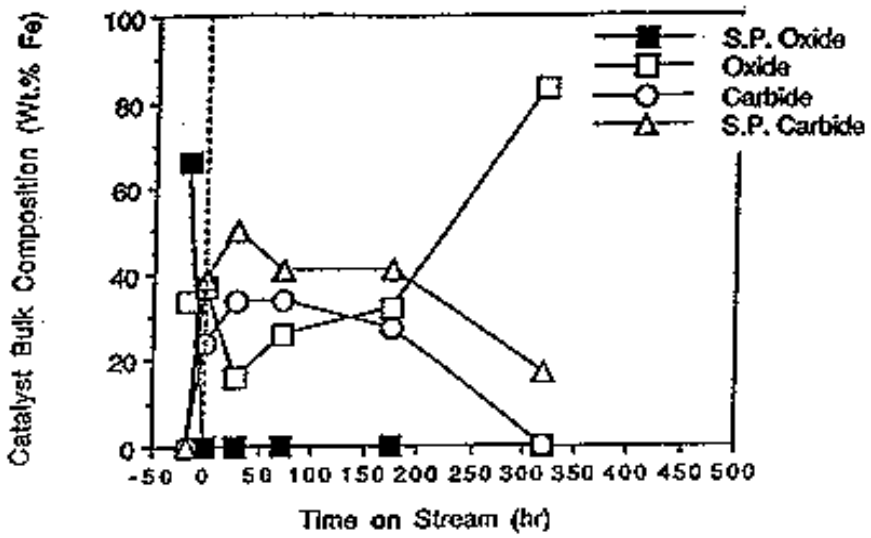

Figure 4. Bulk composition of catalyst: 100Fe/3.6Si/0.71K from Mössbauer spectroscopy as a function of time-on-stream. Negative TOS denote catalyst pretreatment; positive TOS denote Fischer-Tropsch synthesis. S.P. denotes superparamagnetic.

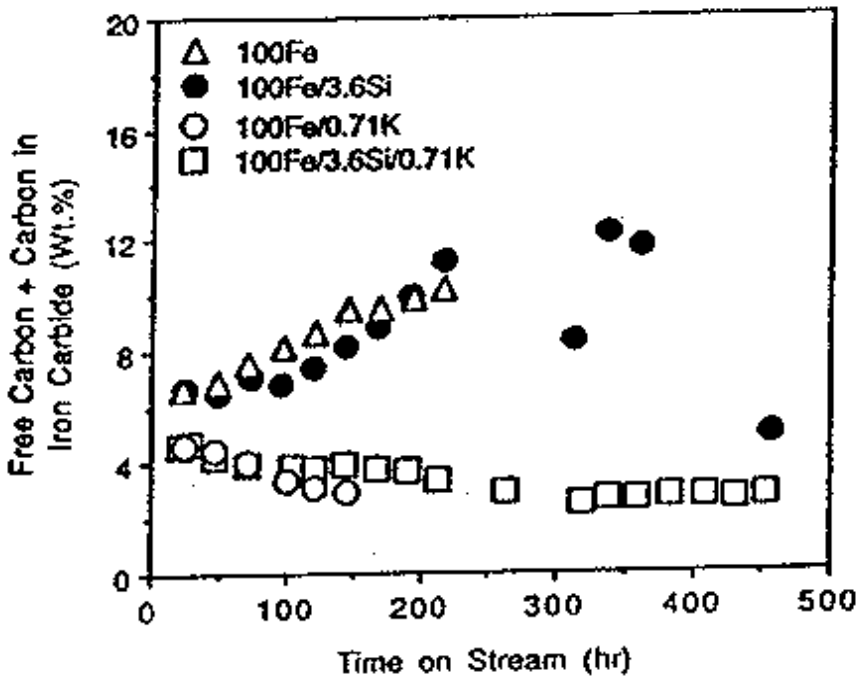

Figure 5. Amount of carbon deposits and carbon in the form of iron carbide as a function of time-on-stream (TOS). Negative TOS denotes catalyst pretreatment; positive TOS denotes Fischer-Tropsch synthesis.

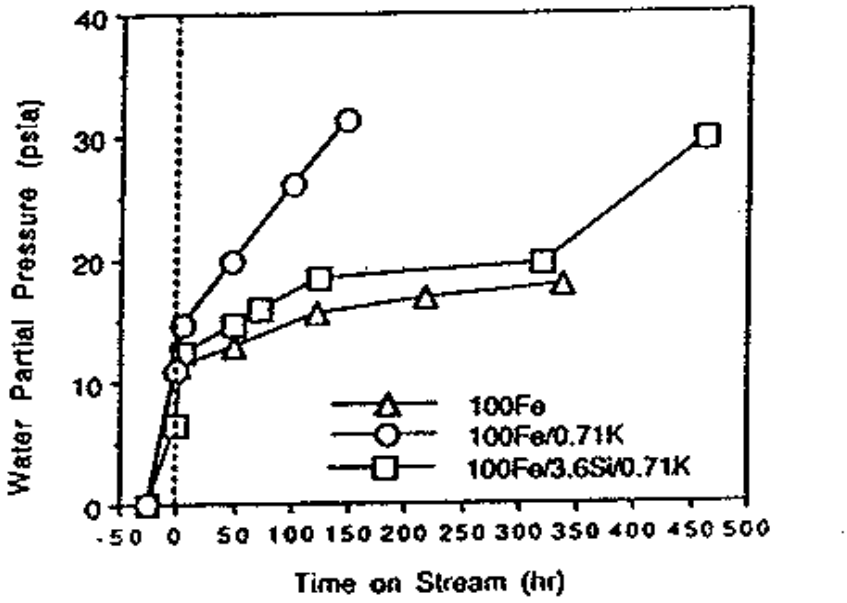

Figure 6. Partial pressure of water as a function of time-on-stream.

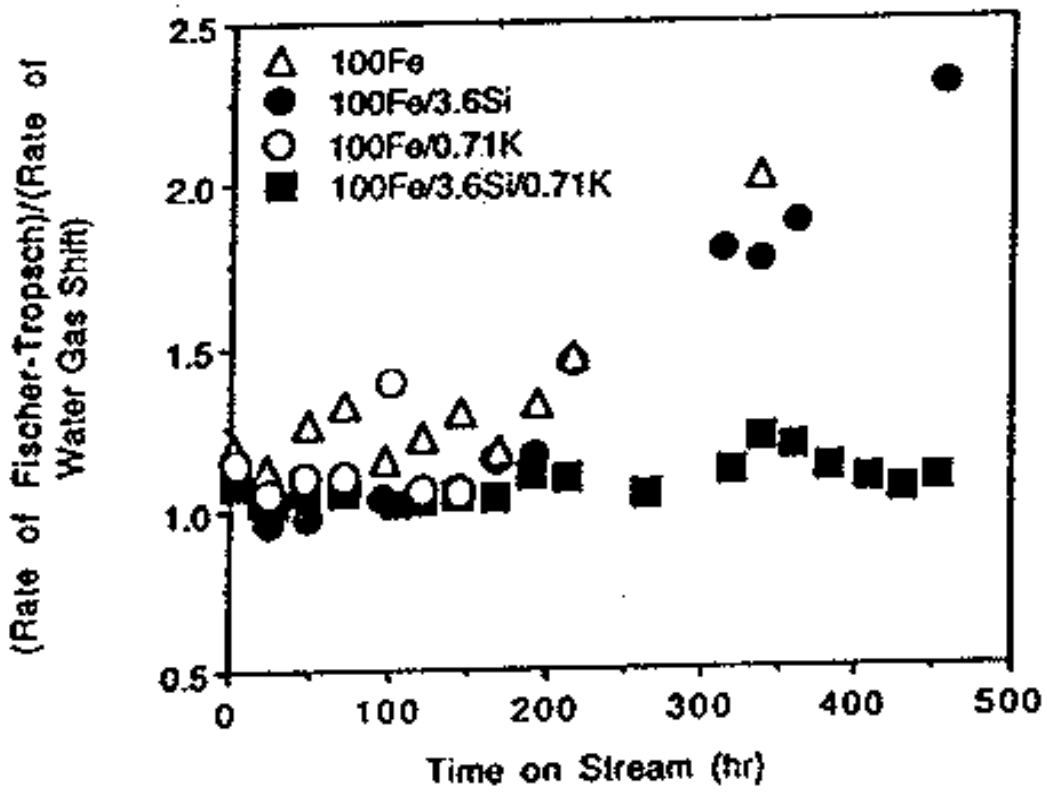

Figure 7. Ratio of the reaction rates of the Fischer-Tropsch synthesis to the water-gas shift reaction as a function of time-on-stream.

3.3.2 Fischer-Tropsch Synthesis. Conversion of Alcohols over Iron Oxide and Iron Carbide Catalysts

ABSTRACT

Both iron oxide (Fe_2O_3) and iron carbide catalysts are active for the dehydration of tertiary alcohols; the oxide catalyst is not reduced nor is the carbide oxidized by the steam generated during the dehydration reaction. Secondary alcohols are selectively converted to ketones plus hydrogen by both the iron oxide and carbide catalyst. Fe_2O_3 is reduced to Fe_3O_4 during the conversion of secondary alcohols. Both iron carbide and oxide catalysts dehydrogenate a primary alcohol (C_n) to an aldehyde; however, the aldehyde undergoes a secondary ketonization reaction to produce a symmetrical ketone with 2n-1 carbons. These results suggest that dehydration of alcohols to produce olefins makes a minor, if any, contribution during Fischer-Tropsch synthesis with an iron catalyst at low pressure conditions.

INTRODUCTION

The conversion of syngas, a mixture of CO and H_2, was initially believed to occur through the formation of an iron carbide which subsequently underwent hydrogenation to hydrocarbons *(1)*. Later, a mechanism was advanced which involved the formation of an oxygen-containing surface species which underwent a series of combination-dehydration steps, ultimately leading to a primary alcohol or an alkene *(2)*. Isotopic tracer studies by Emmett and co-workers provided data which was considered to provide strong support for the oxygen-containing intermediate *(3-11)*. As sophisticated surface science instrumentation became available, their use showed that the metal

surface was covered with carbon but that little, if any, surface oxygen could be detected. Thus, a mechanism involving the dissociation of CO to form C and O adsorbed on the surface became widely accepted *(for example, 12-15)*. In this mechanism, the adsorbed O was hydrogenated to water which rapidly desorbed while the adsorbed C was hydrogenated to form adsorbed CH, CH_2 and CH_3 groups. While any of these groups could be involved in the formation of ethylene and higher hydrocarbons, the methylene groups was considered in most mechanisms to be the surface species which underwent polymerization to produce an Anderson-Schulz-Flory distribution of hydrocarbon products.

In the case of an iron Fischer-Tropsch catalyst, the carbide phase could be formed following activation in either CO alone or with a mixture of CO/H_2 *(16,17)*. In addition, any metallic iron formed by hydrogen reduction of the iron oxide catalyst precursor was quickly converted to iron carbides when the activated catalyst was exposed to the synthesis gas *(18)*. However, during synthesis the iron carbide was gradually converted to a mixture containing both iron carbides and Fe_3O_4; the extent and rate of formation of the iron oxide phase depended upon the operating conditions such as CO conversion, water-gas-shift activity, promoter levels, and time-on-stream. Thus, the iron in a "working, steady-state" catalyst is present as a mixture of the oxide and carbide phases. However, while an attractive model for the working catalyst was a surface layer of iron carbide supported on a core of Fe_3O_4, data to define the structure of the working catalyst is still lacking *(19)*.

Recently, isotopic tracer studies using a variety of alcohols, alkenes and carbon dioxide have produced results for iron catalysts that were consistent with a chain initiating species that contains oxygen *(20-27)*. Thus, it is of interest to define the pathways for conversion of various alcohols using iron oxide and iron carbide catalysts and that is the subject of this paper.

EXPERIMENTAL

Catalyst. The iron oxide catalyst was prepared by adding concentrated ammonia to a 1M iron nitrate solution to produce a pH of about 10.5. The solid was collected and washed by repeated dispersion/filtration cycles; at the end of the washing cycles the pH was in the 7-8 range. After drying overnight at 110°C, the material had a BET surface area of 252 m^2/g. The material following calcination at 300°C had an X-ray diffraction pattern consistent with a-Fe_2O_3. An iron oxide catalyst that contained 6 wt.% thoria was also prepared using a published procedure *(28)*; this material was also a-Fe_2O_3 following calcination at 300°C.

The iron carbide catalyst was prepared by treating the a-Fe_2O_3 sample for 24 hr. in a flow of CO at 1 atm. and 300°C. Prior to use, the sample was flushed with nitrogen for 30 minutes. To obtain a sample of the carbide catalyst for X-ray analysis, the material was passivated at room temperature by passing nitrogen containing 1% oxygen over the iron carbide for about three days.

Conversions. A plug flow quartz reactor with the catalyst located in the middle was utilized. Glass beads were placed on top of the catalyst bed to serve as a preheater and a thermowell extended into the middle of the catalyst bed. During the

run the alcohol was added by a syringe pump at atmospheric pressure without a diluent gas. Liquid samples were collected at appropriate intervals.

The iron oxide catalyst was activated overnight in a flow of air at 300^{o}C prior to a run. To start a run, the air flow was terminated and the catalyst was flushed with dry nitrogen for 30 minutes. The nitrogen flow was stopped and the alcohol flow was then started. The alcohols were purchased from Aldrich and were used without purification. The liquid samples that were collected at appropriate time intervals were analyzed by g.c. using a DB-5 column.

The iron carbide catalyst was prepared and flushed with nitrogen for about 15 minutes immediately prior to use for the alcohol conversions.

RESULTS

The conversion of 2-octanol at 275^{o}C showed that the iron oxide catalyst was very selective for dehydrogenation but had little dehydration activity (Figure 1). Prior to the run the catalytic material was a-Fe_2O_3 (Figure 2a) but following the run the catalyst contained both a-Fe_2O_3 and Fe_3O_4 (Figure 2b). Thus, the hydrogen produced during alcohol dehydrogenation was effective in reducing the catalyst to Fe_3O_4, and the extent of reduction would presumably depend upon the length of the time that the catalyst was exposed to the flow of alcohol.

The conversion results for the thoria-containing catalyst are very similar to the run with the a-Fe_2O_3/Fe_3O_4 catalyst mixture. While the selectivity for dehydrogenation is slightly lower for the thoria containing catalyst, it has a selectivity and activity that is similar to the iron oxide catalyst (Figure 1). Following 5 hr. use as a catalyst for the

conversion of 2-octanol, the X-ray diffraction pattern of this material was similar to that of the a-Fe_2O_3 catalyst that did not contain thoria (Figure 3). However, peaks at 2? = 31.9, 45.8 and 66.8, corresponding to ThO_2, were evident in the X-ray diffraction pattern for this material in addition to those for a mixture of a-Fe_2O_3/Fe_3O_4 (Figure 2c).

3-Methyl-3-pentanol, a tertiary alcohol which cannot undergo direct dehydrogenation to a ketone, was converted with the a-Fe_2O_3 catalyst. At 230^{o}C, the catalyst was active only for dehydration to produce a mixture of cis- and trans-3-methyl-2-pentenes. Following 5 hr. use as a catalyst, the alcohol flow was terminated, the catalyst flushed with nitrogen at reaction temperature, and then cooled to room temperature in a nitrogen flow. The X-ray diffraction pattern of the material was identical to that of the initial catalyst (Figure 3), indicating that the conversion of this tertiary alcohol did not effect any reduction of the catalyst, and this is the expected result. The conversion data for 3-methyl-3-pentanol (Figure 4) show that the tertiary alcohol is converted more rapidly than 2-octanol, a secondary alcohol.

3-Methyl-3-pentanol was also converted with an iron carbide catalyst using similar conditions as with the Fe_2O_3 catalyst except for the flow. Since the flow rate was about 1.7 times greater with the iron carbide catalyst, the iron carbide catalyst is about twice as active for 3-methyl-3-pentanol dehydration as the iron oxide catalyst is.

3-Pentanol was run at 230 and 260^{o}C. At these two temperatures, the selectivity for dehydrogenation is almost the same although the conversion at 260^{o}C is higher than that at 230^{o}C. For both of these runs, the catalytic activity for 3-pentanol conversion did not decline significantly during the run (Figure 5). The X-ray diffraction

pattern of the catalyst exhibited peaks corresponding to both a-Fe_2O_3 and Fe_3O_4 following the conversion of 3-pentanol (Figure 3b) These experiments confirm that the reduction of the catalyst occurs due to exposure to the secondary alcohol.

In another run, the a-Fe_2O_3 was reduced at 270^{o}C for 5 hr. in a flow of hydrogen and then cooled to 230^{o}C in hydrogen flow. A flow of 2-octanol was initiated and the flow of hydrogen was terminated. The catalyst exhibited activity for 2-octanol conversion; however, the selectivity for dehydrogenation was lower (ca. 0.83 vs. 0.96) at 230^{o}C than at 270^{o}C (Figure 4).

The a-Fe_2O_3 was treated with CO at 260^{o}C for 18 hr. to convert the iron oxide to an iron carbide. Following the treatment with CO the catalyst was flushed with nitrogen, then a flow of 2-octanol was started and the nitrogen flow was terminated. This iron carbide catalyst had an activity and selectivity for dehydrogenation that exceeds that of the catalyst comprised of a mixture of a-Fe_2O_3 and Fe_3O_4 (Figure 6) and does not loose activity during 8 hrs. Following use as a catalyst for 8 hrs., the sample was flushed with nitrogen and cooled to room temperature. The X-ray diffraction pattern of this sample following use as a catalyst contains peaks that are consistent with both iron carbides and Fe_3O_4 (Figure 7), with the carbide being the dominant component. A chemical analysis of the sample following use as a catalyst showed that it contained 9.0 percent carbon, a value that is consistent with the sample being $Fe_{2.2}C$ (9.67% C).

While secondary alcohols may be formed during the Fischer-Tropsch synthesis, a primary alcohol is the dominant alcohol for each carbon number. Thus, 1-octanol

was converted over the iron oxide and the iron carbide catalysts. This alcohol underwent conversion by dehydrogenation to the aldehyde. The conversion increased initially and then remained essentially constant with time. The aldehyde underwent a secondary reaction that involved decarbonylation (and/or decarboxylation) to produce CO/CO_2 and the formation of a 15-carbon number symmetrical ketone. This reaction has been observed frequently during the conversion of primary alcohols with metal oxide catalysts that possess dehydrogenation properties *(29)*. Likewise, the selectivity for 1-octanal decreased as the conversion increased. Initially 40 mole% of the products from the conversion with the catalyst was 1-octanal and the remainder was 8-pentadecanone; after the first hour 1-octanal accounted for only 26-29 mole% of the products, the remainder being 8-pentadecanone. As the activity of the iron carbide increased , the selectivity for 1-octanal decreased from 88 mole% to about 65 mole%. Thus, the iron carbide catalyst exhibited an activity for 1-octanol conversion that was about 3-4 times that of the iron oxide catalyst and it had a selectivity for 1-octanal that was 2-2.5 times that of the iron oxide catalyst. Neither the iron oxide nor the carbide catalyzed dehydration of 1-octanol since only traces octenes were observed.

DISCUSSION

The catalytic material remains Fe_2O_3 during the conversion of 3-methyl-3-pentanol. This is not surprising since a tertiary alcohol cannot undergo dehydrogenation; rather it is dehydrated to produce an olefin and water.

The iron carbide catalyst does not undergo measurable conversion to the oxide. Likewise, the greater activity of the iron carbide, compared to Fe_2O_3, suggests that

even the surface remains the carbide during the dehydration of 3-methyl-2-pentanol and the generation of water vapor.

On the other hand, Fe_2O_3 is reduced, at least partially, to Fe_3O_4 during the conversion of secondary alcohol. However, the iron oxide is not converted to an iron carbide during the conversion of this alcohol, at least not to an extent so that the carbide phase can be detected by X-ray diffraction (XRD). The sample containing 6 wt.% ThO_2 also underwent conversion to a mixture of Fe_2O_3 and Fe_3O_4; in addition, a ThO_2 phase was formed so that it could be detected by XRD. This is surprising since it has been reported that when this amount of thoria is present in an iron catalyst it provided a material that had superior activity for the water-gas shift reaction than a similar material that did not contain thoria *(28)*. It is difficult to understand why thoria should impact the activity for water gas shift if phase separation occurs in a reducing atmosphere.

If Fe_2O_3 is treated in CO to produce iron carbides, the material that remains following conversion of 2-octanol during 8 hrs is predominantly iron carbides. Thus, the carbide is not converted to the oxide in the presence of the small amount of water produced during the dehydration of 2-octanol, primarily during the early reaction period, to an extent such that the oxide(s) can be detected by XRD.

Except during an initial break-in period, the pure iron oxide and the iron oxide sample containing 6 wt.% ThO_2 were very selective dehydrogenation catalysts for primary and secondary alcohols. Only with the tertiary alcohol, where dehydrogenation is not possible, was the iron oxide catalyst selective for dehydration.

With the secondary alcohol, the iron oxide catalyst was very selective in dehydrogenating the alcohol to the corresponding ketone. Essentially no secondary reaction products were observed.

With the primary alcohol, the iron oxide catalyst was selective for dehydrogenation to the corresponding aldehyde. However, the aldehyde underwent a secondary reaction in which it was converted to a symmetrical secondary ketone plus either CO or CO_2. This reaction is known to occur when primary alcohols are converted over a variety of metal oxide catalysts *(29)*. In this reaction it resembles the ketonization reaction that many metal oxide catalysts effect when starting with an acid. However, the mechanism for these reactions has not been clearly elucidated to date.

The iron carbide catalyst has a selectivity that resembles that of iron oxide but it is about twice as active for the conversion of the secondary alcohols. The higher activity of the iron carbide catalyst implies that either the surface is not oxidized to the oxide during the conversion of the alcohol or the oxycarbide that is formed on the iron carbide surface is more active that the iron oxide surface. The chemical composition of the gas phase is such that the iron is expected to be present in the carbide phase *(30)*. A similar conclusion is reached for the conversion of 1-octanol over the iron oxide and carbide catalysts. The iron carbide is about 4 times as active for the conversion of 1-octanol as the iron oxide and has only about half the activity for the formation of a symmetrical ketone from the primary dehydrogenation product, 1-octanal.

It has been demonstrated convincingly that alcohols can serve to initiate chain growth during the Fischer-Tropsch reaction (27). Furthermore, when using a promoted

iron catalyst, the alcohol incorporates into the Fischer-Tropsch products about 50-100 times greater than the alkene that would be formed from dehydration of the alcohol. The present data indicate that the primary reaction of an alcohol that is formed during the Fischer-Tropsch synthesis is to undergo dehydrogenation to the aldehyde and this is true for both Fe_3O_4 and iron carbide catalysts. The present results indicate that reincorporation of the alcohol into Fischer-Tropsch products is not through an alkene intermediate that is formed by the dehydration of the alcohol. The results are consistent with the Fischer-Tropsch mechanism requiring an initiation step that involves an oxygen-containing species, and not a surface carbon or carbene intermediate.

ACKNOWLEDGMENT

This work was supported by U.S. DOE contract number DE-AC22-94PC94055 and the Commonwealth of Kentucky.

REFERENCES

1. F. Fischer and H. Tropsch, *Zeit. fur Chem.*, **7** (1926) 97-116.
2. H. H. Storch, N. Golumbic and R. B. Anderson, "The Fischer-Tropsch Synthesis," John Wiley & Sons, Inc., New York, 1951.
3. W. K. Hall, R. J. Kokes and P. H. Emmett, *J. Am. Chem. Soc.*, **79** (1957) 2983.
4. R. J. Kokes, W. K. Hall and P. H. Emmett, *J. Am. Chem. Soc.,* **79** (1957) 2089.
5. J. T. Kummer, H. Podgurski, W. B. Spencer and P. H. Emmett, *J. Am. Chem. Soc.*, **73** (1951) 564.
6. J. T. Kummer and P. H. Emmett, *J. Am. Chem. Soc.*, **75** (1953) 5177.
7. P. H. Emmett, *Oil and Gas. J.*, (Sept. 1951) 82.
8. H. H. Podgurski and P. H. Emmett, *J. Phys. Chem.*, **57** (1953) 159.
9. G. Blyholder and P. H. Emmett, *J. Phys. Chem.*, **63** (1959) 962.
10. G. Blyholder and P. H. Emmett, *J. Phys. Chem.*, **64** (1960) 470.
11. J. T. Kummer, T. W. DeWitt and P. H. Emmett, *J. Am. Chem. Soc.*, **70** (1948) 3632.
12. K. M. Sancier, W. E. Isakson and H.Wise; *ACS Symp Series*, (1979).
13. M. E. Dry, *Appl. Catal. A: General*, **138** (1996) 319-344.
14. (a) R. C. Brady, III and R. Pettit, *J. Am. Chem. Soc.*, **102**, 6181-6182 (1980); (b) R. C. Brady, III and R. Pettit, *J. Am. Chem. Soc.*, **103**, 1287-1289 (1981).
15. M. L. Turner, H. C. Long, A. Shenton, P. K. Byers and P. M. Maitlis, *Chem. Eur. J.*, **1** (1995) 549-556.

16. R. J. O'Brien, L. Xu, R. L. Spicer and B. H. Davis, *Energy & Fuels*, **10** (1996) 921-926.

17. C.-S. Huang, L. Xu and B. H. Davis, *Fuel Sci. & Tech. Intl.*, **11** (1993) 639.

18. C.-S. Huang, B. Ganguly, G. P. Huffman, F. E. Huggins and B. H. Davis, *Fuel Sci. & Tech. Intl.*, **11** (1993) 1289.

19. A. Raje, R. J. O'Brien, L. Xu and B. H. Davis, "Catalyst Deactivation 1997," (C. H. Bartholomew and G. A. Fuentes, eds.), (Studies in Surface Science Catalysis), 111, 527 (1997).

20. H. Dabbagh, L.-M. Tau, S. Bao, J. Halasz and B. H. Davis, "Catalysis 1987" (J. Ward, Ed.) Elsevier, Amsterdam, pp. 61-72 (1988).

21. L.-M. Tau, H. Dabbagh, S. Bao, J. Halasz, B. Chawla and B. H. Davis, *Proc. 9th Int. Congr. Catal.*, **2** (1988) 861.

22. L.-M. Tau, H. A. Dabbagh and B. H. Davis, *Energy & Fuels*, **4** (1990) 94.

23. L.-M. Tau, H. A. Dabbagh and B. H. Davis, *Catal. Lett.*, **7** (1990) 141.

24. L.-M. Tau, H. Dabbagh, S. Bao and B. H. Davis, *Catal. Lett.*, **7** (1990) 127.

25. L.-M. Tau, H. A. Dabbagh and B. H. Davis, *Energy & Fuels*, **5** (1991) 174.

26. L.-M. Tau, H. A. Dabbagh, J. Halasz and B. H. Davis, *J. Mol. Cat.*, **71** (1992) 37.

27. A. Raje and B. H. Davis in "Catalysis" (J. J. Spring Ed), The Royal Soc. Chem., Cambridge, 12, 52-131 (1996).

28. F. Domka and I. Wolska, *Surf. and Coatings Technol.*, **28**, (1986) 187.

29. V. I. Komarewsky and J. R. Coley, *Advan. Catal.*, **8** (1956) 207.

30. S.-J. Liaw and B. H. Davis, submitted.

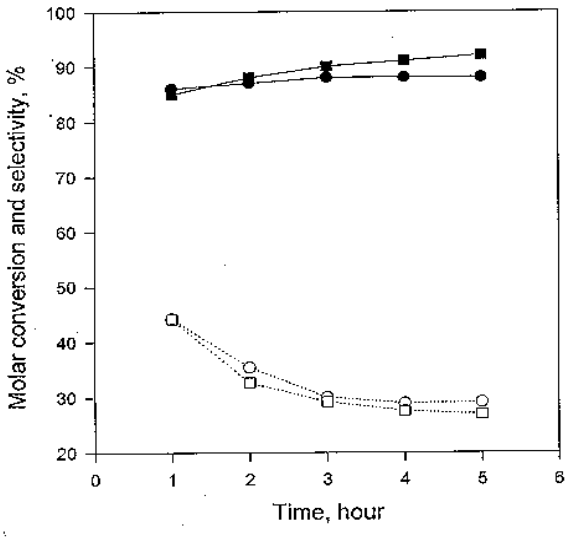

Figure 1. The conversion of 2-octanol for the Fe_2O_3 (**9**) and Fe_2O_3-ThO_2 (**F**) catalysts and the selectivity for dehydrogenation for the Fe_2O_3 (**O**) and Fe_2O_3-ThO_2 (**M**) catalysts [275°C, 1 atm, LHSV = 3.2 h^{-1}].

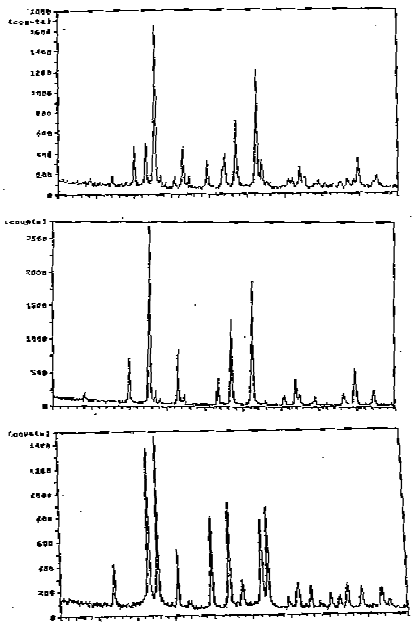

Figure 2. The X-ray diffraction patterns for: (a) the Fe_2O_3 catalyst (bottom); (b) the Fe_2O_3 catalyst after use for the conversion of 2-octanol (middle), and (c) the thoria containing catalyst after use for the conversion of 2-octanol (top).

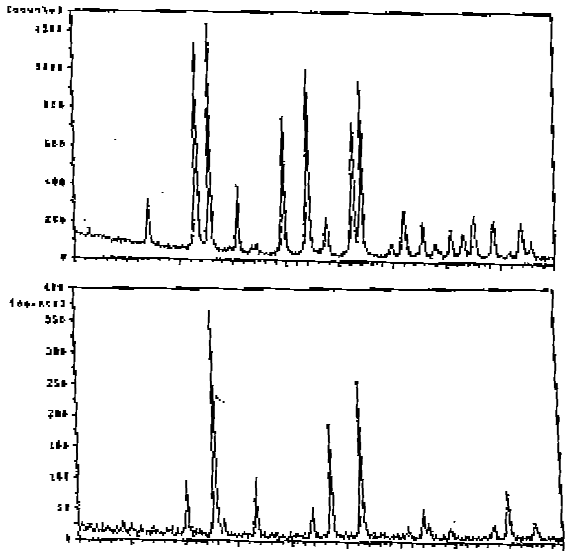

Figure 3. The X-ray diffraction patter for the Fe_2O_3 catalyst following (a) use for the conversion of 3-methyl-3pentanol (top) and (b) of Fe_2O_3 following use for the conversion of 3-pentanol (bottom).

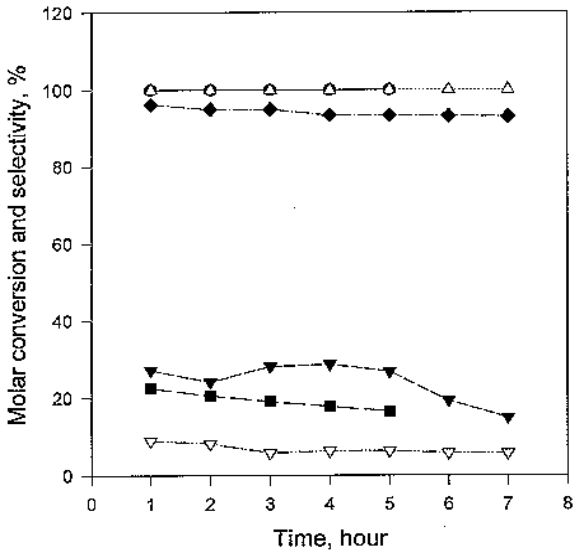

Figure 4. The conversion (L) and dehydrogenation selectivity (,) for 3-pentanol (LHSV = 1.5 h^{-1}) with the Fe_2O_3 catalyst; the conversion (•) and dehydration selectivity (**!**) for 3-methyl-3-pentanol (LHSV = 3.2 h^{-1}) with the Fe_2O_3 catalyst; and the conversion (**–**) and dehydration selectivity (Î) for 3-methyl-3-pentanol (LHSV = 5.4 h^{-1}) the iron carbide catalyst (230°C, 1 atm).

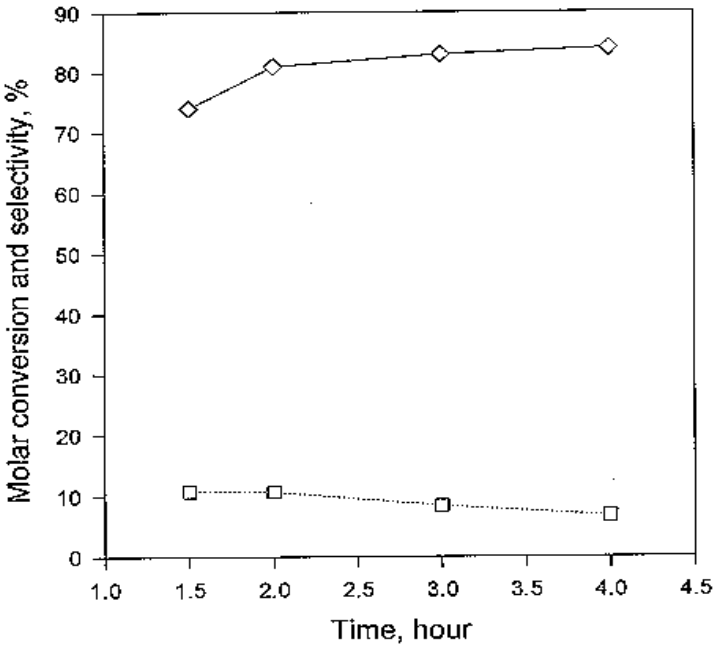

Figure 5. The conversion (**9**) and dehydrogenation selectivity (**"**) for the Fe_2O_3 catalyst following reduction in hydrogen at 230°C, 1 atm, LHSV = 1.5 h^{-1}.

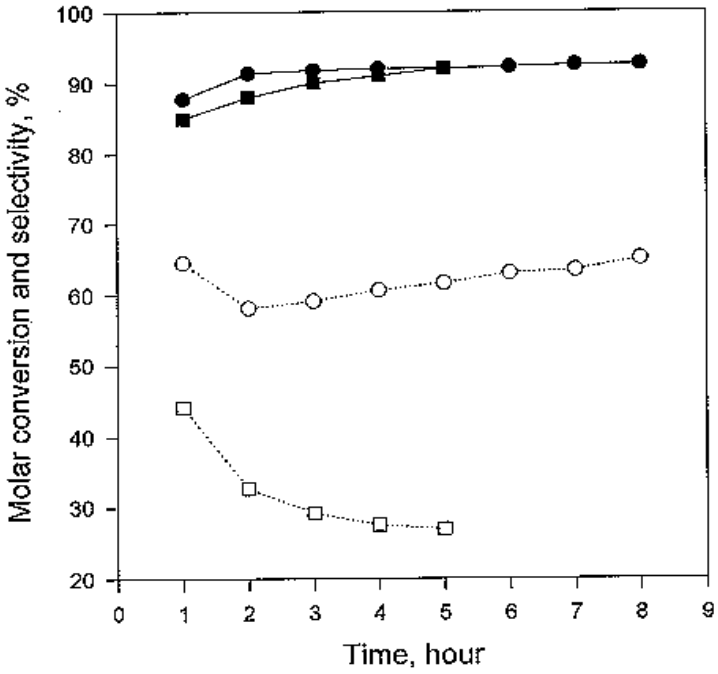

Figure 6. Conversion of 2-octanol with Fe_2O_3 (275°C, 1 atm, LHSV = 3.2 h^{-1}) (**9**) and iron carbide (275°C, 1 atm, LHSV = 3.2 h^{-1}) (**"**) and the dehydrogenation selectivity with Fe_2O_3 (**#**) and iron carbide (**!**).

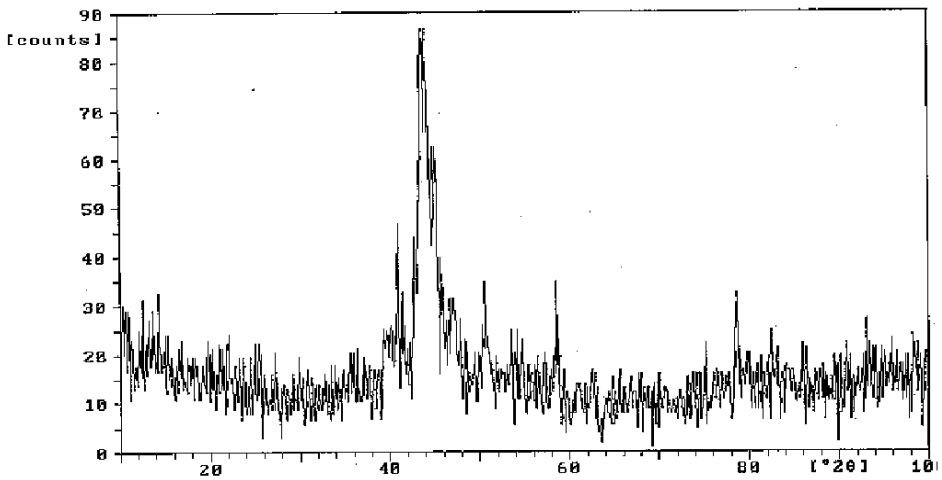

Figure 7. X-ray diffraction scan of the iron carbide catalyst following use for the conversion of 2-octanol at 275°C, 1 atm and LHSV = 3.2 h^{-1}.

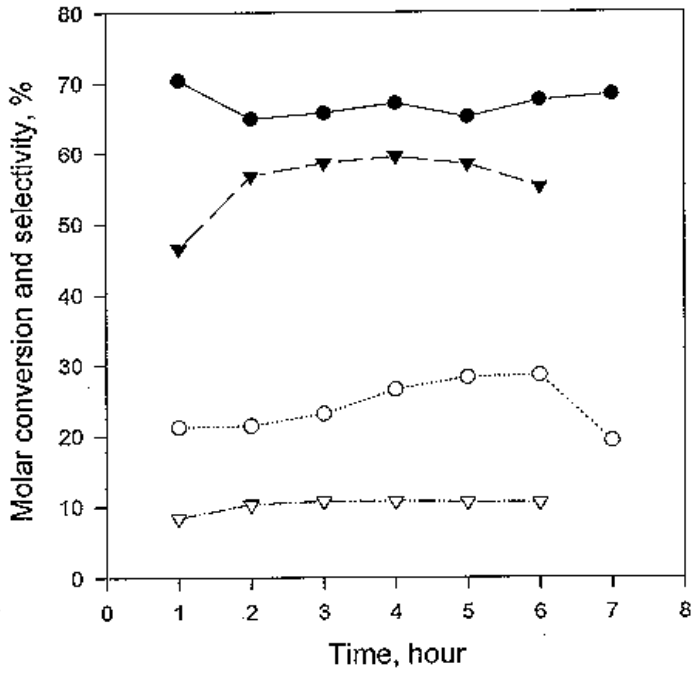

Figure 8. The conversion (L; 275°C, 1 atm, LHSV = 3.3 h^{-1}) of 1-octanol with Fe_2O_3 and iron carbide (**"**; 275°C, 1 atm, LHSV = 3.3 h^{-1}) and the dehydrogenation selectivity to 1-octanal for Fe_2O_3 (**–**) and iron carbide (**!**). [The low selectivity is due to formation of 8-pentadecanal from 1-octanal by secondary reactions].

3.3.3 A Comparison of Fischer-Tropsch Synthesis in a Slurry Bubble Column Reactor and a Continuous Stirred Tank Reactor

Abstract

Fischer-Tropsch synthesis (FTS) was studied using a precipitated Fe/K catalyst in a improved short slurry bubble column reactor (SBCR) equipped with a satisfactory reactor-wax separation system and a continuous stirred tank reactor (CSTR) using the same experiment conditions. The catalyst in the SBCR had a lower catalytic activity. Methane and the products of the gas are higher in the CSTR. Some effects may be related to different mixing heat, mass transfer phenomena between two reactors. The C_3+ hydrocarbons (C_3+H.C.) with synthesis gas (CO+H_2) conversion ratio had similar values.

Introduction

A SBCR is a gas-liquid-solid reactor in which the finely divided solid catalyst is suspended in the liquid by the rising gas bubbles. It offered the following advantages: (a) the ability of the liquid phase to handle the large heats of reaction, (b) low H_2/CO ratio synthesis gas without needing a preliminary water-gas shift step, and (c) relatively low capital and operating cost. A considerable interest has been expressed in using the SBCR to carry out FTS.

FTS takes place in a SBCR where the synthesis gas is converted on catalysts suspended in a liquid as fine particles. The synthesis gas flows as small bubbles through the catalyst suspension. The products are volatile under the synthesis conditions which are removed with unconverted gases, and the liquid products are separated from the suspension. The bubbles in the reactor are produced by the gas

distributor located in the bottom of the reactor. As reported by W-D Deckwer, et al. (1), the higher liquid phase transfer coefficient values were found in short columns, and it can be explained with the increased mass transfer during bubble formation, but the formation of the bubble should be regarded as end effect which will be constant for a given gas distributor. The engineering problem for bubble column reactor that needed to be solved was the catalyst separation from wax.

The improved design of the short bubble column reactor in CAER F-T pilot unit contains a good axial dispersion function and a continuous reactor-wax removal system. This axial dispersion function would cause an increase in gas-liquid backmixing, and would have a great effect on conversion and selectivity. The improved F-T reactor-wax separation system enabled us to increase the flexibility and reduce the manpower requirement for the reactor-wax/slurry separation.

A CSTR is designed to use a powdered catalyst in a slurry. The agitation of the reactor provides optimum isothermal and residence time conditions. A dip-tube fitted inside the reactor provides excellent gas/liquid contact.

The purpose of the present study was to compare certain aspects of the FTS as carried out on the same precipitated Fe/K catalyst in the SBCR and the CSTR using the same experimental conditions. It is expected that there would be some differences in the conversion and selectivities obtained from these reactors, because these reactors differ in the type of mixing and heat and mass transfer phenomena.

Experimental

A schematic diagram of the experimental apparatus is shown in Figure 1 for the SBCR and Figure 2 for the CSTR. The bubble column reactor has 5.08 cm diameter

and a 2 m height. The CSTR is 1 liter autoclave. The SBCR was equipped with a gas distributor and a K-ray detector. The gas distributor produce fine gas bubbles in the liquid phase and the K-ray indicates the catalyst axial suspension inside the reactor. The CSTR was filled initially about 2/3 of the reactor volume and the SBCR filled about 3/4 of the column volume with the slurry that was made of 20 wt% catalyst and the Shell C_{30} oil. The level of the slurry is dependent on the calculation of gas holdup in the SBCR at the synthesis condition (2). Briefly, the synthesis gas was passed continuously through the reactors, the products gas and liquid, at the top of the reactor pass through a separation section to a hot condenser (230^{o}C), and a cold separator (3^{o}C). A dry flow meter for SBCR and a bubble meter for CSTR was used to measure the exit gas flow rate.

The composition of the exit gas was determined by GC techniques. The condensed liquid phases were sampled at periodic times (12 hours for SBCR and 24 hours for CSTR) and the mass of each sample was obtained. The aqueous phase was analyzed for water and oxygenates using a GC fitted with Porpack Q column. The oil and wax phases sample was combined according to the mass fraction, O-xylene was added as an internal standard, then this sample was analyzed for hydrocarbons by GC with the DB-5 column.

The catalyst particle sizes after synthesis for 309 hours (SBCR) and for 253 hours (CSTR) were obtained by SEM. The SEM was carried out after coating the power samples with carbon, using a Hitachi S-2700 scanning electron microscope at 20 KV. EDS was carried out using a thin window Si-Li diode detector.

The operating conditions for both reactor systems are given in Table 1.

Results and Discussion

Catalyst axial dispersion and mixing

The gas-liquid backmixing plays an important role in the performance of the reactor. The quality of the flow is dependent on the type of gas distributor, properties of the liquid, column size, gas velocities, solid concentration and solid particle (3-5). At low gas velocity (<5 cm/sec.), the bubble rise separately in the liquid or slurry and the homogeneous bubble flow regime prevails (3). The solid dispersion, detected by a K-ray at gas velocity 3 cm/sec, shows that the liquid phase is more likely uniform in the column (Figure 3). However, a trend towards bubble coalescence behavior was also observed in this figure. The agitation in the SBCR by rising gas bubbles and in the CSTR by a magnedrive stirrer operated at 750 rpm, so that the agitation of the CSTR provides excellent mixing.

Conversion

Table 2 lists the data obtained from the both reactor systems at same time-on-stream time. It is shown that the difference in conversion between the two reactors is caused by the difference of heat and mass transfer phenomena and gas resident time in the reactor. The gas hourly space velocity (GHSV) based on the volume of reactor is 379 in the SBCR and 209 in the CSTR. Some possible effects of the reactor type on the catalyst activity may be caused by the GHSV based on the liquid volume is slight different (518 in the SBCR and 504 in the CSTR) and the liquid level is much higher in the SBCR, the synthesis products volatile under the operating conditions are removed slowly with the residual gas in the SBCR, so that some high molecular weight liquid products remain in the reactor, fill catalyst pores, and surround the catalyst particles

(6). The H_2O/H_2 ratio is slight higher in the SBCR. This can produce the iron and iron carbides present as magnetite (7,8). Therefore, maximum F-T conversion may be influenced by the reaction of iron carbide with H_2O to form Fe_3O_4, which has no hydrocarbon synthesis activity. A possible explanation of the observed deactivation could be carbon formation as result of the Boudouard reaction. Carbon deposition in the SBCR causes disintegration of catalyst particles to fines. Apparently, carbon nuclei form inside the Fe crystallites and grow to an extent that the particles are broken by the expanding carbon deposit (Figure 5) (9). The mechanically stirring in the CSTR disintegrates the catalyst particles to fines (Figure 6).

Selectivity

The production of methane is slight higher in the CSTR, and the C_3-C_4 olefin/paraffin ratio is not significantly different in the two systems. The gas production is higher in the CSTR (84.4% and 80.6%), because the water gas shift reaction is stronger in the CSTR. The C_3+ H.C. (g/M^3-hr)/$CO+H_2$ conversion ratio is almost same in the two systems (1.63 in the SBCR and 1.65 in the CSTR). Figure 7 illustrates the differences in the products distributions for both reactors. The mole fraction of higher molecular weight products is higher in the SBCR, and the plot of the products breaks sharply at about $C_{12.}$ The alpha values based on total hydrocarbons formation for the SBCR, are 0.68 and 0.93, and for the CSTR, are 0.42 and 0.82. After 240 hours on-stream, the carbon number distributions are similar for both reactors (Figure 8).

Summary

The improved design of the CAER short bubble column reactor offers good gas-slurry mixing and excellent catalyst wax separations. The iron concentration in the wax

collected after passing the separation system is about 10 ppm. The data presented in this study indicate that the catalyst activity is different between two reactor systems at same operating conditions, the activity is about 10% higher in the CSTR than in the SBCR, the water-gas shift reaction is weak and the gas percentage of synthesis products is less in the SBCR, the (C_1+C_2)/total hydrocarbons ratio is higher in the SBCR. The SBCR produced more the higher molecular weight products on-stream for synthesis times of less than 240 hours.

References

1. D. Deckwer, R. Burckhart and G. Zoll, 1974. Chemical Engineering Science, 29, 2177.
2. J. M. Fox and B. D. Degen, 1990. U.S. DOE Report, No.PC89867-T1.
3. Shigeharu Morooka, Tetsuya Mizoguchi, Tokihiro Kago and Yasuo Kato, 1986. Journal of Chemical Engineering of Japan, 19, 6.
4. Serap Kara, Balmohan G. Kelkar, and Yatish T. Shah, 1982. Ind. Eng. Chem. Process Des. Dev., 21, 584.
5. Yasuo Kato, Akio Nishiwaki, Takashi Fukuda and Shigenobu Tanaka, 1972. Journal of Chemical Engineering of Japan, 5, 2.
6. Charles N. Satterfield, George A. Huff, Jr., and Harvey G. Stenger, 1985. Ind. Eng. Chem. Fundam, 24, 450.
7. Robert Bernard Anderson, 1984. “The Fischer-Tropsch Synthesis” Academic Press, Inc.
8. R.D. Srivastava, Burns and Roe Services Corp. And V.U. S. Rao, G. Cinguegrane and G. J. Stiegel, 1990. Hydrocarbon Processing, 69,59.
9. Charles N. Satterfield and Harvey G. Stenger, 1984. Ind. Eng. Chem. Process Des. Dev. 23,26.

Table 1 Operating Conditions		
	SBCR(503)	CSTR(LX238)
Catalyst	4.4 Si/K	4.4 Si/K
Cat. loaded wt%	20	20
Cat. Activation at:		
Gases	$CO+H_2$	$CO+H_2$
H_2/CO	0.7	0.7
Gas space velocity (SL/hr-g Fe)	5.3	5.15
Temperature (^oC)	270	270
Pressure (atm.)	1	1
Synthesis at:		
H_2/CO	0.7	0.7
Gas space velocity (SL/hr-g Fe)	5.3	5.15
Temperature (^oC)	270	270
Pressure (MPa)	1.21	1.21
Gas superficial velocity (cm/sec)	3	Stirred speed 750 RPM

Table 2 Conversion and Selectivity		
	SBCR	CSTR
CO Conversion %	48.63	58.94
H_2 Conversion %	48.38	54.52
CO+H_2 Conversion %	48.48	57.03
Products gas (%)	80.63	84.44
(C_1+C_2)/T.H.C. (%)	16.76	15.45
C_2=/(C_2+C_2=) (%)	45.01	48.66
C_3=/(C_3+C_3=) (%)	87.03	87.99
C_4=/(C_4+C_4=) (%)	84.27	84.23
C_3+H.C.(g/M_3-hr)/CO+H_2 (%) Conversion	1.63	1.65
H_2O/H_2 Ratio	1.26	1.2
H_2/CO Usage	0.69	0.67

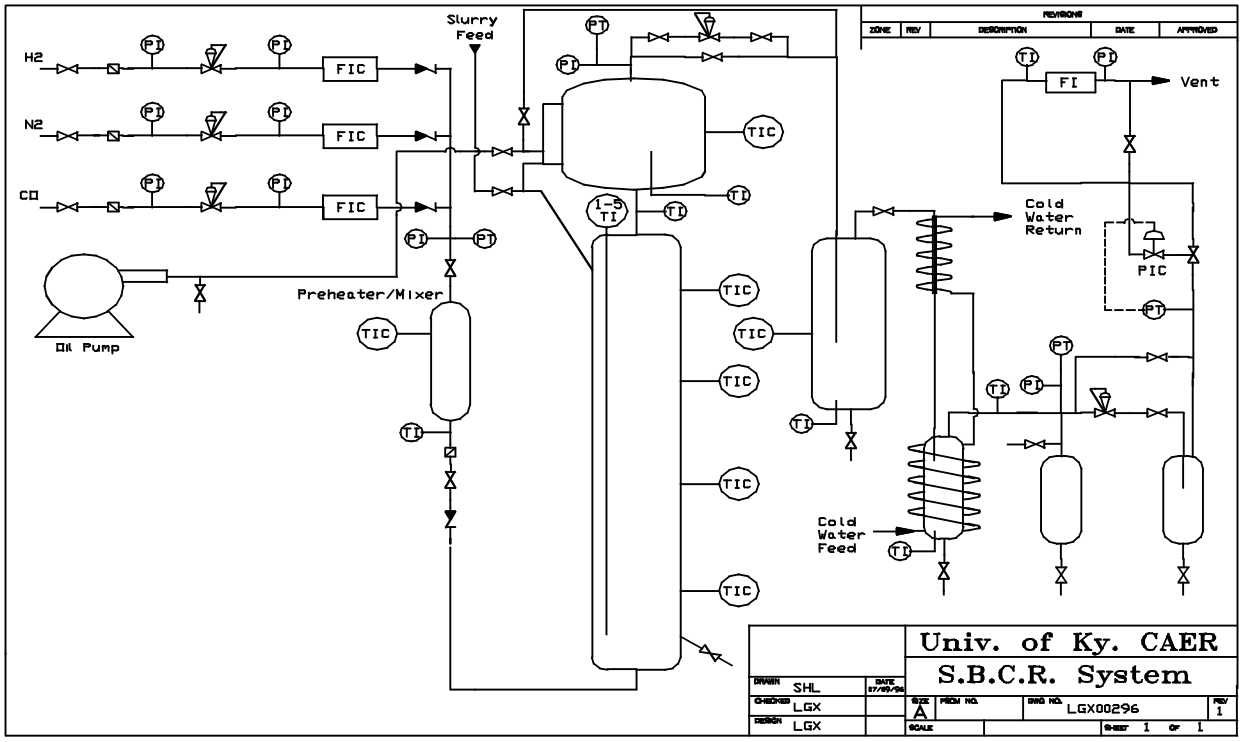

Figure 1. Schematic of the FTS slurry bubble column reactor.

Figure 2. Schematic of the CSTR FTS reactor system.

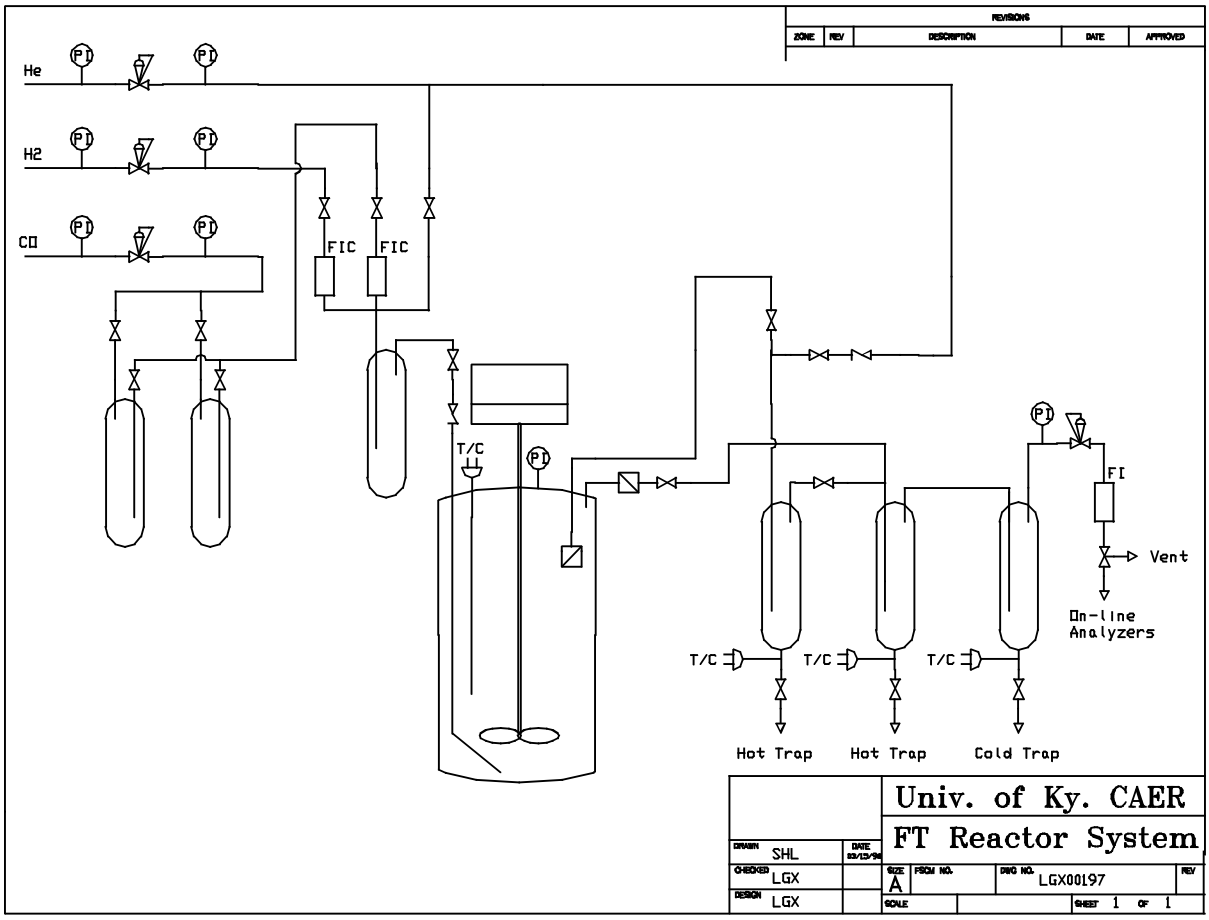

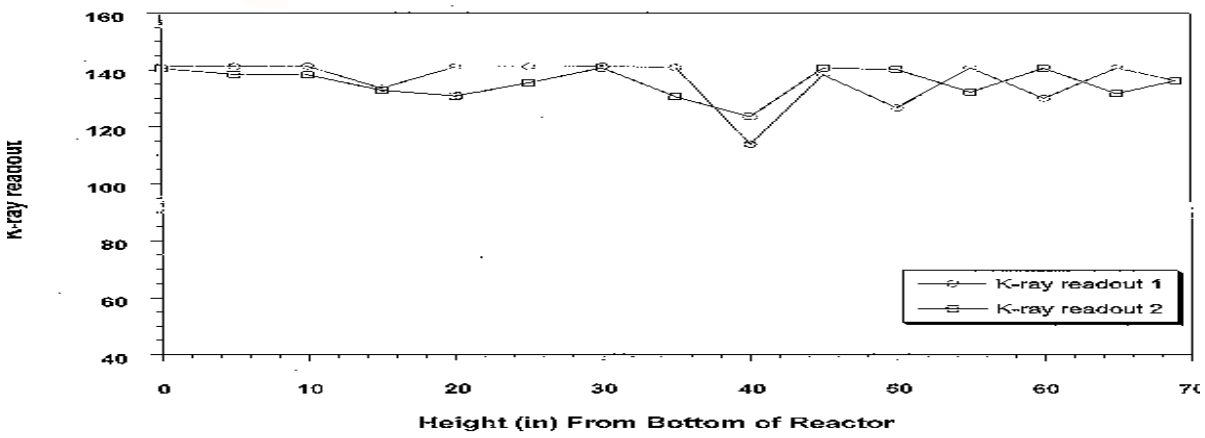

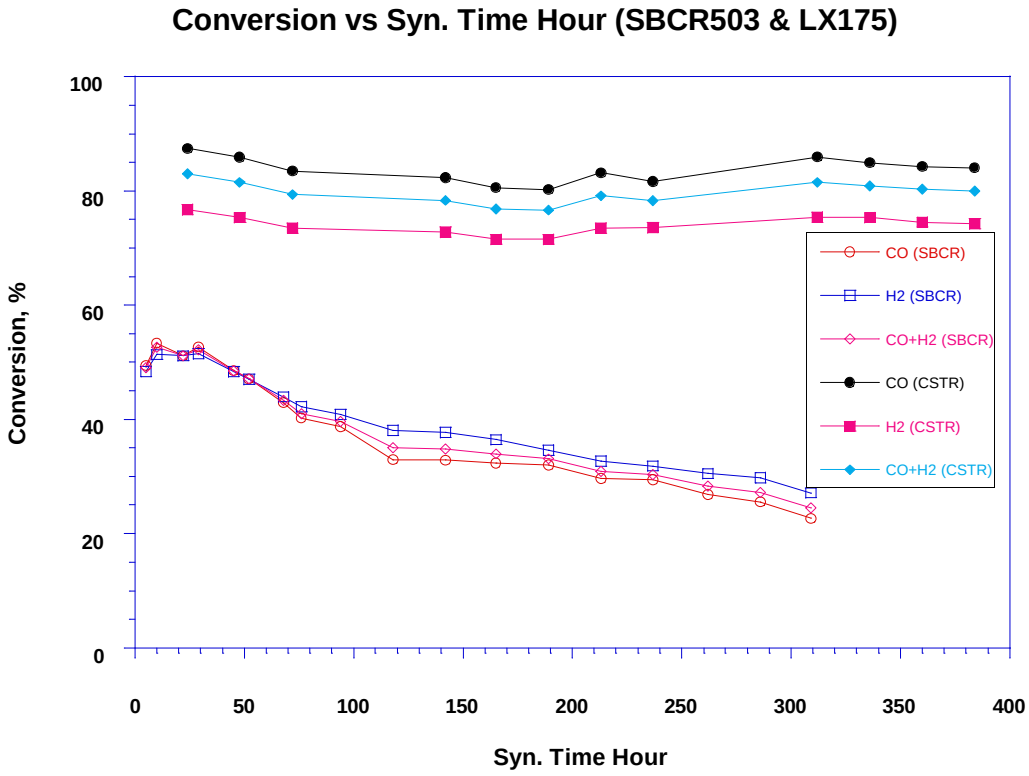

Figure 3. K-ray data for the SBCR indicating uniform catalyst distribution.

Figure 4. Conversion comparisons for the CSTR and SBCR systems.

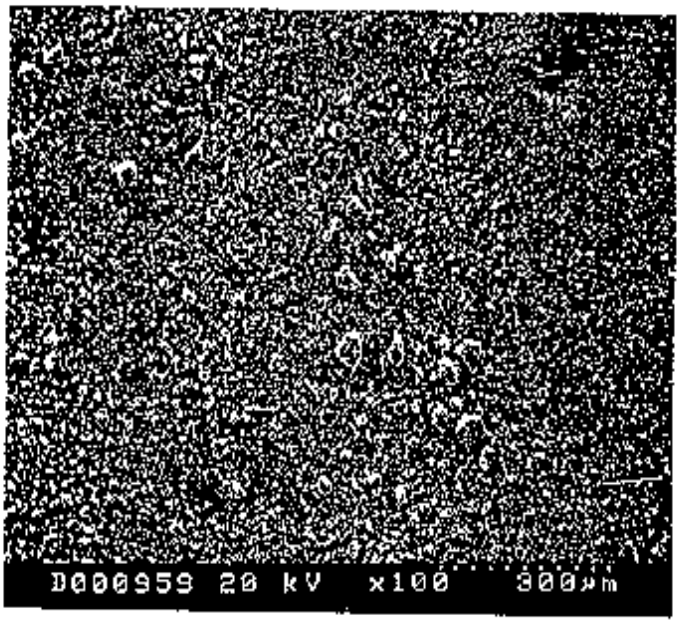

Fig. 5. SEM Scanning, the sample from the SBCR after synthesis 309 hrs.

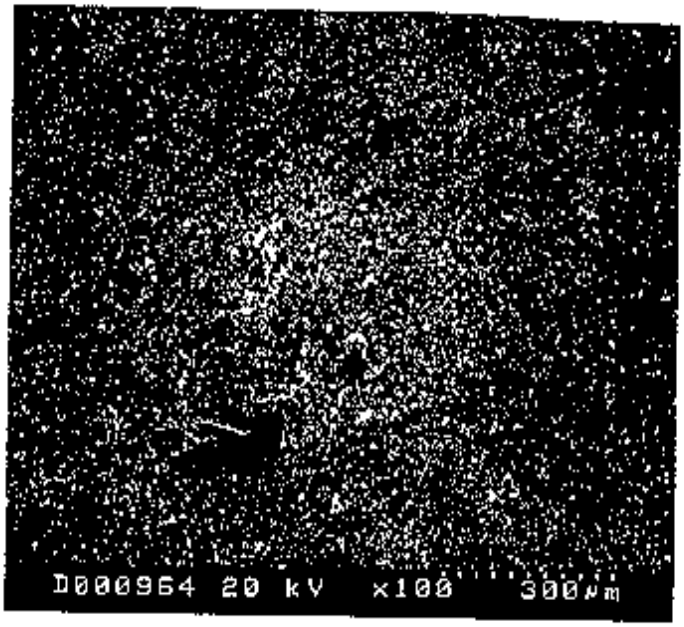

Fig. 6. SEM Scanning, the sample from the CSTR after synthesis 253 hrs.

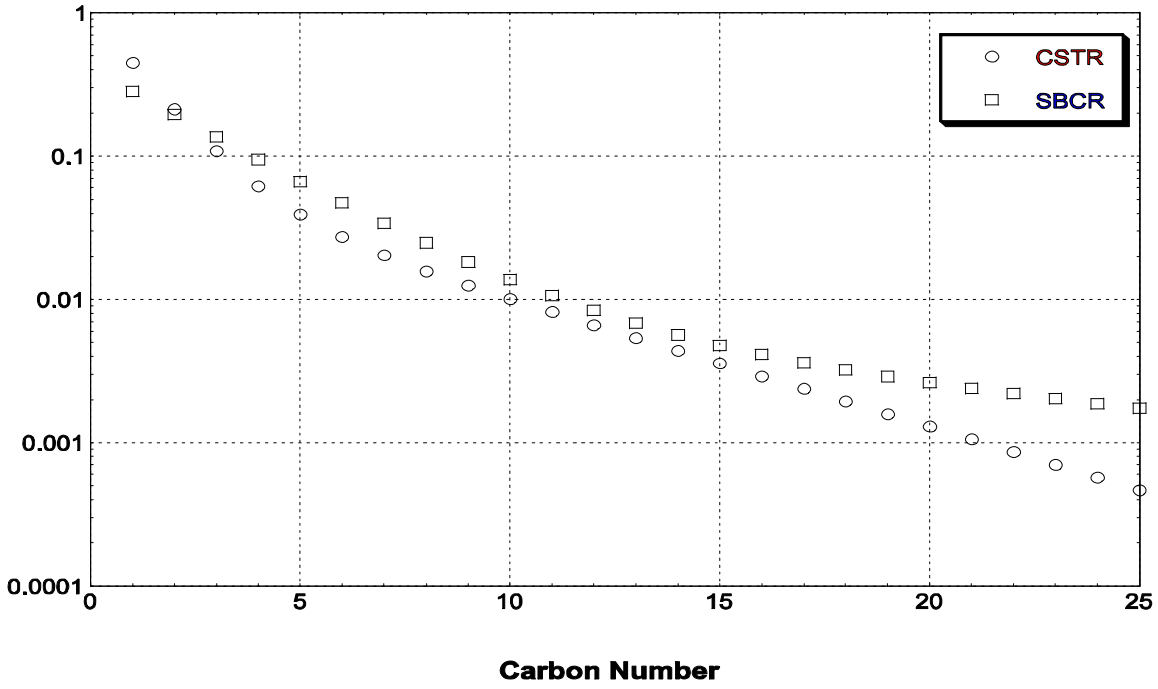

Figure 7. Comparison of the product distributions obtained in the CSTR and SBCR systems.

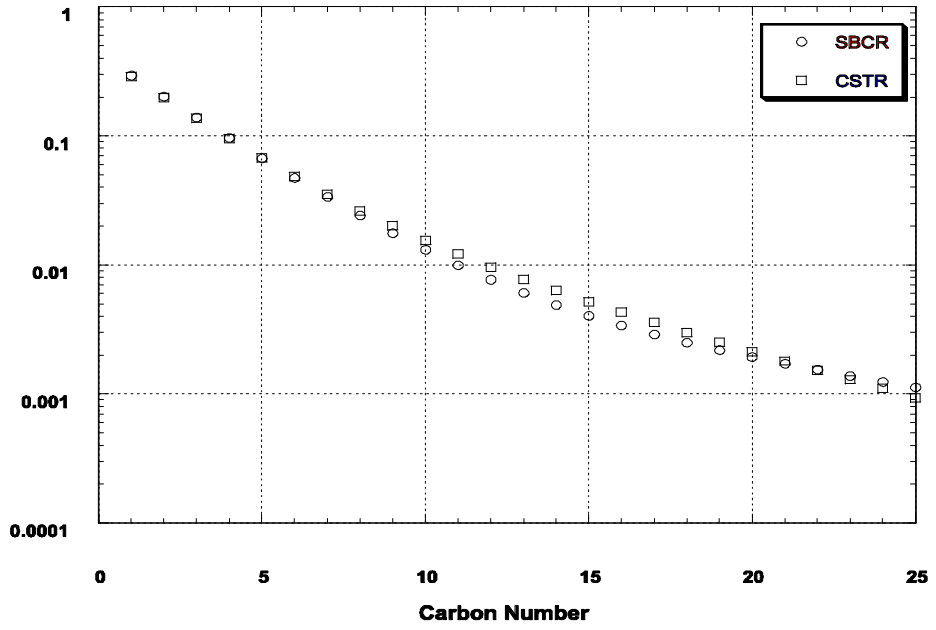

Figure 8. Comparison of the product distributions obtained in the CSTR and SBCR systems.

3.3.4 Additional Research

3.3.4.1. Verify the Quality of Data Obtained from the CSTRs.

The previously unexplained loss and re-establishment of activity has been found to be due to the lowering of the liquid level in the reactor. The conversion data shown in Figure 1 clearly show the loss of activity when rewax (wax from the reactor) was collected on a daily basis in the first 500 hours of the run. When the sampling of the rewax was stopped the activity recovered to approximately the initial level. Repeating this cycle produced a loss and gain of activity again. From these data, it was suggested that removing the reactor wax lowered the liquid level by physically removing the wax material and thus allowed more of the lighter material including the start-up oil to be removed from the reactor. After most of the start-up oil was removed and the reactor contained a sufficient amount of FTS wax, the reactor liquid level became stabilized and sampling of the reactor wax could be done without affecting the activity.

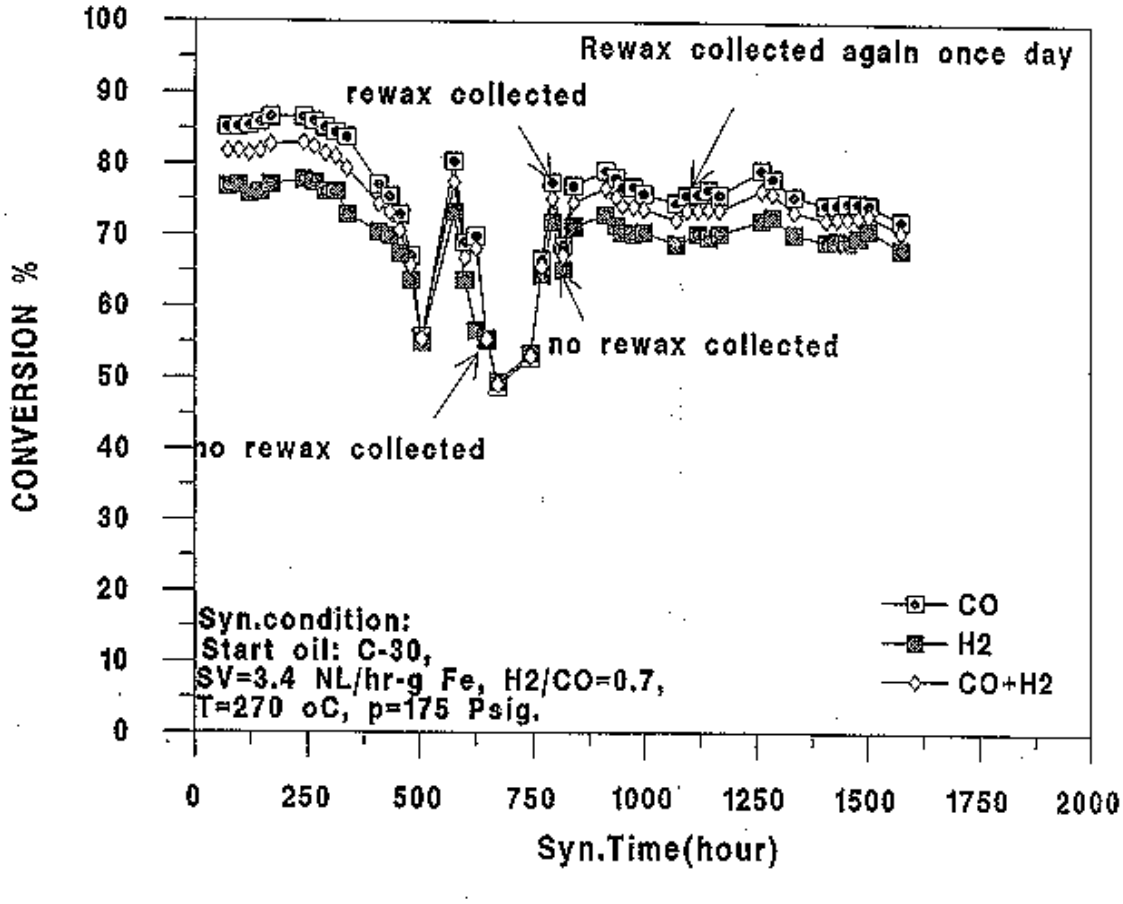

Figure 1. %CO conversion vs. Time on stream for runs LGX276-279 and LGX283 (4.4at%Al/3.0wt.%Cu/2.5-10.0wt.%K with T_{syn} = 230°C).

3.3.4.2 Comparison of Silica Based Hi-Alpha Catalyst at 230ºC and 250ºC With C-30 oil at a 5.0wt% Catalyst Loading

Two series of runs using five catalysts at synthesis temperatures of 250°C and 230°C were performed in the one liter continuously stirred tank reactors (CSTR). For all the runs, the reactor solvent was C-30 oil with a catalyst loading of 5.0wt%. The iron-based catalysts used in these tests had been co-precipitated so that the atomic ratio of silicon to silicon + iron ,i.e., [Si] /[Si+Fe], was at 0.044, or 4.4atomic(or mole)%. All the catalyst had been impregnated with copper such that the weight percentage of copper (relative to Fe) was at 3.0wt%Cu. Each of the five catalysts had a different amount of potassium present, specifically, 0.0wt%K, 2.5wt%K, 5.0wt%K, 7.5wt%K, and 10.0wt%K. As was the case for the copper, the potassium wt%'s are also relative to Fe. The list below shows the five catalysts tested and designates the atomic(mole) ratios of Si, Cu, and K, based on 100 atoms(moles) of Fe.

RJO228 (0.0wt%K) 100Fe:4.60Si/2.72Cu/0.00K

RJO229 (2.5wt%K) 100Fe:4.60Si/2.72Cu/3.66K

RJO230 (5.0wt%K) 100Fe:4.60Si/2.72Cu/7.52K

RJO231 (7.5wt%K) 100Fe:4.60Si/2.72Cu/11.58K

RJO232 (10.0wt%K) 100Fe:4.60Si/2.72Cu/15.87K

The first five runs performed were at 250°C and designated LGX236(0.0wt%K), LGX239(2.5wt%K), LGX240(5.0wt%K), LGX241(7.5wt%K), and LGX242(10.0wt%K). A comparison of the %CO conversion versus days on stream is shown in Figure 1. The second series of runs, specifically LGX235(0.0wt%K), LGX244(2.5wt%K), LGX245(5.0wt%K), LGX246(7.5wt%K), and LGX247(10.0wt%K), was performed at the

synthesis temperature of 230^{o}C and the %CO conversion versus days on stream is given in Figure 2.

In general, the catalysts performed better in regards to CO conversion at the synthesis temperature of 250^{o}C. At both temperatures, the catalyst run with the 5.0wt%K loading (RJO230) had the best CO conversion, while also for both temperatures, the 0.0wt%K loaded catalyst (RJO228) runs produced the poorest CO conversions. Again, for both temperatures, the catalysts at 2.5wt%K and 7.5wt%K (RJO229 and RJO231, respectively) produced comparable CO conversions, slightly lower than the CO conversion exhibited by the 5.0wt%K (RJO230) loaded catalyst runs, and the catalyst runs with the 10.0wt%K loadings were the fourth best with respect to the CO conversions, these also at both synthesis temperatures.

Note that for the 230^{o}C synthesis conditions (Figure 2), the CO conversions for the 2.5, 5.0, 7.5, and 10.0wt%K loaded catalysts all fell within a 20% band at the start of the run and improved to a band of 10% or less by the end of the run. This band of CO conversions was also observed for the runs performed at 250^{o}C, but only for the 2.5, 5.0, and 7.5wt%K loaded catalysts. The CO conversions were at ~80% for the 2.5, 5.0, and 7.5wt%K catalysts, while the CO conversion for the 10.0wt%K catalyst had a starting value of only ~50%. This justified another run using the 10.wt%K catalyst, RJO232, at the synthesis temperature of 250^{o}C. Run LGX250 was performed and the results of the CO conversion are given in Figure 3 and it can be seen that the %CO conversion did improve to values greater than 70%, with the exception in the drop of conversion starting at run hour 168 and reaching a minimum at ~run hour 264, which was found to be due to a faulty inert gas valve. After corrective action was taken in

regards to the valve, it can be seen the CO conversion did rebound and if these results were plotted with the 2.5, 5.0, and 7.5wt%K data, they would all fall into a band even tighter than that found with the 230^{o}C CO conversions (i.e., bandwidth of ~10% CO conversion for the 250^{o}C synthesis conditions).

Thus, in general, based on %CO conversions for these catalysts,

$$T_{syn} = 250^{o}C \; > \; T_{syn} = 230^{o}C$$

$$5.0wt\%K \; > \; 2.5wt\%K \; - \; 7.5wt\%K \; > \; 10.0wt\%K \; > \; 0.0wt\%K.$$

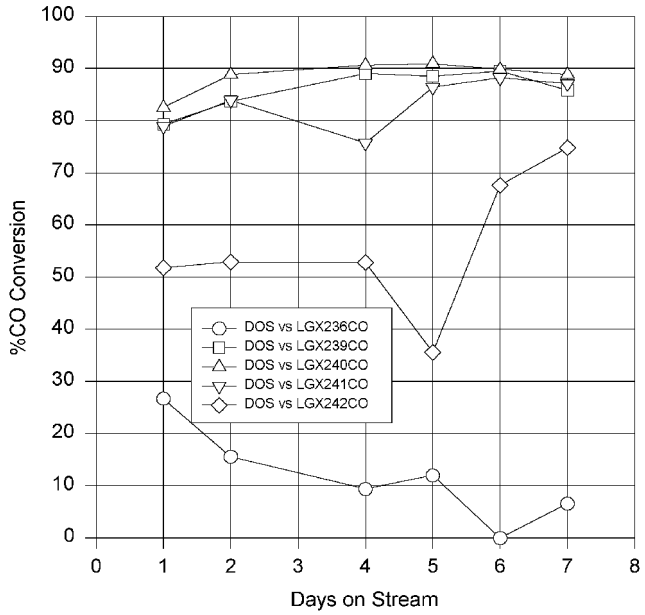

Figure 1. %CO Conversion vs Days on Stream for Runs LGX239-242 @ 250°C.

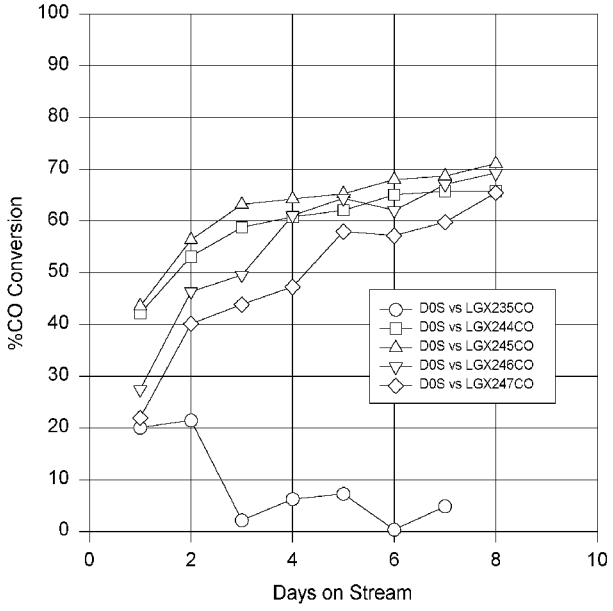

Figure 2. %CO Conversion vs Days on Stream for Runs LGX244-247 @ 230°C.

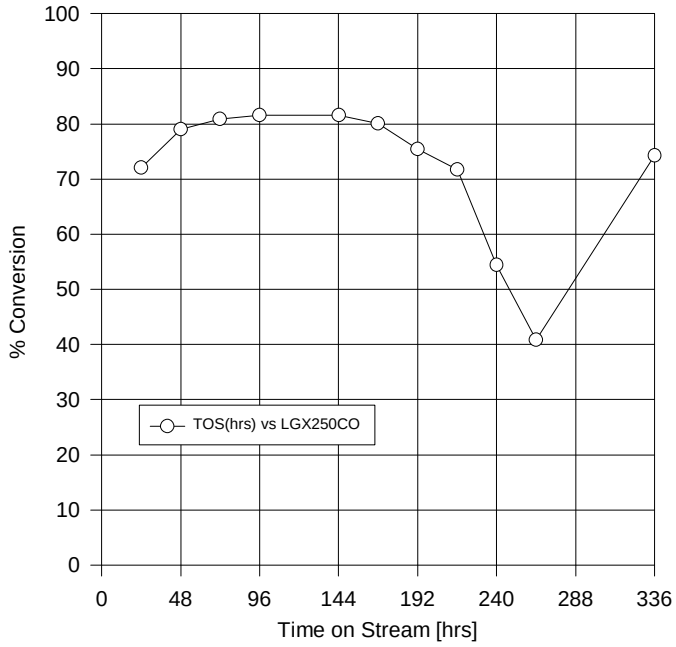

Figure 3. %CO Conversion vs Time on Stream for Run $LGX250_{R7}$ with T_{syn} @ 250°C.

3.3.4.3 Comparison of Reactor Solvents (C-30 oil vs PW_R3000 Wax)

This series of runs involves comparing the performance of a high molecular weight polyethylene wax, Polywax PW_R3000, for use as a reactor solvent, to that of the typically used C-30 oil. For this comparison, the well studied 4.4Si150 cyclone catalyst was used (4.4atomic%Si and 1.0atomic%K, both relative to Fe, i.e., [Si(or K)]/[Si(or K) + Fe]). 32.22g of the catalyst was used in all of the runs, and for the C-30 oil application the catalyst loading was at 10.0wt%, while for the PW_R3000 wax a 11.1wt% catalyst loading was used. This difference in weight% loadings stemmed from attempts to establish equivalent volumes of solvent during the initial loading of the continuously stirred tank reactors (CSTR). These runs were modeled after previous runs that used the C-30 oil as a solvent, which were normally loaded at a 10.0wt% catalyst loading, specifically 32.22g of catalyst along with 290.0g of C-30 start up oil/solvent. With the density of the C-30 oil at ~0.80g/cm^3, this yielded a start up solvent volume of 362.5cm^3, thus the target volume for the PW_R3000 wax was 362.5cm^3. As the PW_R3000 wax is a solid at ambient temperatures, it was heated until it melted, i.e., at ~130^{o}C, at which point the density was determined to be 0.71g/cm^3. Thus at 130^{o}C, it requires 257.4g of PW_R3000 wax to obtain a volume of 362.5cm^3. Note that the density of the C-30 oil should have been determined at a temperature of 130^{o}C, instead of at ambient temperature (at a later date the densities and specific volumes(cm^3/g) of the PW_R3000 and C-30 oil were determined up to 210^{o}C, as well as the densities and specific volumes for the C-28 (octacosane) and the PW_R2000 high molecular weight polyethylene wax, and that algorithms were then developed for the densities and specific volumes as a function of temperature from ambient through 210^{o}C).

Run LGX248 was performed as the baseline case with the C-30 oil and the %CO conversion results are given in Figure 1. The %CO conversion results for the PW_R3000 run, LGX249, are shown in Figure 2. Both reactor solvents produced CO conversions of 80-90%, until gas feed tube pluggages occurred (at ~run hour 550 for the C-30 oil and at ~run hour 460 for the PW_R3000 solvent). These two runs showed the feasibility of using the PW_R3000 polyethylene wax as a reactor solvent. It was then decided to repeat the PW_R3000 run to confirm the reproducibility of the results obtained in run LGX249. Run LGX251 was started and it was observed that the pretreatment pressure had climbed to ~40psig (pretreatment is to be carried out for 24 hours at 0psig), but aborted after two days at synthesis conditions. Thus run LGX252 was initiated, but it too was aborted after three days at synthesis conditions, due to a pressure of ~100psig during the pretreatment period. It was discovered that the reason for the elevated pressures during the pretreatment period was caused by the restriction of the gas out and due to blinding off and/or plugging in the 7F-wax filter and the wax line out of the reactor, which functions as a continuous line out for the gas products produced during the FTS reaction. It was found that the restrictions were caused by the condensing and solidifying of the PW_R3000 polywax (melting point at ~130^oC) which possibly had been entrained in the gas out of the reactor via the wax line out. To rectify this problem, the wax filter was fitted with a thermocouple and an additional heat tape was installed on the wax line, as well as increasing the amount of insulation on the wax line out (this was also done for the rewax line out to allow for the removal of the reactor liquid products). This allowed for the monitoring and adjustment, if necessary, of the temperature of the 7F-wax filter and wax line. After these modifications, run LGX253

was started and the pretreatment period was successfully completed at the desired pressure of 0psig. Figure 3 gives the %CO conversions for runs LGX251, LGX252, and LGX253 and shows an inverse relationship with %CO conversion and pretreatment pressures. Note that the %CO conversion for run LGX253 agrees rather well to that of the %CO conversion for run LGX249. That is, for run LGX253 the CO conversion starts at ~90% and is maintained at ~85% or greater up through run hour 500. It was thus shown that the PW_R3000 polyethylene wax could be used as a suitable reactor solvent for the FTS synthesis.

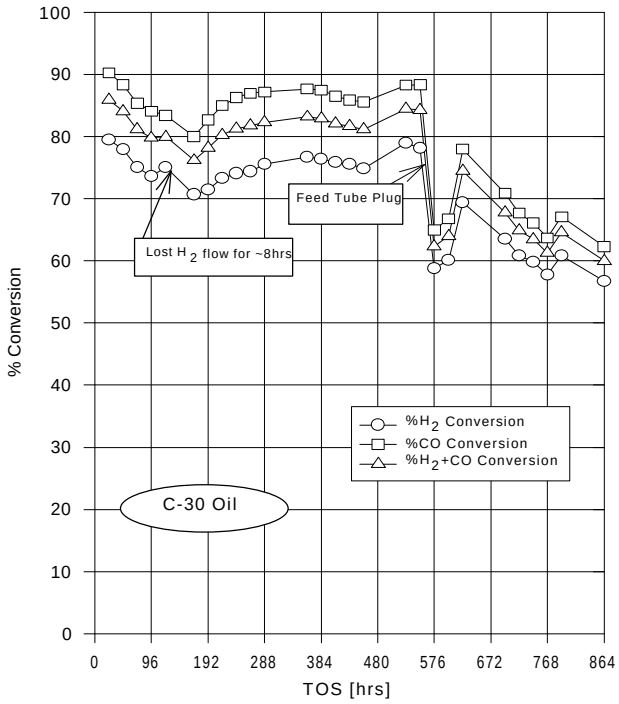

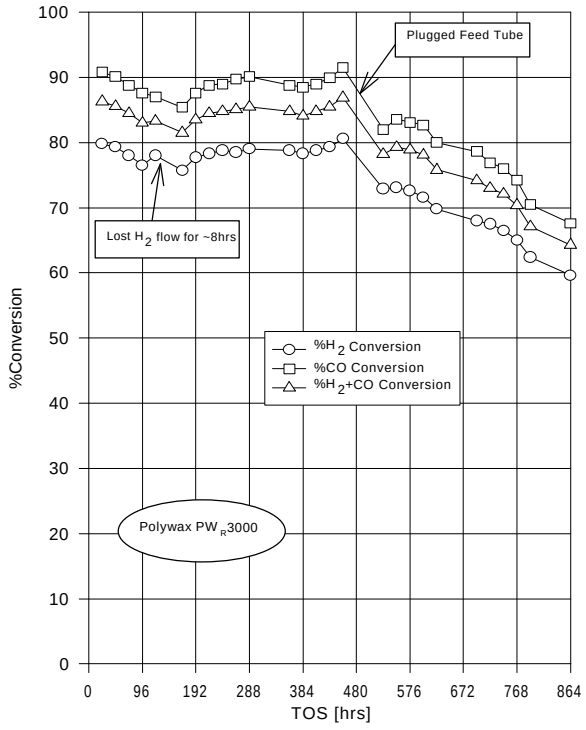

Figure 1. %CO Conversion vs Time on Stream [TOS] for Run $LGX248_{R1.}$

Figure 2. %CO Conversion vs Time on Stream for $LGX249_{R2.}$

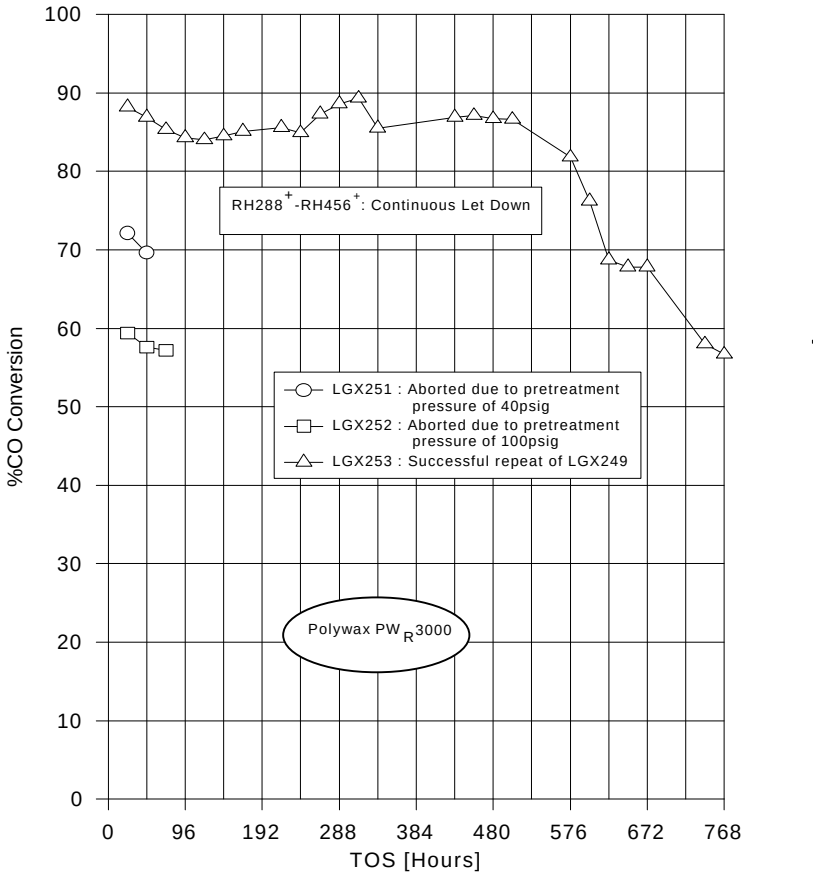

Figure 3. %CO Conversion vs Time on Stream for Runs LGX251-253.

3.3.4.4 Comparison of Alumina and Silica Based High-Alpha Catalyst at 230°C and 250°C

Once it was shown that the Polywax PW_R3000 was a suitable reactor solvent, five Fe-based/silica catalysts and five Fe-based/alumina catalysts were tested at both 250°C and 230°C for their conversion performance in the one liter continuously stirred tank reactors (CSTR). The ten catalysts tested at the two synthesis temperatures are referred to as the hi-alpha catalyst studies. The alumina and silica series catalysts were both co-precipitated with the iron such that atomic ratios of aluminum(silicon) relative to Fe was 0.044 or, 4.4atomic% Al(Si). All ten catalysts were impregnated with copper so that the copper was present at a 3.0wt%Cu, relative to iron. Both the silica and alumina series Fe-based catalysts had varying amounts of potassium, specifically 0.0wt%K, 2.5wt%K, 5.0wt%K, 7.5wt%K, and 10.0wt%K, relative to Fe. The following list identifies the catalyst and gives an atomic(mole) representation of the Si/Al, Cu, and K, based on 100 atoms/moles of Fe.

Silica Series:

RJO228(0.0wt%K) 100Fe:4.60Si/2.72Cu/0.00K

RJO229(2.5wt%K) 100Fe:4.60Si/2.72Cu/3.66K

RJO230(5.0wt%K) 100Fe:4.60Si/2.72Cu/7.52K

RJO231(7.5wt%K) 100Fe:4.60Si/2.72Cu/11.58K

RJO232(10.0wt%K) 100Fe:4.60Si/2.72Cu/15.87K

Alumina Series:

RJO250(0.0wt%K) 100Fe:4.60Al/2.72Cu/0.00K

RJO251(2.5wt%K) 100Fe:4.60Al/2.72Cu/3.66K

RJO252(5.0wt%K) 100Fe:4.60Al/2.72Cu/7.52K

RJO254(7.5wt%K) 100Fe:4.60Al/2.72Cu/11.58K

RJO255(10.0wt%K) 100Fe:4.60Al/2.72Cu/15.87K

The silica series catalysts at a synthesis temperature of 250^{o}C were tested first and Figure 1 shows the %CO conversion versus time on stream. These runs were designated as LGX254-258 and used the RJO232, RJO231, RJO230, RJO229, and RJO228 catalyst, respectively. The %CO conversion for the silica series at 230^{o}C is presented in Figure 2 (runs LGX259-263 utilizing the RJO232-228, respectively).

For the alumina series at 250^{o}C, the CO conversion is given in Figure 3 (runs LGX267-271 utilizing the RJO250, RJO251, RJO252, RJO254, and RJO255 catalysts, respectively) while Figure 4 shows the %CO conversion for alumina at 230^{o}C (runs LGX276-279 using the RJO251, RJO252, RJO254, and RJO255 catalyst, respectively, and run LGX283 using the RJO252 catalyst). Note that for the 230^{o}C alumina series that the catalyst with 0.0wt%K was not tested and that run LGX283 is a repeat run of LGX277 (the 5.0wt%K catalyst). Also note for runs LGX276, LGX278, and LGX279, at ~run hour 183, a re-pretreatment of the catalysts with only CO gas was performed, which did not appear to help.

In general, the following trends were observed for the %CO conversion,

L For Both 230^{o}C and 250^{o}C Synthesis Temperatures

Silica Series Better Than Alumina Series

L For Both Alumina and Silica Series

%CO Conversions Better at 250^{o}C than at 230^{o}C

L For The Alumina Series

230°C : 2.5wt%K . 5.0wt% > 7.5wt%K > 10.0wt%K

250°C : 2.5wt%K >> 5.0wt%K > 7.5wt%K >> 10.0wt%K >0.0wt%K

L For The Silica Series

230°C : 7.5wt%K $ 5.0wt% $ 2.5wt%K >> 10.0wt%K > 0.0wt%K

250°C : 2.5wt%K $ 5.0wt%K $ 7.5wt%K >> 10.0wt%K >0.0wt%K

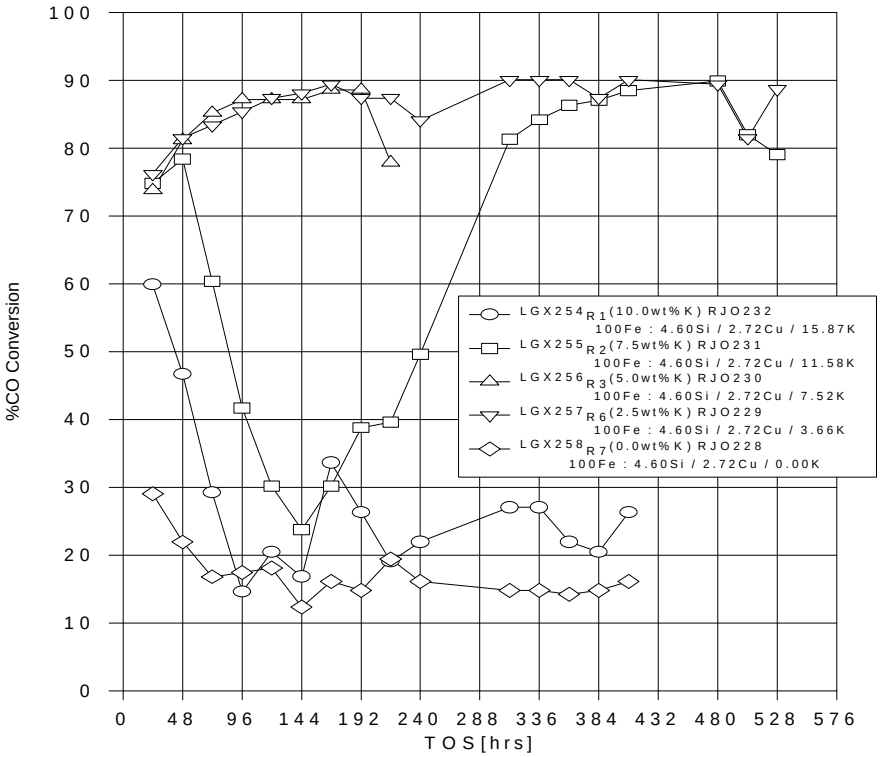

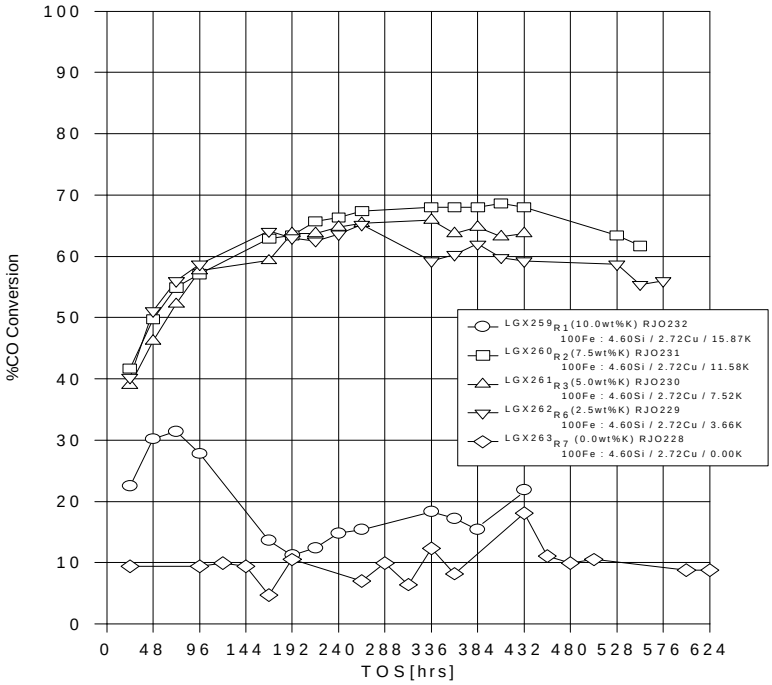

Figure 1. %CO Conversion vs Time on Stream for Runs LGX254-258.

Figure 2. %CO Conversion vs Time on Stream for Runs LGX259-263.

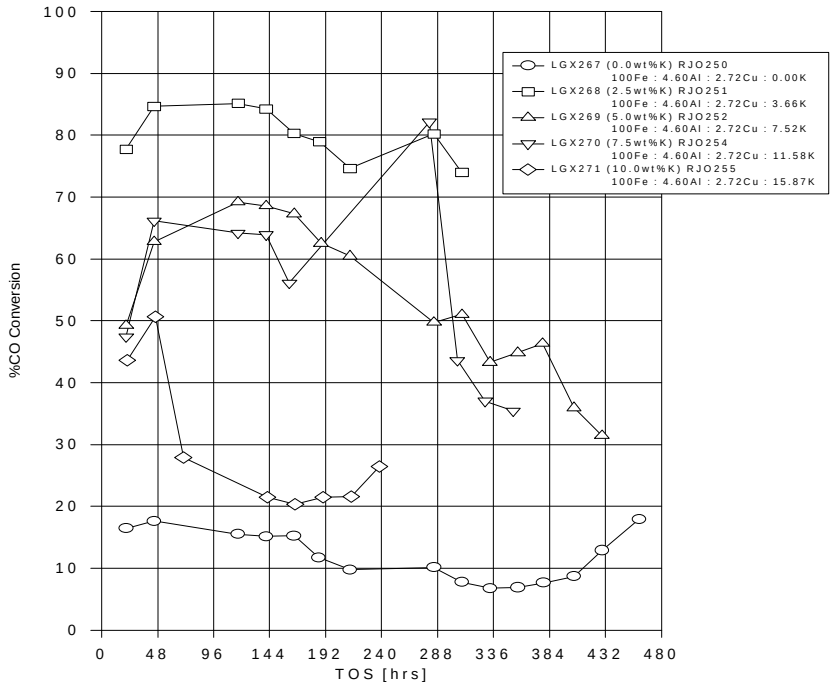

Figure 3. %CO Conversion vs Time on Stream for Runs LGX267-271.

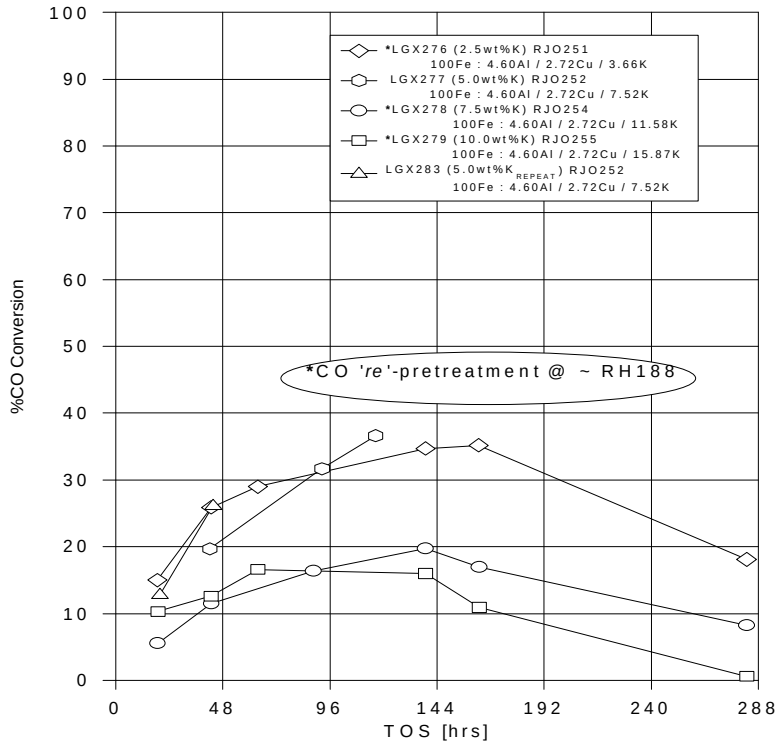

Figure 4. %CO Conversion vs Time on Stream for Runs LGX276-279 & LGX283.

3.3.4.5 High-Aluminas

A series of runs was performed using catalyst that contained varying amounts of alumina as a support. The alumina, Al_2O_3, varied nominally from ~10wt% to ~53wt% for the four catalysts used in this series of runs and each catalyst had different amounts of Al, Cu, and K. The reactors had a 10.0wt% catalyst loading in the PW_R3000 polyethylene wax reactor solvent and a synthesis temperature of 270°C was used for these runs. The following list identifies the catalyst and gives an atomic(mole) representation of the Al, Cu, and K, based on 100 atoms/moles of Fe.

a. RJO274 (10.15wt%Al_2O_3 & 52.69wt%Fe), 100Fe:21.1Al/2.73Cu/11.8K

b. RJO275 (17.74wt%Al_2O_3 & 46.93wt%Fe), 100Fe:41.4Al/2.72Cu/11.6K

c. RJO276 (37.58wt%Al_2O_3 & 35.19wt%Fe), 100Fe:117Al/2.72Cu/11.6K

d. RJO277 (53.13wt%Al_2O_3 & 23.47wt%Fe), 100Fe:248Al/2.74Cu/11.6K

Figure 1 shows the %CO conversion for runs LGX284, LGX285', LGX286 and LGX287, which used catalysts RJO274, RJO275, RJO276, and RJO277, respectively.

Run LGX284 was aborted after 144 hours on stream due to the inability to withdraw liquid reactor product through the 2F-rewax filter, which is located inside the reactor and submerged in the catalyst/wax reactor slurry at start up . It is not certain if the 2F-rewax filter for LGX284 was blinded off from previous runs or if the tubing run from the reactor to the rewax trap (vessel for the collection of liquid reactor product) was plugged, or a combination of both. Modifications to the tubing run from the reactor to the rewax trap have been implemented to allow for a repeat of this run.

Run LGX285' was a repeat run of LGX285, as LGX285 was aborted during the 24 hour pretreatment period due to the reactor pressure rising to ~400psig (as the pretreatment pressures are fixed at a nominal 0psig).

Although there was an inability to remove reactor product via the rewax filter for run LGX284, difficulties in catalyst/wax separation and reactor product removal was not encountered for runs LGX285'-287. In fact, there was no plugging or blinding off of the rewax filters over the course of these runs and the reactor product removed through the rewax filter was visibly free from catalyst contamination. The increased amounts of Al_2O_3 and the lower Fe content associated with these catalysts are thought to be mainly responsible for the ease of reactor product removal through the rewax filter. This, along with the fact that there were problems associated with the mass balance resulted in removal of too much reactor product via the rewax filter for runs LGX285'-287. Specifically, after the completion of these runs, the reactor contents were collected and measured and deficits of 84g 186g, and 213g from the initial catalyst/PW_R3000 wax loading of 344.0g was found for runs LGX285', LGX286, and LGX287, respectively. In effect, this results in higher percentage catalyst loadings for these runs, as well as a reduced residence time in the reactor slurry, but the effect on CO conversion is not well understood.

The previously mentioned problems present some difficulty in attempting to compare this series of runs, but with respect to the data for %CO conversion over time, the best results were obtained using the RJO276 catalyst (run LGX286) as CO conversions were maintained at levels of 70-80%. The CO conversion for runs LGX287(RJO277) and LGX285(RJO275) were comparable to one another for run

hours 100-336, but both had CO conversions of 40% at run hour 336 while for run LGX286, the CO conversion was at +70%.

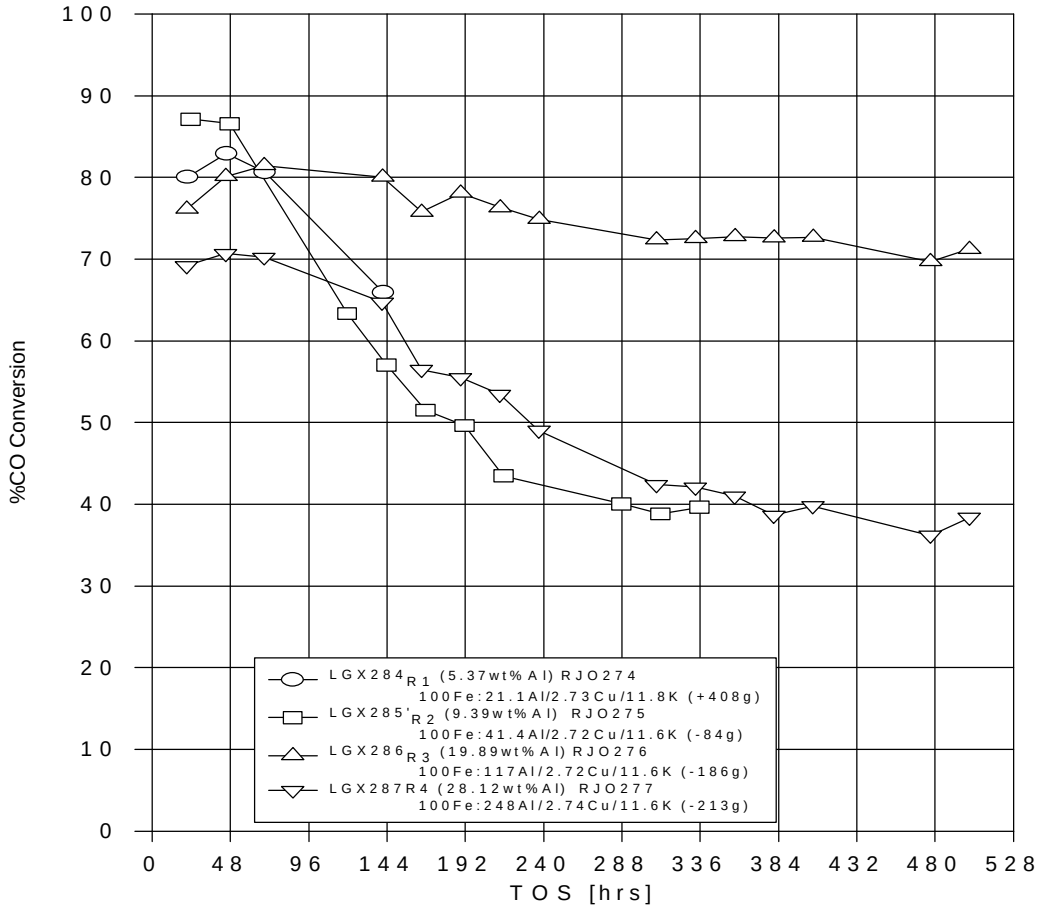

Figure 1. %CO Conversion vs Time on Stream for Runs LGX284-287.

3.3.4.6 Reactor Wax Withdrawal Modifications

In the past, reactor product and catalyst separation has been accomplished using a ½µ-grade Mott Metallurgical Corporation sintered stainless steel filter (½"OD and **f** " in length for a surface area of 0.0109ft^2). This filter was positioned so that when it is installed to the reactor head that it's bottom surface is ~3" down from the upper internal surface of the head of the one-liter CSTR, which has an internal diameter of 3" and an internal height of 10¼", with a hemispherical bottom and a cylindrical shaped top. Since using the Polywax PW$_R$3000 hi-molecular weight wax as a reactor solvent (LGX249 first PW$_R$3000 run) problems have persisted in that the filter was increasingly being blinded off, resulting in an increasing inability to remove the reactor product (i.e., the heavy liquid product at reactor temperature and pressure referred to as 'rewax'), allowing the reactor to fill up, ultimately resulting in aborting the runs. Potential solutions to this problem have been suggested and/or implemented.

The first of the solutions which has been incorporated, was to lower the filter to insure that it is completely immersed in the wax/catalyst slurry. The thinking here is that with the filter immersed in the slurry, it would be out of the gas/froth space (which may or may not contain smaller ebullated catalyst particles) and would be continually washed by the slurry and eliminate or at least minimize the blinding off of the filter. To accomplish this end, the filter was lowered to an elevation so that it's bottom surface is ~7" below the upper surface of the reactor (specifically, the bottom of the filter is positioned ~¼" above the upper surface of the gaspersator blades). At this elevation there is no doubt that the filter is covered by the slurry for the current loadings of PW$_R$3000 polywax and hi-alpha catalysts. The first run using this lowered filter

configuration was LGX263 (100Fe:4.60Si/2.72Cu/0.00K) and as can be seen in Figure 1 (i.e., 'Rewax Flux Density vs Sample Day for Run LGX263') problems were encountered in attempting to remove the rewax for the first 12 sample days. It was found that this inability to remove the rewax during this period was not due to blinding off of the filter, but instead by the line from the reactor head to the rewax trap being heated at a too low of a temperature, specifically lower than the melting point of the reactor product (note that the melting point of the Polywax PW_R3000 is ~130^oC at ambient conditions). Once additional heat tracing was applied to the line, rewax removal was then permitted as can be seen for sample days 13-17. The rewax collected during this run showed no visible traces of iron. The next run utilizing the lowered filter was run LGX266 (100Fe:4.60Si/2.72Cu/7.52K) and from Figure 2, the performance of the filter, as measured by flux density (gpm/ft^2), can be seen in general to decrease with time. The implication here is perhaps there is increased blinding of the filter with subsequent rewax letdown periods. As in run LGX263, the rewax product was visibly free of iron, and in fact LGX266-005 and LGX266-007 each were tested for iron content and tested at 0.03wt% Fe and 0.01wt% Fe, respectively. Also, note that on this figure there is reference to the Regimesh Filter that has a flux density of 0.13-0.20gpm/ft^2, surface area of 0.175ft^2, and a porosity of 18µ (corresponding to ~16 times the area and an increase of 36 times the porosity of the Mott SS-filter that we were using). With the maximum ?p across the Mott SS-filter at 75psid and the ?p across the Regimesh filter not known, there is difficulty in making a comparison of the performance of the filters, but from liquid flow characteristic graphs supplied with the Mott product catalog, if the µ-grade is increased from ½µ to 20 µ (with ?p and viscosity held

constant), the flux density (gpm/ft^2) increases ~100-fold. However, if the ?p is varied and the µ-grade and viscosity held constant, there seems to be a linear relationship with flux density.

After the completion of run LGX266, an attempt was made to test out a 2µ-grade Mott SS-filter, the second of the modifications to improve the rewax removal. This was accomplished by opening up the reactor once it had cooled to 130^{o}C and replacing the ½µ-filter with a 2µ-grade filter. Comparing the liquid flow media charts in the Mott catalog for the ½µ and 2µ filters, at equal ?p's and viscosities (for ?p's of 100, 60, 10, 6, and 1 psid and viscosities of 500, 100, 20, and 5cP's, as well as for water), the average flux density increased by a factor of seven. Once the reactor was back to normal operating conditions, the rewax valve was opened for a rewax letdown period of one hour and unfortunately ~300g of reactor contents were removed. The collected reactor product did in fact have catalyst present, but at the time , it was not known if;

1) the wax/catalyst leaked through an improperly tightened filter fitting,
2) had it passed straight through the 2µ-grade filter,
3) was due to the fact that the level had dropped so much that the filter was exposed to the gas/froth space that may contain finely ebullated catalyst particles,

or possibly a combination of the above.

Since the 2µ-grade filter test was inconclusive for run LGX266, after the completion of run LGX268 (100Fe:4.60Al/2.72Cu/3.66K) which also used a ½µ-filter, another test of the 2µ-grade filter was attempted. The results from this series of rewax letdowns was more promising in that the rewax product collected appeared catalyst free

and thus was justification for the installation of a 2µ-grade filter prior to the start of a run. Subsequent iron based catalyst FTS runs have incorporated the use of the 2µ-grade rewax filter.

The third of the potential solutions to address the problem of rewax removal and reactor overfilling was to develop a mass balance for the system to allow for the prediction of the amount of rewax to be removed so as to maintain a constant reactor inventory. Simply stated,

Reactor Accumulation(g) = Gas_{in}(g) - Gas_{out}(g) - Trap $Products_{out}$(g).

Two versions of this mass balance were developed. The first just accounts for the mass of the gas out based solely on the Carle Series 400 AGC chromatographic data and is referred to the simplified mass balance , while the second, and certainly more sophisticated, utilizes chromatographic data from the HP-5790 as well as the AGC data (this second mass balance was developed by Scott Lambert and is referred to as Scott's mass balance). Both mass balance methods also account for the liquid and solid products out, i.e., water, oil, wax, and rewax. By adding either reactor accumulation terms to the starting weight of the wax/catalyst, a predicted reactor inventory is determined. Figure 3 shows run LGX267 (100Fe:4.60Al/2.72Cu/0.00K) using Scott's mass balance which predicted that there was ~127g remaining in the reactor, while in fact the reactor contents were measured at 92g after the completion of the run. Note that the dashed line across the graph indicates the starting weight of the of the reactor solvent and catalyst in the reactor, which was 318.68g. Figure 4 is for run LGX269 (100Fe:4.60Al/2.72Cu/7.52K), which also had a staring weight of 318.68g. Both the simplified and Scott's mass balances are presented here and up until run hour

144, agree rather well with one another. After run hour 144 there is a divergence of predicted reactor contents in which there is an approximate 50g difference in values. At the end of the run the disagreement between the two mass balance methods was at ~40g (346g for the simplified and 386 for Scott's), but the actual measured amount of wax/catalyst in the reactor for this run was at 598g, 55% more than what Scott's mass balance predicts and 73% more than the simplified mass balance prediction. These discreprancies have yet to be resolved. Figure 5 shows the results of the two mass balance methods applied to run LGX270 (100Fe:4.60Al/2.72Cu/11.58K). For this run the predicted reactor contents agree to within ~20g of one another (384.8g for the simplified and 363.2g for Scott's method, within 6% of each other), and both prediction models compare well to the final measured wax/catalyst weight of 310g (24% high for the simplified method and 17% high for Scott's method).

Figures 6 and 7 are plots of the 'Net Reactor Accumulation' (i.e., gain/loss from initial starting weight of 344.0g of catalyst/solvent) for runs LGX284 and LGX285', respectively. For run LGX284 (Figure 6), the simplified mass balance was better (95% of the actual/measured value of +408g) at predicting the reactor accumulation than was Scott's mass balance (121% of actual/measured value). The opposite is true for the net reactor gain/loss for run LGX285' (Figure 7). Scott's method predicted a loss of 35g from the starting weight of 344.0g (within 49g of the actual/measured loss of 84g), while the simplified mass balance predicted a gain of 130g. Referring to Figure 7, it can be seen that the two prediction methods agreed with one another to within ~50g, up through run hour 360, but then they diverged to predicting values in disagreement of

165g for the end of the run. It is unclear as to what caused this divergence, when they had agreed so well with one another.

The problems concerning the disagreement with the two methods are presently being addressed, as this is potentially a very useful technique for maintaining and predicting reactor inventory, as well as predicting the amount of rewax to be removed from the reactor on a daily basis.

A fourth solution has been incorporated in attempts to aid in the removal of the rewax product. In the past, rewax letdown was accomplished by opening the rewax letdown valve while closing the wax letdown valve. With the wax valve closed and the rewax filter submerged, there is no discharge path for the gas (unless the reactor's contents are at a level lower than the rewax filter) to exit the reactor and subsequently the reactor pressure climbs. To eliminate excessive increases in reactor pressure, the wax valve would be periodically cracked to vent excess gas in the reactor. This required constant monitoring of reactor pressure and as a result of pressure variations, the FTS reactions were probably affected. With both the wax and the rewax valves open, an exhaust path for the gas is available, as is a path for the removal of reactor product. Although this letdown procedure does not allow for as large of a ?p across the rewax filter as that which occurs when using the former (with wax valve closed), it has been shown that there was sufficient ?p to let down rewax through the filter. Not only was it possible to remove reactor product using this method, but the rewax collected was , visibly clean, which is also a testament to the use of the 2.0µ-rewax filter. The only difficulties encountered in using this method has been in the prediction of the amount that can be removed over a given period of time.

To enhance the predictability in removing a desired amount of rewax (as determined from the mass balance techniques) a more recent modification of the rewax letdown procedure incorporates the use of Boyle's law to attempt rewax removal. As the rewax sample bomb can be totally isolated from the reactor system without interruption to reactor operation, and the fact that volume of the rewax receiver is known and that the rewax sample receiver can be independently charged to any pressure, we should be able to predict at what pressure to charge the empty rewax bomb so as to allow for a volume of rewax to be collected. As the rewax is collected, the bomb pressure should increase until it equilibrates to that of the reactor. The verdict is still out on this method of predicting specific amounts of rewax removal, but appears to be promising.

A final method for addressing the problem of reactor rewax removal and that of avoiding reactor overfilling involves the installation of a liquid back flush bomb for the rewax filter. Presently, the rewax bomb itself can be used as a gas charging vessel by isolating the bomb by closing the rewax letdown valve and the equalizing valve between the rewax and wax traps. An inert gas can then be introduced into the rewax bomb at a pressure higher than that of the reactor and the rewax valve can then be opened and the gas pressure can force the hydraulic column of rewax (contained in the rewax line and the rewax filter) to back flush the filter. Although this capability does exist, it is felt that there is simply not enough rewax present in the line and filter to perform an adequate backflush as well as the fact that the rewax letdown valve is of the flow control/throttling type of valve and does not allow for an instantaneous surge of higher pressure gas to back flush the rewax material such as a ball valve would offer. With a bomb installed on the branch of a tee (with a ball valve separating the bomb and the branch of the tee) and the run of the tee plumbed between the reactor head rewax

discharge port and the existing rewax valve, liquids such as C-30 oil could be used to facilitate this back flush.

The importance of cleaning the filter cannot be understated, and can be demonstrated by returning to Figure 2 of Section 3.3.7.6, where it is seen that as time progresses, the flux density decreases, requiring longer periods of letdown time to remove the desired amounts of rewax, which are determined by using either of the reactor mass balance techniques.

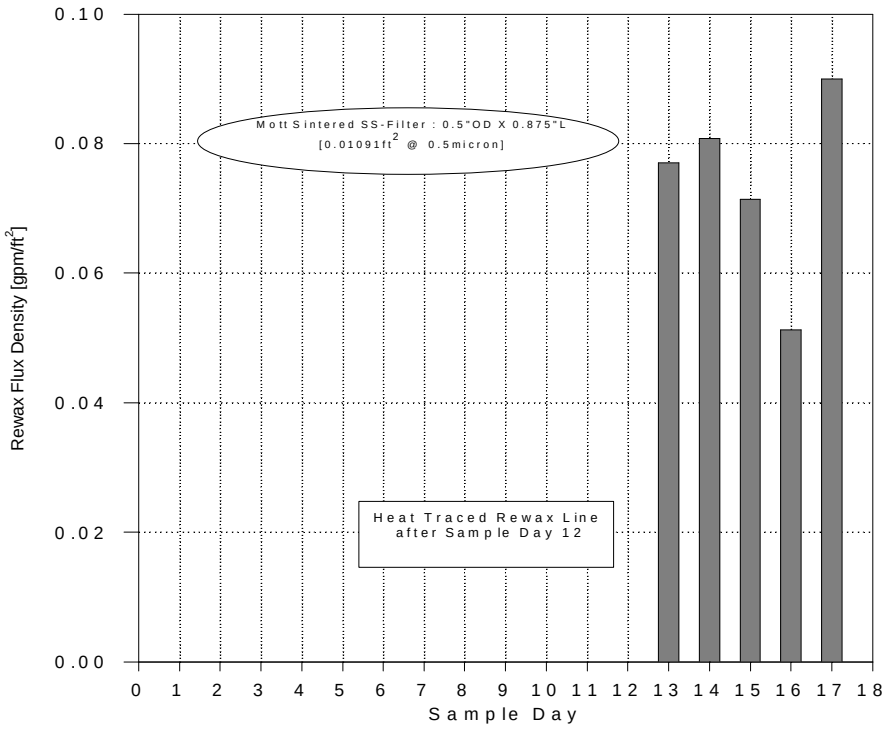

Figure 1. Rewax Flux Density vs Sample Day for Run $LGX263_{R7}$.

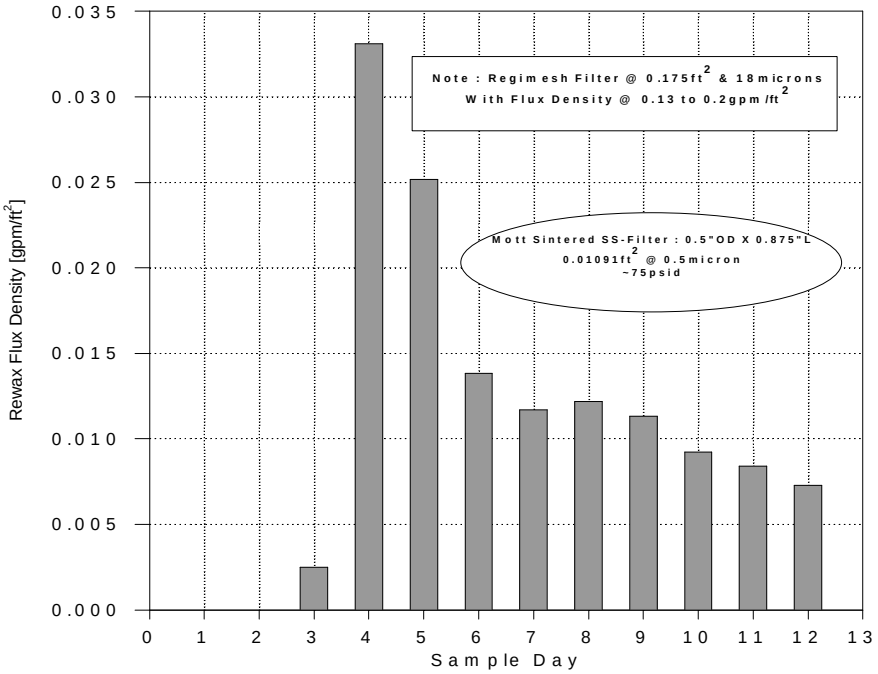

Figure 2. Rewax Flux Density vs Sample Day for Run $LGX266_{R7}$.

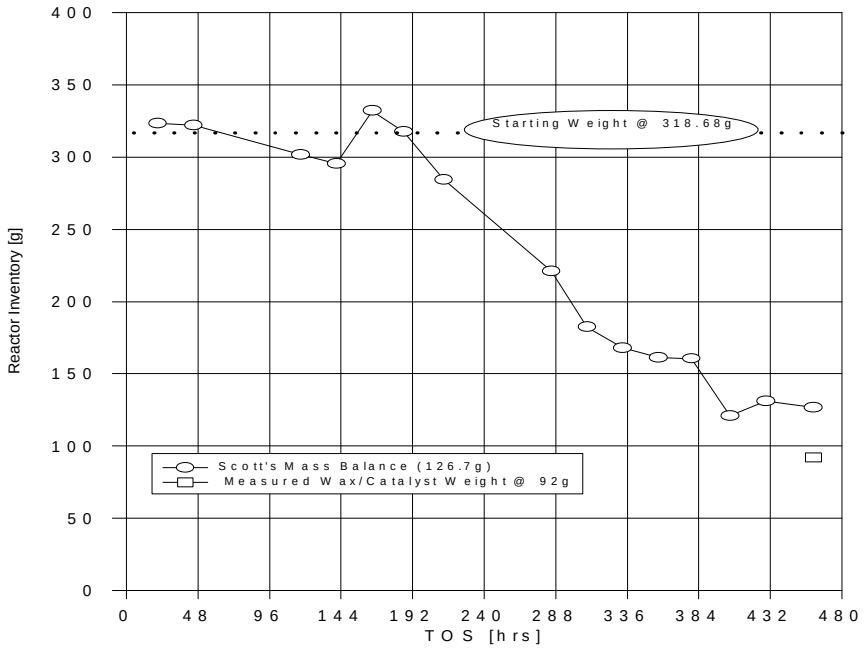

Figure 3. Predicted Reactor Inventory vs Time on Stream for RunLGX267$_{R1}$.

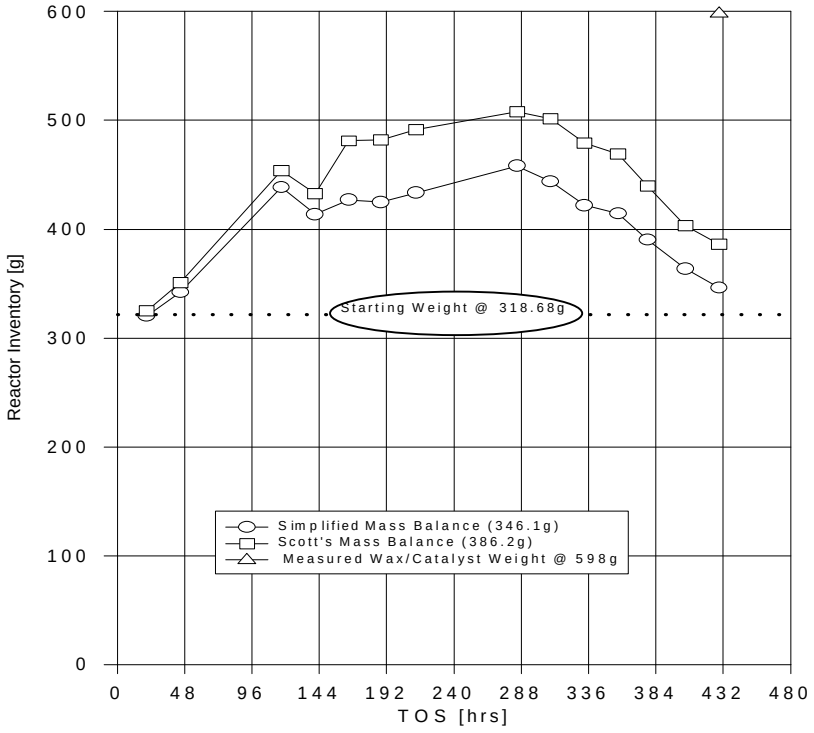

Figure 4. Predicted Reactor Inventory vs Time on Stream for RunLGX269$_{R3}$.

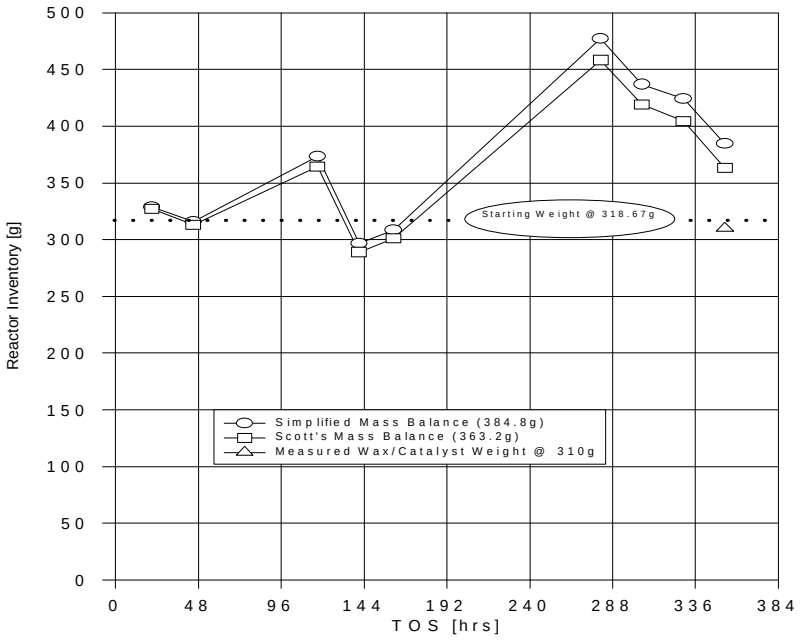

Figure 5. Predicted Reactor Inventory vs Time on Stream for Run LGX270$_{R4}$.

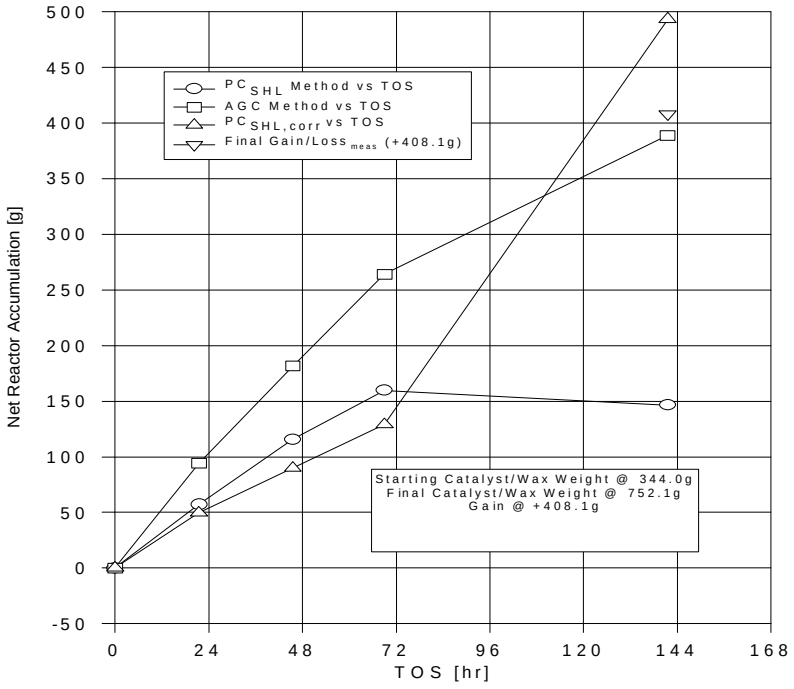

Figure 6. Net Reactor Accumulation vs Time on Stream for Run LGX284.

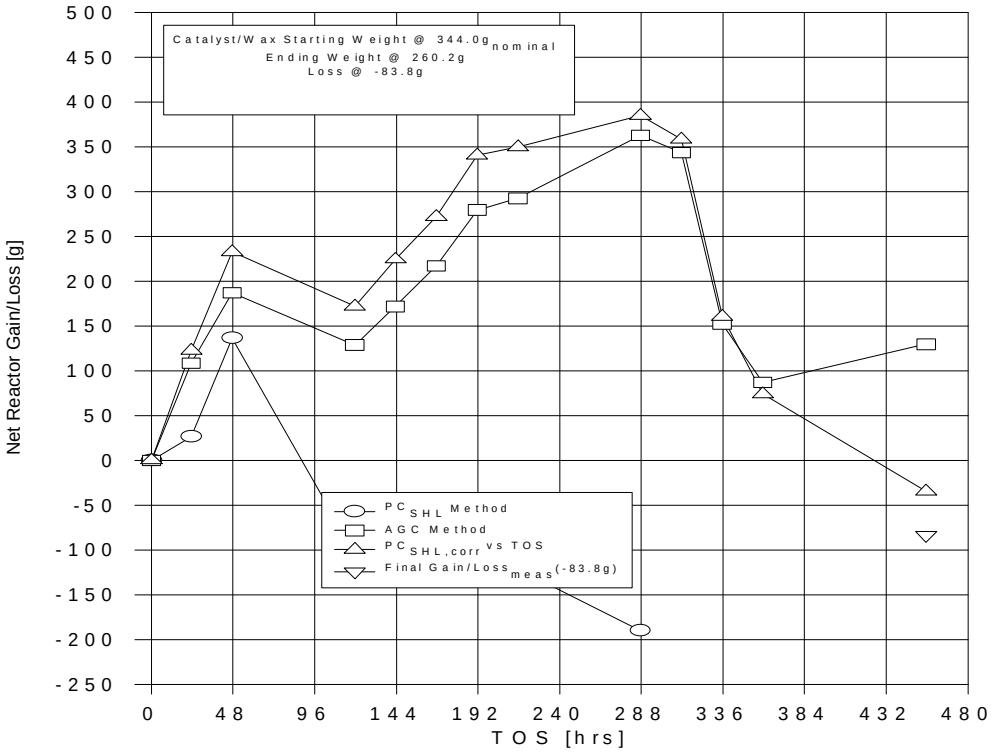

Figure 7. Net Reactor Accumulation vs Time on Stream for Run LGX285'.

3.3.4.7 Technical Assessment of the Fischer-Tropsch Synthesis

1. **Executive Summary**

A technical assessment of the Fischer-Tropsch synthesis was completed.

2. **Abstract**

The objective of this research project is to develop the technology for the production of physically robust iron-based Fischer-Tropsch catalysts that have suitable activity, selectivity and stability to be used in the slurry phase synthesis reactor development. The catalysts that are developed shall be suitable for testing in the Advanced Fuels Development Facility at LaPorte, Texas, to produce either low- or high-alpha product distributions. Previous work by the offeror has produced a catalyst formulation that is 1.5 times as active as the "standard-catalyst" developed by German workers for slurry phase synthesis. The proposed work will optimize the catalyst composition and pretreatment operation for this low-alpha catalyst. In parallel, work will be conducted to design a high-alpha iron catalyst this is suitable for slurry phase synthesis. Studies will be conducted to define the chemical phases present at various stages of the pretreatment and synthesis stages and to define the course of these changes. The oxidation/reduction cycles that are anticipated to occur in large, commercial reactors will be studied at the laboratory scale. Catalyst performance will be determined for catalysts synthesized in this program for activity, selectivity and aging characteristics.

The research is divided into four major topical areas: (a) catalyst preparation and characterization, (b) product characterization, (c) reactor operations, and (d) data assessment.

To accomplish the objectives of the project, these topics have been organized into the following technical tasks:

a. Task 1.0 Development of Optimum Promoter Levels for Low- and High-Alpha Catalysts

The goal of this task is to identify and optimize procedure for the preparation of iron-based catalysts that combine high activity selectivity and life with physical robustness. Each of the subtasks address an area of considerable uncertainty in the synthesis of catalysts.

1.1 Determine Optimized Synthesis Procedure for High-Alpha Iron-Based Fischer-Tropsch Catalysts

- Role of precursor particle size on activity.
- Role of Cu in precipitated catalysts.
- Define attrition resistance.

1.2 Prepare Catalysts that can be Used to Determine the Role of Promoters for Low- and High-Alpha Catalysts

- Define optimum SiO_2.
- Define optimum Al_2O_3.

1.3 Prepare Catalysts that can be Used to Quantify the Role of K on Product Selectivity in both Low- and High-Alpha Catalysts.

1.4 Complete the Optimization of the Two Best Low-Alpha, Iron-Based Fischer-Tropsch Catalysts Developed during the Previous Contract.

b. Task 2.0 Definition of Preferred Pretreatment for both Low- and High-Alpha Fischer-Tropsch Catalysts.

The goals of this task are to define the preferred treatment, to define the role of Cu and K during the pretreatment on activity and selectivity and to define the chemical and physical changes which occur during the preferred pretreatment. The subtasks address each of these goals.

2.1 Determine the Role of Cu in the Activation of Precipitated Low- and High-Alpha, Iron-Based Fischer-Tropsch Catalysts.

2.2 Determine the Effect of K Content on Activation Procedures and Determine if the Method of Addition has any Effect on Catalyst Activity and Life.

2.3 Determine the Physical and Chemical Changes that Occur during Catalyst Pretreatment and Use and Determine how these Changes Effect the Strength of the Catalysts.

2.4 Evaluate the Effect of Carbon Deposition during Catalyst Activation on Activity, Selectivity and Aging Characteristics.

c. Task 3.0 Catalyst Structure and Characterization.

The goal of this task is to provide basic analyses (surface area, XRD) of all catalyst prepared and to provide additional techniques as required (Mössbauer, SEM, XPS, etc.) to answer specific questions or to provide basic required characterization data for the catalysts.

d. Task 4.0 Catalyst Testing.

The goals of this task are to operate the eight CSTR reactors, measure catalyst performance, determine the stable phases that exist during synthesis at low and high conversions and to determine the rates of interconversion of iron oxide and carbide.

4.1 Verify the Quality of Data Obtained from the CSTR's.

4.2 Measure Catalyst Performance.

4.3 Determine the Stable Phases that Exist during Synthesis at Low and High CO Conversion Levels.

4.4 Obtain Data on the Rates Involved in the Interconversion of Iron Oxide and Iron Carbide.

3. **Results and Discussion**

Following the nomenclature of Sasol, we shall refer to low temperature and high temperature operational modes. As practiced at Sasol, the high temperature mode produces lower boiling products than the low temperature synthesis. Thus, the high temperature operation may be viewed as a low-alpha operation whereas the low temperature operation may be viewed as a high-alpha operation. The current production capacities at the Sasol plants are summarized below according to reactor and temperatures modes (1):

Capacities	Bbl/Day			
	CFB	SAS	TFB	SP
Total installed cap	110,000	11,000	3,200	2,500
Capacity/reactor	6,500	11,000	500-700	2,500
Potential/reactor	7,500	20,000	1,550	10,000

CFB = Circulating Fixed Bed
SAS = Sasol Advanced Synthol Fixed Fluid Bed
TFB = Tubular Fixed Bed
SP = Slurry Phase

The product selectivities on a carbon basis for these two operational modes are:

PRODUCT	LTFT	HTFT
Methane	4	7
C_2-C_4 olefins and paraffins	8 (50%)[a]	30 (80%)[a]
Gasoline	18	36
Middle distillate	19	12
Heavy oils and waxes	48	9
Water soluble oxygenates	3	6
a. Number in parenthesis is the carbon % olefins.		

Both of these distributions are fit by a "two-alpha" plot corresponding to synthesis by chain growth to produce a low molecular weight and a high molecular weight products. Based on the Sasol data for the low-temperature operation, it is calculated that about 50 carbon % is produced by each synthesis mode; however, for the high temperature mode 75% of the products are produced by the low-alpha synthesis pathway. As stated above, the high-temperature mode (low alpha mode) accounts for more than **95%** of the total installed capacity at the Sasol commercial plants.

During about 40 years of operation Sasol has made significant advances in their reactor technology. Thus, the older-type fixed bed reactors (Arge) have been replaced by a slurry-phase reactor; the slurry reactor has been operated for more than 2 years without problems and at, or above, the design capacity. One Sasol Advanced Synthol (SAS) fixed-fluidized bed reactor has been installed to replace Synthol-circulating fluidized bed (CFB) reactors and sufficient SAS reactors have been ordered to replace all of the remaining older CFB reactors.

The capacity of the high-temperature, low-alpha CFB and SAS units compared to the low-temperature, high-alpha units is overwhelming and corresponds to over 95%

of the production capacity. The transportation fuel is split 60:40 gasoline:diesel in South Africa. Since most of the reactor-wax produced in the low-temperature process is refined to supply the world's demand for paraffin wax, the contribution by Sasol to the diesel fuel requirements for South Africa must come from their high-temperature, low-alpha operation.

Sasol plans to replace the 110,000 capacity currently supplied by the CFBs with SAS fixed-fluidized bed reactors, and not with the high-molecular weight, low-temperature slurry reactors. Presumably Sasol is taking the view that the low-alpha, high-temperature synthesis will be an economical process for the next 20+ years. It should be obvious that Sasol considered both low- and high-temperature modes of operation before deciding to take the high-temperature route. Thus, Sasol's actions do not agree with the opinion of many that the only route available to produce transportation fuel is the low-temperature, heavy-product route.

It does not appear to be possible to operate with a cobalt or ruthenium catalyst in a mode other than one leading to high molecular weight products (high alpha mode). However, even for the cobalt catalyst the published data show the two-alpha product distribution. This means that 50%, and usually greater than 50%, of the products from the Co or Ru catalyst are too heavy to be utilized directly as transportation fuels. Thus, a second process step (hydrocracking) must be utilized to convert these high molecular weight products to transportation fuels.

In order to develop a process based on the cobalt catalyst, Shell has opted to utilized a fixed-bed reactor F.-T. process. Shell acquired the Gulf-Badger catalyst process technology from Chevron. The Shell fixed-bed operation in Malaysia utilizes a

reactor system that is virtually identical to the one utilized by Sasol for their ARGE reactors that utilized an iron catalyst and that are now being replaced by slurry reactor technology. The Exxon AGC-21 process utilizes a proprietary catalyst for both the F.-T. (presumably based on cobalt) and hydrocracking steps that are included in their process.

3.1. Iron Catalyst Preparation

Considering the vast literature back through the German work prior to and during WWII, it appears that the preferred iron catalyst is obtained through a precipitation procedure. The most economical source of iron in the U.S. is a concentrated solution of ferrous sulfate that is produced as a by-product in the manufacture of iron and/or steel. However, it is virtually impossible to remove all of the sulfate that is incorporated during the precipitation step even by repeated washing. Thus, in spite of the greater cost of iron, ferric nitrate appears to be the preferred source of iron for the preparation of iron Fischer-Tropsch catalysts.

3.1.1. Sasol

Catalyst robustness is a problem. Sasol utilizes a precipitation step for the preparation of the catalyst that is utilized in the fixed-bed ARGE and the slurry reactor (2). The same procedure is used to add the chemical and structural addition step that follows the precipitation and washing steps. Further processing of the fixed-bed ARGE catalyst involves filtering the slurry, extruding the "paste" and then drying the extrudate. For the preparation of the slurry-phase catalyst, the catalyst slurry is spray dried; the dried particles of the desired size are separated from fines and/or oversized particles using a cyclone/screening/scribbing system. It is found that the breakage of the

spherical catalyst particles formed for the slurry reactor is inversely proportional to the mechanical strength of the particle. **However, it is reported that the formation of ultra fine particles due to abrasion does not necessarily follow this trend [of abrasion/mechanical strength]**. This implies that the measurement of the mechanical strength of the oxide catalyst precursor does not have predictive value for catalyst integrity during use in a slurry reactor.

Sasol provides pictures representing a batch of **good** catalyst particles and **bad** catalyst particles (Figure 1). The good particles are spherically shaped and do not exhibit imperfections. The poor catalysts exhibit indentations that extend into the body of the pellet and is indicative of an operation that involves non-uniform drying during the spray-drying process. The catalysts spray-dried at UCI for the La Porte runs exhibit the characteristics of the **good** catalysts described by Sasol (Figure 2) (3). Furthermore, the attrition of the carbide form of the **good** spheres prepared by UCI show a gradual decrease in size during tumbling experiments under non-reacting conditions (3).

3.1.2. Ruhrchemie

Kuntze, et al. (4) tested a precipitated iron catalyst that they report to be similar to one used in the ARGE-process, at least during the early work at Sasol. The composition of the catalyst was (mass units): $Fe:SiO_2:Cu:K_2O = 100:25:5:5$. When this catalyst was reduced in hydrogen at 220^{o}C, it was reported to have a reduction degree of 32% (not defined as to whether this means to Fe_3O_4 or to Fe; similar catalysts at CAER would be reduced to Fe_3O_4 under these conditions) and had a surface area of 235 m^2/g.

3.1.3. The "Reichsamt" Comparative Experiments

This test utilized six different catalysts representing the major German developers of the F.-T. process at that time (WWII period) (5). These tests were under the supervision of Herbet Kölbel. The tests were conducted at temperatures not to exceed 225^{o}C, 10 atm. pressure, without recycle, and were to last for three months without change of catalyst. The products that were produced had to resemble sufficiently those obtained with cobalt catalysts so as to be marketable as substitutes for the cobalt-produced products. The catalyst compositions are summarized below:

ORGANIZATION	CATALYST COMPOSITION
KWI	Fe,100:Cu,1:K_2CO_3,1
Lurgi	Fe,100:Cu,1.0:SiO_2,30:K_2O,2.0
Brabag	Fe,100:Cu,2.0,Zn,20:K_2CO_3,1
IG	Sintered iron containing Al_2O_3 and K_2O and CaF as support
Rührchemie	Fe,100:Cu,5:CeO_2,10:kieselguhr,50
Rheinpreussen	Fe,100:Cu,5:$CaCO_3$,100:K_2CO_3,0.5-1.0

The above catalysts were tested in a 5-liter reactor and were presumably sufficiently robust to be utilized in a fixed-bed reactor. In general, there were only minor differences in the activity and limited product selectivities that were reported.

Sasol also uses a precipitation procedure that was described above.

3.1.4. Mobil

These workers utilized a precipitated iron catalyst that contained copper and potassium. Several formulations were utilized but the compositions appear to be considered proprietary and were not provided in their DOE report. In one run, the Mobil workers changed from a low-alpha operation to a high-alpha operation merely by

adding a soluble organic potassium salt at a point during the run; thus, they utilized the same base catalyst for both the low- and high-alpha in at least one of their runs. Based on a Mobil patent for an iron catalyst, we speculate that the Mobil low-alpha catalyst resembled the catalyst used in La Porte run II (except for the Cu level which was in the 2% range in the Mobil patent and was 12% in the La Porte run).

3.1.5. Rentech

The catalyst preferred by Rentech was an unsupported precipitated iron catalyst promoted with copper and potassium (6). Metallic iron and copper were dissolved in nitric acid to form a mixture of ferrous/ferric iron and precipitation was effected by adding ammonium hydroxide to produce a pH of 7.4. The precipitate is washed free of ammonium nitrate. A slurry containing the proper amount of potassium carbonate was then spray dried to produce particles with diameters in the range of 5 to 50 microns. The final step in catalyst preparation was heating in a fluidized bed at 600^{o}F (315^{o}C).

3.1.6. China

These workers used a continuous precipitation procedure to produce their catalysts (7). They report that both low and high pH conditions are to be avoided in order to obtain a high surface together with the preferred pore size distribution.

3.2. Iron Catalyst Activation

3.2.1. The "Reichsamt" Comparative Experiments

A variety of activation procedures were utilized in this test (5). Presumably these were specified by the organization that provided the catalyst and represented the preferred procedure for each catalyst formulation. For the KWI catalyst listed above the activation consisted of reduction in synthesis gas (H_2/CO = 2) at 325^{o}C and 0.1 atm.

(absolute) for 24 hours. The Lurgi catalyst was reduced in hydrogen at about 250°C. The Brabag catalyst was activated by treatment in water gas at 235-240°C for 48 hours and the Rheinpreussen catalyst received a similar activation at atmospheric pressure. The Rührchemie catalyst was reduced in hydrogen at 300°C. The catalyst preparation and activation procedures are summarized in the following table:

Table 1
Summary of the Catalyst Preparation and Pretreatment Procedures

Company	Catalyst Preparation	Pretreatment
Ruhrchemie	Conventional precipitation with Fe,100:Cu,5:CaO,10:kieselguhr,150	Hydrogen reduction, 1 hr., at 300°C; or recycle gas.
Kaiser Wilhelm Inst., Mülheim)	Precipitated from nitrate solution Fe,100:Cu,1-3:K_2CO_3,0.1-1.0	CO at 325°C, 0.1 atm.; Fe_3C formed, claimed as active phase.
I.G. Farbenindestrie A.G.	Paste of iron powder (from decomp. of $Fe(CO)_5$, 1% borax, sinter 800-900°C.	Hydrogen reduction at 800-850°C
I.G. Farbenindestrie AG (foam process)	Paste of iron powder (from decomp. of $Fe(CO)_5$ with K_2CO_3 or borate.	Hydrogen reduction at 350-400°C.
I.G. Farbenindestrie AG (tubular react.)	Paste of iron oxide powder with 5-25% 5-25% MgO or $MgCO_3$ and 1-2% K_2CO_3 or borate, sinter at 850°C in nitrogen.	Hydrogen reduction at 350-450°C.
I.G. Farbenindestrie AG (Synol process)	Melting iron in oxygen incorporating 2% alumina and 1% K_2O	Hydrogen reduction at 450°C.
Lurgie Gesellschaft für Wärmetechnik	Precipitated from nitrate solution with with sodium carbonate at boiling point, wash and add K_2CO_3. Fe,100:Cu,2.5:alumina,9:K_2O, 2:kieselguhr,30.	Hydrogen reduction at 250-350°C, 1 hr.
Rheinpreussen	Precipitated catalyst with Fe,100: Cu,1.0:kieselguhr,50:K_2CO_3,2.	CO at low partial pressure.

3.2.2. Rentech

These workers (6) report that "Determining the 'best' activating procedure for a catalyst is difficult at best even if it is known what changes in the catalyst are needed to give the desired activity, selectivity and stability." They utilized a complex recipe, initially starting by heating in an inert gas, then switching to synthesis gas at a temperature higher than the synthesis temperature using a hydrogen-rich synthesis gas. The inventors indicate that "It is believed that the presence of this water [from the activation] prevents over-carburization of the catalyst and thereby improves the activity and selectivity of the catalyst." and quote Koenig et al. as support for this view (8).

3.2.3. China

These workers made a study of the effect of activation on the catalytic properties of their iron catalyst (7). They report that reduction of the catalyst with hydrogen leads to the production of Fe and a catalyst with a low surface area and low catalytic activity. They conclude that reduction in hydrogen is not a preferred activation procedure. They also studied the use of syngas mixtures in which the H_2/CO ratio was varied from 1 to 9. The more active catalyst appeared to be produced following activation with the lower H_2/CO synthesis gas at the lower activation pressure (0.3-1.0 MPa). However, they preferred a staged activation in which the treatment with syngas is carried out in steps of increasing temperature.

3.2.4. CAER

Extensive pretreatment studies have been conducted at the CAER with a variety of iron catalysts. Initially, the catalyst activation approach followed a staged heat-up in syngas (H_2/CO = 0.7) to finally attain a temperature of about 20^{o}C higher than the

reaction temperature (270^{o}C). Presumable because of some residual sulfur in the catalysts prepared to by UCI to be screened for La Porte Run II, sufficient sulfur accumulated on the surface so that the catalytic activity was low following this pretreatment procedure. The same catalysts could be activated successfully in pure CO, either at atmospheric or reaction (170 psig) pressure.

Using pure CO, CAER workers found that they could obtain an active material following 24 hours in CO at 270^{o}C. Four activation runs were made at the CAER in the 2 inch diameter x 6 foot long using the spray-dried Round-Robin batch of unsupported iron catalyst of the same formulation used for La Porte Run II. These runs were made to produce activated (carbided) catalyst samples to be used in filtration studies at Mott. The first resulted in a "poor" run due to the use of a low CO flow rate; the other three runs were at a lower pressure and provide reproducible data (Figure 3). These runs were conducted until the catalyst had accumulated an amount of carbon, based upon the cumulative production of CO_2 measured in the exit gas, to produce about 10% more carbon that required to produce $Fe_{2.2}C$. The data generated in the CSTR studies at the CAER had the same shape as those obtained in the 2"x6' slurry reactor except that it took 17, rather than 18 hours, to attain the desired amount of carbon deposition. The activation at LaPorte for Run II used a similar activation procedure (40 wt.% slurry) and produced data that followed closely the "poor" curve in Figure 4.

Synthesis gas and pure hydrogen streams are, or can be, easily attained at a commercial F.-T. site. However, it is not easy to obtain a pure stream of CO at a commercial F.-T. site. Thus, while CO pretreatment may be of interest for laboratory

studies or for use at La Porte, it does not appear to be easily practiced at a commercial site.

Activation in CO occurs in steps. Initially, there is a rapid reaction to convert the Fe_2O_3 to Fe_3O_4; the formation of Fe_3O_4 has been confirmed by Mössbauer spectroscopy. After the formation of Fe_3O_4 is complete, a slower reaction occurs to deposit carbon in the form of an iron carbide (and possibly carbon to coat the iron carbide particle).

Activation in synthesis gas at reaction pressure appears to be dependent upon the catalyst formulation. For instance, the catalyst that Ruhrchemie provided to DOE could be successfully activated in syngas at reaction pressure. A catalyst with a similar composition that was prepared at the UCI could not be successfully activated using syngas. It appears that it is essential to have copper (or some metal that functions in a similar manner) present if the catalyst is to be activated in synthesis gas at or near reaction pressure. Even when copper is present, it appears that the approach to maximum activity requires days of operation in the synthesis mode.

The effectiveness of an activation at reaction pressure using gas flow rates at or near to those to be used for the synthesis depends upon the hydrogen partial pressure. Thus, an active catalyst was obtained when pure CO was passed over the catalyst for 24 hours prior to changing to the synthesis conditions (Figure 5). However, there appears to be a linear decline in activity as the partial pressure of hydrogen in the feed gas is increased.

On the other hand, activation with synthesis gas was easily accomplished at atmospheric pressure during 24 hours at reaction temperature. This observation is in agreement with much of the early German work on activation of iron catalysts.

Reduction in hydrogen is a complex operation. Initially Fe_3O_4 is formed; this stage is followed by the reduction to metallic iron at a higher temperature and/or longer reaction time. During a 24 hour period at 270°C it is found that about 30% of the iron is present in the metallic form and the remaining iron is present as Fe_3O_4. When synthesis gas contacts the reduced catalyst at reaction temperature, within 2 hours or less the metallic iron is converted to iron carbides. The presence of copper has been shown to result in a lowering by 20-40°C the temperature where each of these two reductions occur. In general, reduction in hydrogen prior to contact of the catalyst by synthesis gas can produce an active catalyst, and this appears to be the procedure that is utilized at Sasol in their commercial operation. On the other hand, it does not appear that the optimum degree of conversion to metallic iron has been reported in the open literature. It has been reported that complete reduction to metallic iron is to be avoided since the metallic iron sinters rapidly at this temperature to produce a low area material that results in a low-activity catalyst.

3.3. Cobalt Catalysts

The catalysts utilized in the German commercial plants prior to and during WWII was primarily based upon cobalt and these were operated at atmospheric or low pressure conditions. Roelen encountered severe loss in activity during the use of the cobalt catalyst in the early plants but overcame these problems, primarily by separating the interfering elements from the cobalt by precipitation prior to catalyst preparation (9).

During the past 30 years, a vast amount of patent and open literature has developed on cobalt catalyst; these are primarily devoted to the use of one or more elements to modify the catalytic properties of the cobalt.

During the 1970s, Gulf Oil workers found that a Group VIII element, such as ruthenium (Ru), incorporated in a much smaller amount compared to cobalt (Co), greatly increased the activity of the finished catalyst; as an example, a catalyst containing 20 wt.% Co would contain 1 wt.% Ru (10). In addition to cobalt and the Group VIII metal, other components, such as magnesia and thoria (Shell now uses zirconia) were incorporated in order to improve the performance of the catalyst. A catalyst based upon the Gulf patent formulation became the basis for the Gulf-Badger process for the production of hydrocarbons using the Fischer-Tropsch synthesis. Two designs were tested - fixed-bed and fluidized-bed reactors - were tried. The operation of the fluidized-bed reactor was not satisfactory. Gulf Oil, working with Badger, designed, built and operated a 1 inch diameter, 40 ft. length (two-section) tubular reactor using the Gulf cobalt catalyst. The aged catalyst was reported to be restored to its original activity following an oxidation and reduction cycle.

Gulf Oil workers also patented the use of two stage operation with the first stage employing a Fischer-Tropsch catalyst and the second stage employing an acidic catalyst such as the silicalite catalyst developed by Union Carbide. Alternatively, both the F.-T. and the acidic catalyst could be added to a single reactor. The utility of this concept was adequately demonstrated by the Mobil work carried out under DOE contract.

Unsupported cobalt catalysts have not been found to be satisfactory. A wide range of supports have been utilized; these include alumina, silica, titania, zirconia, magnesia, silica alumina, carbon, and molecular sieves. Recently, Statoil has been issued patents in which it is claimed that the use of alumina, in contrast to other supports, leads to the catalyst with a superior activity compared to Co on other supports (11). The Statoil work also indicates that the incorporation of alkali decreases the catalytic activity and increases the alpha value from about 0.7 for the cobalt only catalyst to 0.9 or greater as the K/Co ratio increases. However, the conclusion for the alteration of the alpha-value by cobalt, from a scientific viewpoint if not from a patent viewpoint, is tenuous at best.

Exxon workers contend that the activity of all cobalt catalysts, with the exception of a titania supported cobalt, exhibits the same activity (site time yield) (Figure 6) (12). Thus, it appears that the Statoil and the Exxon data may be in conflict provided one makes the comparison upon the cobalt dispersion. In the Exxon view, the preferred catalyst involves placing cobalt on the external portion of the support ("egg-shell" type) to improve the selectivity towards the C_{5+} fraction. Exxon workers have provided extensive published work to indicate that, because of olefin reincorporation, a balance between the kinetics and the diffusional factors must be taken into account. Thus, a structural parameter (? in Figure 7), dependent upon the pellet diameter, the average pore size of the support, and the density of the metal sites within the pellet, acts to determine the F.-T. product distribution for supported Ru and Co catalysts. Thus, the proper control of the parameter ? allows one to maximize the production of C_{5+} products and, at the same time, minimize the amount of undesirable methane.

There are many patents that purport to provide recipes to prepare cobalt catalysts in such a manner that a superior catalysts is produced with respect to activity, selectivity, and/or ability to handle the exothermic reaction. Unlike the case of the Exxon open literature reports on scientific aspects of the catalyst impact upon the F.-T. synthesis, little exists in the open literature to evaluate the various claims of these patents. It appears that legal actions are underway to resolve some of the perceived or real differences among some of the patents.

For cobalt catalyst, those containing magnesia had been in use in Germany since 1938. The introduction of the magnesia catalysts were claimed to have made possible catalyst lives of up to eight months at normal pressure. According to the managing director of Ruhrchemie A.-G. the magnesia was added **solely** to increase the hardness of the resulting catalyst and thus to reduce its tendency to disintegrate to dust in the reactor (13).

3.4. Comparison of Cobalt and Iron Catalysts

A major difference between cobalt and iron catalysts is the ability of iron to catalyze the water-gas-shift (WGS) reaction:

$$CO + H_2O \; W \; CO_2 + H_2 \; .$$

At Fischer-Tropsch synthesis conditions, the equilibrium for the above WGS reaction lies far to the right; that is, WGS is a thermodynamically favored reaction. Furthermore, the reverse reaction is slow, compared to the forward reaction, under Fischer-Tropsch conditions. However, the forward reaction depends upon the partial pressure of water.

For the F.-T. reaction, cobalt produces hydrocarbons and water whereas the iron catalyst, in the extreme condition, will produce hydrocarbons and carbon dioxide.

Thus, for each CH_2 produced as hydrocarbon, cobalt will produce a H_2O whereas iron will produce CO_2. In this instance, iron will consume two CO molecules for each CH_2 formed whereas the cobalt catalyst will consume only one CO for each CH_2 formed. Thus, the "conventional wisdom" is that cobalt is the preferred catalyst since it makes more efficient use of the CO in the syngas.

For a coal derived syngas, this "conventional wisdom" is an illusion. To produce CH_2 and H_2O by the F.-T. reaction two molecules of H_2 are required as shown in the following equation:

$$CO + 2\ H_2\ 6\ \text{-}CH_2\text{-} + H_2O\ .$$

Thus, using a ratio of $H_2/CO = 0.7$ (the "middle-ground value" for a syngas produced from coal), there is a deficiency of hydrogen when the cobalt catalyst is used. The above F.-T. reaction can only take place provided an additional amount of CO is converted to CO_2 and H_2 to provide a synthesis gas to pass over the cobalt catalyst that has a ratio $H_2/CO = 2$. Thus, with a syngas derived from coal the only difference between the use of the two catalysts is that with the iron catalyst the WGS reaction can be carried out in the same reactor as the F.-T. reaction whereas with the cobalt catalyst the WGS reaction must be carried out in a process operation that precedes the F.-T. reactor. The preferred catalyst, on the basis of the usage of syngas to produce hydrocarbons, will depend only on the economics of whether it is preferable to conduct the WGS reaction in the F.-T. reactor or in a separate operation.

With a syngas derived form natural gas, the H_2/CO ratio is 2 so that "conventional wisdom" teaches that cobalt, without WGS activity, is definitely the preferred catalysts. This assertion is both "true" and "false." At high CO conversions,

the WGS reaction is an important component of the synthesis using an iron catalyst and hydrogen is formed in excess of that needed to produce CH_2. Thus, the "conventional wisdom" assertion for iron catalysts is "true" at high CO conversion levels. However, the extent of WGS reaction relative to the F.-T. reaction is very dependent upon the CO conversion level for an iron catalyst. Thus, the fraction of CO converted by the WGS reaction is low at low CO conversions (Figure 8). Thus, up to CO conversion of about 60%, the WGS reaction does not make a significant contribution to the overall reaction of CO. **Thus, below about 60% CO conversion iron and cobalt catalysts produce essentially the same products and therefore the same relative utilization of hydrogen and carbon monoxide**. Therefore, it is only true that a cobalt catalyst is preferred for an operation that derives the syngas from natural gas when the iron catalyst is to be utilized in a process configuration that requires high CO conversion in a single-pass operation. Thus, the "conventional wisdom" assertion to favor cobalt over iron catalyst is "false" for operations with an iron catalyst involving recycle or multiple reactors so that CO conversion is kept at about 60% or less.

Thus, iron and cobalt catalysts have a similar selectivity for CO conversions at the 60% or lower levels.

The other "conventional wisdom" viewpoint that favors the cobalt catalyst over the iron catalyst is that the cobalt catalyst is more active. Again, this "conventional wisdom" is both "true" and "false." The CO conversion for a cobalt catalyst is considered to depend only upon the dispersion of the cobalt as shown in Figure 9. This is not the case with an iron catalyst. As shown in Figure 10, the rate of F.-T.

synthesis with an iron catalyst increases nearly linearly with time up to a conversion level of about 60% and then to increase only slowly with time above this level. Furthermore, the usage of hydrogen and carbon monoxide varies with CO conversion. Thus, if we compare cobalt and iron catalysts at high CO conversion levels the "conventional wisdom" that Co is more active catalyst than iron is "true". However, if we compare the two catalysts at temperatures where the production of CH_4 is low (e.g., 220^{o}C for cobalt and 270^{o}C for iron), the grams of hydrocarbon produced per gram of catalyst is comparable. Thus, based on an operation using iron catalysts at 60% conversion and using recycle or multiple reactors to a attain the high overall conversion of syngas, the "conventional wisdom" is "false".

The above is based upon an analysis of the situation by CAER. Similar conclusions have been reached by Sasol investigators (14). Based upon syngas conversion, they show that using an iron catalyst at 240^{o}C at high relative space velocities, the iron catalyst matches or even exceeds the activity of the cobalt; only at short relative space velocities (high conversion levels) does the conversion obtained with a cobalt catalyst exceed that of the iron catalyst. Furthermore, on the basis of a comparison of the two catalysts, the cobalt catalyst is more productive than an iron catalyst only at the lower relative space velocities and lower pressures (Figure 11). Also, as the operating temperature for the iron catalyst is increased, the dividing line in Figure 12 will lower so as to favor iron over cobalt to even higher conversions. Presumably the data in Figure 12 is for an iron catalyst designed to produce higher molecular weight products (high-alpha catalyst); thus, the use of an iron catalyst to produce low molecular weight products (low-alpha catalyst) would lower the dividing

line to favor the iron catalyst by an additional amount. The Sasol workers report that the activity of their cobalt catalyst compares favorably with patented alternative cobalt catalysts. The above comparison was at an $H_2/CO = 2$ ratio; i.e., a syngas that would be produced from natural gas.

The Sasol workers provide stability data for their cobalt catalyst operated at 220°C, 20 bar (essentially 20 atm, 290 psi) and 0.5 relative space velocity. The authors state that a commercial syngas feed was used that contained $H_2/CO = 2$ and contained 25 vol.% inerts. Under these conditions there was a rapid decline in activity during about 5 days and then a very slow decline in activity during the next 20 days. These authors attribute the initial decline with build-up of waxes in the catalyst pores and the slow decline as probably due to a low level of sulfur poisoning.

Based upon the knowledge in the open and patent literature, it does not appear valid to make a choice between a cobalt and an iron catalyst unless the choice is based upon a particular process in which the operational conditions are specified.

3.5. Slurry Reactor Studies

3.5.1. German

3.5.1.1. Roelen

In spite of studies directed toward industrial development, the KWI pilot plant studies showed that the optimal stoichiometric ratio of $CO:H_2$ was 1:2 (9). **In November 1930 the pilot plant staff attempted to run the F.-T. in the liquid phase, and they were successful in maintaining the heat flow problem.** However, the typical catalysts of that day had an activity that was too low to have practical commercial interest.

3.5.1.2. Kölbel

Until the start-up of the slurry reactor by Sasol, the Rheinpreussen-Koppers demonstration plant was the largest slurry reactor that had been operated successfully. The reactor was 1.55 m in diameter and 8.6 m in height. Kölbel states that at the time that most work was conducted using the demonstration plant (1952-53), the operation was confined almost exclusively to the production of gasoline (15). The results of the operation of this plant and the smaller laboratory scale slurry phase reactor produced data that have become the "standard" that is used to compare with other slurry phase studies. A typical catalyst used by Kölbel would have a composition of Fe:Cu:K_2O = 100:0.1:0.05-0.5; thus, the catalyst used by Kölbel would be consistent with the objective of producing gasoline range material, and not high molecular weight reactor-wax. The catalyst used by Kölbel would be similar to a low-alpha iron catalyst described in a Mobil patent and the one used for La Porte run II (low, not the actual high Cu content).

Table 2
Operating Data and Results of Liquid-Phase Synthesis for One-Step Operation with a Single Passage of the Gas Over Iron Catalysts (from ref. 15)

	Demonstration Plant (a)	Laboratory Plant (b)
Effective reaction space (volume suspension including dispersed gas) (L)	10,000	6
Catalyst (kg Fe)	800	0.4
Synthesis gas pressure (bar)	12	11
Synthesis gas (volume ratio, CO:H_2)	1.5	1.5
Quantity of synthesis gas (Nm^3/hr)	2,700	1.3
Linear velocity of the compressed gases at operating temperature referred to the free reactor cross section (cm/sec)	9.5	3.5
Total CO + H_2 used (Nm^3/hr) Per m^3 of reaction chamber (Nm^3/hr) Per kg of Fe (Nm^3/hr)	2,300 230 2.6	1.1 183 2.45
Average synthesis temperature, °C	268	266
CO conversion, %	91	90
CO + H_2 conversion, %	89	88
Synthesis products referred to CO + H_2 used: Hydrocarbons C_1^+ (g/Nm^3) $C_1^+ + C_3$ (g/Nm^3) C_3^+ (g/Nm^3)	 178 12 166	 176 11 165
O-containing products in the synthesis water (g/Nm^3)	3	2
Space-time yield of C_3^+ products including O-products in 24 hr (kg/m^3 of reaction chamber)	930	740

At the conversion level shown in the above table, only 178 g of hydrocarbons were produced per m^3 gas (from the original paper in German, it was not possible for even a native German to tell whether this volume of gas refers to the amount of gas fed or to the amount of gas converted). Even if it is taken as the amount fed, at the 90% conversion level, more than 178 g. of hydrocarbons should have been produced. For

example, in the Mobil runs more than 200 g hydrocarbon were produced. Sasol workers indicate that they could not repeat Kölbel's results in their early studies (2). Kölbel et al. report that through polymerization of lower olefins, about 18 g/Nm^3 CO+H_2 of alkylate gasoline can be produced. When this was mixed with the reformed gasoline (112 g/Nm^3 CO+H_2), 130 g/Nm^3 CO+H_2 of finished gasoline could be produced. For a CO conversion of 91%, the H_2 + CO conversion was 89%; the feed gas ratio was H_2/CO = 0.67. With this gas ratio the only way, based upon CAER results, that Kölbel could have obtained such similar high CO and CO + H_2 conversions would be to operate so that the single pass conversion was 50-60% and to recycle the unconverted gas. It has not been widely appreciated that much of the work that Kölbel reports has been conducted under conditions designed to produce gasoline; in this mode the demand on wax/catalyst separation is minimal. Thus, much of Kölbel's work can be viewed as being conducted under conditions that make the operation of a slurry reactor much easier than the current goal of operating to maximize the reactor-wax fraction to subsequently hydrocrack to produce diesel fuel.

Kölbel stressed that the low viscosity and surface tension of the liquid was crucial for maintaining the small bubble size needed to maintain gas-liquid mass transfer. Kölbel maintained the view that it was necessary to establish upper limits upon the solids content of the slurry in order to maintain a low viscosity.

3.5.2. British

The operation of the British plant was terminated about the time that they had solved most of the operating problems and considered themselves to be at a point where they could operate to produce reliable data. For example, low catalyst activity

and rapid catalyst aging were problems than limited the usefulness of the data produced during the period of operation of the plant.

3.5.3. U.S. Bureau of Mines

The Bureau of Mines operated a 3 inch diameter x 8 foot long reactor as well as a larger 8 inch diameter reactor in the oil-recycle mode. These units were operated with a precipitated and a fused iron catalyst that has a very low activity compared to the high surface area precipitated iron catalyst. The fused catalyst was used because it was hard and seemed to have the physical strength needed. Some experimental operating difficulties made it difficult to maintain constant temperature during significant portions of the runs. While it was demonstrated that this mode of operation was viable, little else was obtained that merit further consideration here.

3.5.4. Mobil

The initial runs in the pilot plant (Figures 13 and 14) at Mobil Oil, based upon the catalyst compositions in Mobil's patents, would utilize a catalyst with a composition that resembles the one reported above for Kölbel's work and the catalyst intended (low, not high, Cu content) for the La Porte Run II. Mobil's data from work funded by DOE have become the "standard" for both economic (e.g., 16) and technological evaluations (e.g., 17). The first three runs in the Mobil plant were conducted using a catalyst that produced low molecular weight materials; during the third run a potassium salt was added at 81 days-on-stream and this decreased the methane + ethane production from about 13 to 18 wt.% without significantly lowering the CO conversion; however, operational upsets prevented a valid assessment of the impact of the added alkali (18). The later runs were in the high molecular weight product mode (wax mode). In most

runs Mobil operated with about a 20 wt.% slurry catalyst loading. In run 8, the aging rate of the iron catalyst operated at 250°C, 1.48 MPa (about 15 atm; 215 psi) and 1.4 NL/gFe-hr was such that half the activity would be lost during 24 days; later in the run the catalyst half-life was 13 days when the temperature and pressure were increased. Mobil workers indicate that the catalyst used in this run was not acceptable because of its high aging rate. In run 9, a surprisingly low methane + ethane make (about 5.4 wt.%) was obtained. The catalyst was the "same" as had been used in a prior run where this was not observed; the only difference noted was that the low methane + ethane catalyst had a lower surface area. An operational upset terminated the effective operation at day 10. In run 10, Mobil workers reported that the catalyst could not be fully activated at synthesis conditions.

Run 12 was operated for 17 days at constant conditions and "This period represented the finest example of low methane + ethane [4.1 wt.%] mode operation we have ever produced in the pilot plant." Wax production was about 60 wt.%. An operational upset occurred on day 17 and afterwards catalyst settling and low catalyst activity were problems that could not be overcome.

Run 13 was a repeat of run 12 and good operation was accomplished for 35 days-on-stream, after which catalyst settling became a problem. Viewing the pictures of the catalyst, Mobil was utilizing particles in the 1-5 micron range, and the final catalyst particles were considerably larger following removal from the reactor. It is not clear whether this is due to catalyst particle growth or, more likely, cementing together several particles by reactor wax. It is not clear, if wax caused the particle size increase,

whether this occurred in the reactor itself or was an artifact introduced during catalyst collection and subsequent treatment.

As stated above, the Mobil data have replaced the Kölbel data as the "standard" for slurry F.-T. operation. Data for reactor wax yield of 46 wt.% are shown in Figure 15. This data has been utilized by Bechtel Corp. for their analysis of slurry F.-T. operations. They consider the data to consist of three regions: methane (a_1) that is higher than ASF; C_2-C_4 (a_2) and reactor wax (a_3). Theoretical curves for reactor wax make of 9.49 wt. % (low alpha data), 46.02 (intermediate alpha data) and 75.95 (high alpha data) are shown in Figure 16.

Thus, the Mobil data, in spite of operational problems, represents the best data that is available in the open literature in sufficient detail that its quality can be adequately judged.

3.5.5. Sasol

Sasol has reported general, but few specific, details about the development and operation of their slurry reactor operations. Sasol's work on a small scale began in the early 1980s (2). In 1990, a slurry bed with a diameter of about 1 m was commissioned and the results confirmed their early expectations. In a bold move, Sasol decided to construct a commercial scale slurry reactor (5 m diameter, 22 m high) rather than two 5,000 tube tubular-fixed-bed reactors for the expansion of their low temperature operation. The commercial reactor was commissioned in May 1993 and has been reported to operate successfully since that time.

Sasol uses a separate catalyst pretreatment reactor in which hydrogen reduction (extent of reduction not specified) is used to activate a catalyst prior to its introduction

into the slurry reactor. During operation, it is understood that an activated catalyst batch is on "stand-by" so that if a significant upset, such as a slug of sulfur to cause severe catalyst poisoning, causes a significant loss in productivity, the reactor is emptied and a fresh catalyst batch added during a short period. On-line catalyst removal and additions are reported to be done without difficulty. Based upon reports of the extent of sulfur poisoning in the fixed-bed ARGE reactors, it should not be surprising if Sasol operators had made several replacements of the catalyst inventory during the four years of commercial operation.

The authors (2) describe the churning nature of the slurry-base bubble interactions, implying that the Sasol operation operates in the bubbly, rather than slug, flow condition. Because of the isothermal nature of the slurry reactor, operating temperature can be much higher than in a fixed-bed tubular reactor without fear of hot spots leading to carbon formation and break-up of the catalyst. Hot-spots in the fixed-bed reactor presumably allows for the catalyst in the hot-spot to reach a temperature sufficiently above that of the reactor set-temperature so that carbon formation becomes possible.

It is reported that for an iron catalyst, the product slate is considerable affected by the age of the catalyst, with wax selectivities decreasing with time. It is reported that "by proper scheduling of catalyst renewal, it is possible to maintain a steady selectivity profile for a single reactor while minimising the catalyst consumption." It therefore appears that the Sasol operation involves a regular schedule of catalyst addition, presumably to replace catalyst that is intentionally withdrawn as well as that which is lost as catalyst fines due to catalyst attrition.

Foam was found to build up in the reactor under certain conditions but it was reported that this could be prevented by modifying operation procedures. "Separation of gas from the entrained slurry was another development that was easily resolved.", implying that slurry carry-over can be a problem if not properly handled.

Several approaches were tried at Sasol in order to effect wax separation form the catalyst containing slurry. These included close attention to the production of the catalyst and its physical characteristics and to the separation processes. The technique currently in use in the commercial operation is considered to be proprietary information.

3.5.6. China

The Chinese have operated a two stage process involving slurry F.-T. synthesis with an iron catalyst and fixed-bed cracking/oligomerization processing using a ZSM-5 catalyst to convert the F.-T. product to gasoline range products (7). The F.-T. slurry reactor was 4 cm in diameter and 450 cm in height. The reactor, in a schematic form, is very similar to the one used by Mobil Oil (Figures 13,14). They used an unsupported precipitated iron catalyst with a typical composition of Fe:Cu:K_2O = 99.5:0.5:0.29. The sample of catalyst used in the slurry reactor had obviously been calcined (based on CAER work, at temperatures of at least 300^oC) since the XRD analysis showed that the main crystal phase was a-Fe_2O_3. The authors indicate that diffusion effects could be neglected for their runs. It appears that they used a slurry that contained 12% catalyst. Most of the published data concerning runs with their pilot plant are for the product following processing with the ZSM-5 catalyst. However, based upon data presumed to be for the F.-T. only operation, the liquid phase is reported to have a composition of

approximately 70% C_{5-12}, 27 % C_{13-22} and 3% C_{22+}. Thus, based upon the catalyst composition, the product distribution would be considered to originate from a low-alpha mode of operation, and the composition of the catalyst is consistent with this. Furthermore, the low-alpha mode would probably be preferred for subsequent conversion of the F.-T. products with a ZSM-5 catalyst in the second stage.

The output during the course of a 1,000 hour (40 day) run declined due to loss of catalyst. From the published data on the Chinese F.-T. only operation, it is difficult to reach definitive conclusions or catalyst performance.

3.6. Products

3.6.1. Low Temperature vs High Temperature

The product distribution reported by Kölbel was typical of high temperature (low alpha) operation: C_{1-2}:C_{3-4}:gasoline (25-190°C):diesel oil (190-310°C):heavies (>310°C) = 7:17:62:10:3 (19). The olefin content of the C_{2-4}, gasoline and diesel fractions were 72, 74, and 45%, respectively. Kölbel reported in less detail on runs made to produce "medium" and "high" molecular weight products in addition to the ones described above. These products are shown in the following table:

Table 3

Variations in Product Composition from the Kölbel Reactor (from ref. 19)

Molecular Weight Goal	"Low"	"Medium"	"High"
Single-pass C_3^+ product yield (g/m^3 feed)[a]	166	175	182
Distribution of C_3^+ products (%)			
C_{3-4}	18	7	2
Gasoline (C_5-190°C)	68	40	7
Diesel fuel (190-310°C)	11	26	8
310-450°C	2.5	18	33
> 450°C	0.5	9	50

As noted, the production of hydrocarbons per m^3 gas increases as the molecular weight of the products increases; however, in no instance does it approach the theoretical yield of 208 g/m^3. On the other hand, Mobil runs consistently produced greater than 200 g/m^3. This low hydrocarbon productivity in Kölbel's work is apparently a problem that many investigators have struggled with.

The quality of a diesel fuel can vary considerably. Cetane number is used as one measure of the quality of a diesel fuel much in the same manner as octane number is used for gasoline. However, octane number and cetane may be viewed as opposites. Thus, highly branched paraffins, olefins and aromatics are desirable, and normal paraffins undesirable, components of a fuel if one wants a high octane number; on the other hand, n-paraffins are desirable and highly branched paraffins, olefins and aromatics are undesirable components for diesel fuel with a high cetane number. In viewing the **high molecular weight product** slate in the above table, it is noted that 33% of the product is diesel and 50% is heavier molecular weight material that must ultimately be cracked to produce gasoline and diesel. As produced with an iron catalyst, the diesel fraction of the products (straight-run diesel) contains a significant amount of olefins, and consequently a relatively low cetane number. However, when this fraction is hydrogenated it will contain predominantly (90% or greater) n-paraffins, and this fraction will have a high cetane number (at or approaching 70). Because there is little difference in the ratio of i-/n-paraffin fraction of the hydrogenated straight-run diesel from an iron catalyst and the straight-run diesel from a cobalt catalyst, the straight run diesel produced by either catalyst will be the same, or very similar. Furthermore, it requires the same amount of hydrogen to produce a paraffin

irrespective of whether it is produced indirectly by hydrogenating an initially formed olefin produced by iron catalysis or produced directly using a cobalt catalyst. Based upon straight-run diesel, there should therefore be no difference in the quality of the materials produced using either catalyst. Likewise, the >450^{o}C fraction of the iron and cobalt catalyst is composed essentially of n-paraffins, either before or following a hydrogenation step, so that, while the quality of the diesel fuel produced by hydrocracking may depend upon the hydrocracking process utilized, it should not depend upon whether the >450^{o}C fraction is obtained by iron or cobalt catalysis.

It cannot be overemphasized that diesel is not a sufficient specification to use to compare catalysts and/or processes. Straight-run diesel and diesel obtained from hydrocracking will not, in general, have the same properties even when both are composed only of paraffins. The major reason for this is that hydrocracking normally produces a significant fraction of monobranched paraffins; in fact, the classical bifunctional hydrocracking mechanism would produce an i-/n-paraffin ratio of 1 or even greater. Thus, it is important, when discussing cetane number, to specify whether one refers to what is straight-run diesel, diesel produced by hydrocracking or some blend of these two products. For blending with petroleum-derived diesel to produce a more environmentally friendly transportation fuel, it is desirable that the F.-T. product have the highest possible cetane number. From the point of view of obtaining a superior diesel for blending with petroleum-derived diesel, it appears that straight-run F.-T. diesel would be preferred over hydrocracked diesel.

In considering the medium and high molecular weight cases shown above, an equal amount of blended diesel would be produced by combining the straight-run and

hydrocracked diesel fraction only if the hydrocracking selectivity was such that it produced only 32 % diesel fraction. The selectivity for hydrocracking is much greater than 32% so that it is obvious that more diesel will be produced from the "high" operation in the above table. However, for a run at La Porte to generate diesel to make a large-scale test, both straight-run and hydrocracked diesel could be produced using either the medium or high molecular weight mode of operation. For the medium molecular weight case the straight-run fraction would dominate over the hydrocracked diesel whereas the opposite would result from the high molecular weight mode of operation.

3.6.2. Deviations from Anderson-Schulz-Flory

3.6.2.1. Positive Deviations

Since its introduction about 1950, the Anderson-Schulz-Flory distribution for the products from Fischer-Tropsch synthesis has been accepted. However, only a few investigators have been able to attain a product distribution that adheres to this single alpha distribution. Anderson, in his review in the 1950 showed data for products from large scale German and U.S. plants and these exhibited the "double-alpha" plot that has now been reported by many. Donnelly et al. (20) published an approach to calculate the two alphas from the experimental product distribution. Sasol workers report that it is difficult to obtain an accurate evaluation of the higher alpha value because of the small amount of wax production in laboratory studies. These workers report, however, that the Donnelly et al. approach is "suitable for the extrapolation of selectivities," (14). On the other hand, Shell workers (21) report that "In a few hundred independent F.-T. synthesis experiments with various catalyst formulations [iron,

ruthenium and cobalt] under different operating conditions it was confirmed that the carbon number distribution were in close agreement with the AFS chain growth kinetics discussed above, with a values varying between 0.7 and 0.95 (Figure 17)." However, these authors did not provide data in their paper (Figure 17) that would cover adequately the carbon number ranges of both alpha values.

^{14}C tracer studies carried out at the CAER using an iron catalyst produced data that led to the postulation of a double alpha ASF distribution with the additional provision that the lower alpha produced all F.-T. products but that the higher alpha pathway produced only alkanes. More recent ^{14}C tracer studies included a measurement in the activity in the higher carbon number alkenes. This more recent data indicate that the ^{14}C distribution in the alkenes is consistent with a single ASF pathway. Accumulation of paraffins in the reactor provide a "product accumulation disguise" so that the second alpha products are due to reactor operation and not to two reaction pathways. Thus, based upon CAER data, the observation of a double alpha value is introduced by the operation of the reactor and not by the F.-T. mechanism.

As noted in another section, Sasol workers consider that an iron catalyst can be modified by the use of chemical promoters (e.g., potassium) but that cobalt cannot. On the other hand, the selectivity of cobalt is sensitive to the pressure but not the iron catalyst. Thus, the Sasol workers attribute the observations of the impact of chemical promoters as being due to pressure effects. Thus, they report the chain growth probability as a function of pressure (Figure 18). This translates into the product selectivities shown in Figure 19. It is obvious that if wax is the desired product pressure makes very little difference with the iron catalyst (25 atm appears optimum)

but for the cobalt the wax production is still increasing relative to other products even at 40 atm pressure. The Sasol workers report that the wax boiling above 350°C can be easily hydrocracked to extinction, yielding about 80% diesel with a cetane number of at least 70.

3.6.2.2. Positive Deviation at Higher Carbon Numbers

There are many examples of this type of deviation and these examples have been produced in many laboratories as well as at large pilot or commercial plants (22). A number of reasons have been advanced to account for this distribution. Included among these are two or more chain growth pathways, the impact of alkali, and alkene reincorporation.

A more logical explanation for the deviation is reactor operation and the hold-up of heavier materials.

3.6.3. Cut Off of Product Distribution

At the start-up of a slurry or even fixed-bed reactor a period of time is required until the vapor-liquid equilibrium is established. The length of time that it takes to reach vapor-liquid equilibrium depends upon carbon number; the higher the carbon number the longer the time it takes. Satterfield, Bell and others have shown the impact of this factor. This effect is a result of normal reactor operation and is independent of F.-T. selectivity deviations.

3.6.3.1. Chinese

Yang et al. (23) considered literature reports and proposed a new product distribution formulation. They proposed that ASF growth was followed but that on any metal crystal size, only molecules with a lower carbon number than the cut-off value

could be produced. They fit an equation they derived to three sets of data and showed a good correlation between theory and experimental data. One set of data was for a series of carbon supported iron catalysts that had different distribution of metal crystallite sizes (24). There are two problems with the use of these data: (1) the metal crystallite size will have little meaning since under reaction conditions the supported Fe crystallites will be converted to iron carbide and/or iron oxide and (2) products were analyzed by an on-line g.c. with a transfer line that was heated only to a temperature that is consistent with the cut-off of products being due to vapor pressure effects rather than metal crystallite size. A consideration of other data (25-35) show that the selectivities were most likely due to operational rather than F.-T. mechanistic factors.

Thus, while many accounts have been provided to show that cut-off has been accomplished, none of these studies have been conducted under realistic conditions for a sufficient length of time to ensure that liquid-vapor equilibrium had been established.

3.6.3.2. Syntroleum

The Syntroleum Process involves the conversion of gas to liquids and offers a variety of options. Agee (36) reports that work began on a program to produce a catalyst that limits the growth of hydrocarbon chains to eliminate wax production and at the same time minimizing the production of light hydrocarbons (C_1-C_4). Agee reports that multi-week test runs in a fluid bed reactor at the pilot plant yielded a product profile that indicates success. Based upon data presented at the AIChE meeting, and repeated at the Spring ACS meeting (37), the C_1-C_4 gases are low, and the products cut off by carbon number 25. The most surprising feature of this example is that there

is a linear decline in the products with increasing carbon number in the C_1-C_4 range. This cannot happen in a normal polymerization reaction unless the higher carbon number components also continue a similar decline. Agee indicates that the new chain-limiting catalyst eliminates the need for a hydrocracking step; presumably he did not eliminate hydrocracking as an operation that is combined with F.-T. However, this would have to be a new kind of hydrocracking since significantly more C_4 is produced than C_1-C_3 during normal hydrocracking. Based upon currently practiced petroleum technology, it appears that the only way that the distribution shown Figure 20 is possible, would be for the C_2-C_4 products to be converted to higher carbon number materials. This would imply that either the C_2-C_4 fraction is primarily alkenes and that these alkenes are in some manner caused to reincorporate in the F.-T. process to produce higher carbon-number products or to be oligomerized by some proprietary catalyst; this would explain the absence of the usual amounts of the C_2-C_4 fraction but still would not explain how these authors are able to terminate chain growth. If on the other hand, the products from the F.-T. step are not olefinic, then olefin reincorporation cannot explain their results and they would have to have discovered some new catalysis that will activate saturated alkane hydrocarbons, something that is being widely investigated today but so far with little success. In any event, the Syntroleum process produces a better product distribution than the very severe hydrocracking of F.-T. wax in the Shell process (Figure 21). At this time, Syntroleum has non-exclusive licensing agreements with three companies: Marathon Oil Co., Texaco, Inc. and Arco.

3.7. Slurry-Wax/Catalyst Separation

3.7.1. British

The catalyst, after "break-in," was 1-3 Fm in size. A liquid slip-stream was withdrawn continuously from the reactor and catalyst was recovered in a multiple-stage, gravity-settling apparatus. Because of the relatively rapid catalyst aging rates as well as significantly coke formation, reliable data for wax/catalyst separation is not available.

3.7.2. Kölbel

A finely divided powder catalyst was utilized; the starting material has a particle size <30Fm but sizes during or after use is not provided. The liquid level in the reactor was maintained by a float-device. A slip-stream, utilized when excess liquid was produced, allowed for wax/catalyst separation by pressure filtration. [Kölbel operated most of the times under conditions where the liquid inventory of the reactor could be maintained **only by adding** heavier liquid products along with the synthesis gas and wax/catalyst separation was not a problem.] As an alternative, wax/catalyst separation could be effected by centrifugation. Capability for replacement of the catalyst was included in the process although catalyst replacement rates are not given. Data are not available to enable one to reach valid conclusions about the effectiveness of the wax/catalyst separation because of the lack of knowledge of catalyst addition rates. Based on the data in Table (Kölbel) for the "low" operating conditions, an upper limit of 15% reactor-wax removal can be set, and in practice it should have been much lower.

3.7.3. U.S. Bureau of Mines

The U.S. Bureau of Mines operated a 7.6 cm ID x 3.05 m high slurry reactor (e.g., 38). This unit utilized a parallel downflow slurry recycle line that was equipped with a porous metal filter. During a 52 day operating period, upsets in maintaining slurry circulation through the recycle line were encountered. It is not known whether this effect was responsible for the catalyst activity decline that occurred during the period of operation. For either the precipitated or fused iron catalyst, the original oxidic material was ground to provide <60 Fm particles; following use the particle size was reduced to about 1 Fm.

3.7.4. Mobil Oil

Mobil operated a slurry reactor and performed 13 runs during the course of its DOE contract (18). A simplified flow diagram of the two-stage plant is shown in Figure 13. During this run it is reported that:

> "The improved on-line F.-T. reactor-wax separation system enabled us to increase the flexibility and reduce the manpower requirement for the reactor-wax/slurry separation. A schematic of this system is shown in Figure 14. During normal operation, slurry is withdrawn continuously from the F.-T. reactor at the 610 cm level [762 cm to start of the conical shaped reactor area in Figure 14], and entrained gas is disengaged in a small disengager pot which is connected to the reactor-top. The gas-free slurry is passed through a dip-tube into a two-liter settling pot. The dip-tube length is designed to maintain 80% of the settling pot volume above its tip. The concentrated slurry exits the settling pot through a conical section, and is pumped back to the slurry

reactor at the 305 cm level through a positive-displacement slurry pump. The pump is inverted, i.e., feed enters at the top and effluent exits at the bottom. This prevents catalyst settling in the feed line to the pump, but requires spring loading of the pump check valves. The clean reactor-wax is withdrawn from the top of the settling pot either semi-continuously by periodically opening a valve, or it can be withdrawn continuously by using a metering valve."

It was reported that the clean reactor-wax contained 0.03 % solids. During this operation the reactor slurry was reported to contain 25-27 wt% solids. This means that 0.12% of the solids in the reactor are removed in the clean wax. While this type of reactor-wax/catalyst separation may work at the pilot plant, it appears that the separation/reactor volumes would be very large for a commercial plant reactor.

3.7.5. Sasol

In a patent specification, Sasol workers define a wax/catalyst separation device and operational procedures for its use (Figure 22). A number of these separation devices are located in the reactor slurry. Reactor-wax can be withdrawn through the separation device; depending upon the catalyst size distribution some portion of catalyst fines will be removed together with the reactor-wax. The design of the separation device is illustrated in Figure 23. A unique feature of this design is the use of a trapezoidal shaped wire utilized so that the filter exposes the smaller opening-size to the catalyst/wax slurry side and its larger opening-size to the clean reactor-wax side. This design is utilized so that any blockage of the separation device opening occurs on the catalyst/reactor wax side and can be easily removed by over-pressuring on the

clean wax side at appropriate intervals. A unique feature of this design is that any particle that passes through the opening on the catalyst/reactor-wax side will be able to traverse the pore without being impeded by a pore constriction.

3.7.6. Exxon

Included in the more than 200 patents issued to Exxon is one that describes "a reactor housing having a plurality of reaction tubes vertically disposed therein for conducting slurry phase hydrocarbon synthesis reactions under substantially plug flow conditions, and wherein provision is made for uniformly distributing gas bubbles in slurry liquid into the reaction tubes (Figure 24).

Included in this patent is a description of a reactor-wax/catalyst separation device. This device is described thusly (39):

> "...Above the liquid space is another tube sheet **30** holding filter cartridges **31** which may contain sintered metal mesh, woven metal fibers, glass fibers, cloth, fibrous carbon that can remove the catalyst particles while allowing passage of the liquid. The filter cartridges are each vertically aligned with each reaction zone and prevent catalyst particles from reaching the upper portion of the housing **8**. Above the filter cartridge tube sheet is a gas-liquid disengagement zone **36** topped by a foamy interface **38**. Liquid product from the hydrocarbon synthesis may be removed via line **40**, or alternately vis line **33** at or above the filter cartridge tube sheet. A demister **41** finally separates gas from liquid droplets and residue gases are withdrawn via line **42**. Thus, the liquid space above the upper tube ends and below the filter tube sheet allows

fluid communication between the upper tube ends and the alternate slurry addition/removal conduit **32** as well as the space above the filter tube sheet. The space above the filters and filter tube sheet allows fluid communication of the gas outlet means, the liquid outlet means and the space below the filter tube sheet, thereby further allowing fluid communication to the upper ends of the reaction tubes."

3.7.7. Statoil

Patent applications by Statoil describe a recent report identified only as "a report issued by the United States Department of Energy." The DOE report addressed the question of catalyst/wax separation in Fischer-Tropsch slurry reactor systems and concludes:

"Internal filters immersed in the reactor slurry, as used in some bench-scale or pilot-scale units, do not work successfully due to operational difficulties. A reactor with a section of its wall as a filter may be operable for a pilot plant but is not practicable for commercial reactors. Internal filters are subject to plugging risks, which may cause premature termination of the run, and commercial plants are not allowed to take chances."

The patent applicants have discovered that, contrary to the teachings of the DOE report, "...it is possible to provide a continuous reaction system for a Fischer-Tropsch synthesis in which it is not necessary to perform the solid/liquid separation in an external filter unit. Furthermore, a sufficiently high flow rate of filtrate for commercial

operation can be achieved." (40). The drawings included in these applications are similar to the word description and/or the schematic drawings in the above patents.

The only examples of actual operation given in the Statoil patent applications are for a cold model using oil, alumina and nitrogen gas. The cold model was operated for about 40 hours without major plugging problems that inhibit liquid flow. However, it does not appear that the applications provide any data to substantiate the claims that they have overcome the problems enumerated in the DOE report.

3.7.8. China

The operators encountered problems in separating reactor-wax from the catalyst slurry in both the bench scale and the large plant. The data reported for the small bench scale plant indicated that the reactor wax discharged contained consistently 7.5 wt. % catalyst. Considering that the reactor contained a slurry with 12 wt.% catalyst, the separation was not very efficient. These workers indicate that the catalyst loss is the reason for the decline in activity and state that "...if we solve the problem of catalyst loss, long-term operation is very possible." (7).

3.8. Process Considerations

The relative usage of hydrogen and carbon monoxide depends upon the CO conversion level (Figure 10). A similar curve has been obtained by UOP workers (41). Thus, the hydrocarbon productivity per gram of iron and per reactor volume is higher at lower CO conversion levels. Furthermore, the fraction of CO that is converted to hydrocarbons is greater at lower CO conversion levels. Thus, up to CO conversion levels of about 50%, the iron and cobalt catalyst will exhibit similar activity and hydrocarbon distribution selectivity properties. However, the iron catalyst operated at

50% or lower CO conversion will produce a very olefinic product. From the point of view of chemicals, such as could be utilized with a pioneer plant, the iron catalyst would provide a significant advantage. In fact, iron would be the preferred catalyst for any operation where chemicals would be a serious consideration.

Thus, in order to take full advantage of the activity and selectivity properties of the iron catalyst, it should be utilized in a process employing recycle or multiple reactors. It would appear that a process utilizing multiple reactors with water knock-out between reactors and the addition of make-up syngas, would be the preferred option.

An additional advantage of the iron catalyst is that it can be operated at a higher temperature than the cobalt catalyst. This would permit the generation of higher quality steam and with the iron catalyst the generation of electricity could be considered as an approach to utilize some of the energy rejected during the hydrocarbon synthesis step.

3.9. Supercritical Phase Fischer-Tropsch Synthesis

It is claimed that three main advantages of the supercritical synthesis are: (1) rapid diffusion of reactants, (2) effective removal of reaction heat and (3) effective extraction of wax, a-olefins and water. Thus, the supercritical operation could, if item 3 is accomplished, decrease or eliminate secondary reactions.

Yokota et al. (42) compared the results of the operation of three types of reactors: fixed-bed, liquid and supercritical. In order to make an effective comparison the feed consisted of 22-36 % synthesis gas with the remainder being diluent (nitrogen for the fixed-bed, hexadecane and nitrogen for the liquid, and n-hexane for the supercritical). An iron catalyst was utilized and had the following composition by wt. fraction: Fe, 83.5; Ca, 2.1; Al, 1.5; Si, 0.4; K, 0.5 or Fe, 99; Cu, 0.3; K, 0.3. Thus, both

iron catalysts were of the low alpha type utilized by Mobil Oil and La Porte Run II. The total pressure was 5 MPa (about 50 atm.; 728 psi), 270°C, H_2/CO = 1 and W/F (CO + H^2) = 10 g-cat h/mol. **Each run was conducted for 6 hours. Under no circumstances should it be considered that a steady-state operation was attained**.

The authors show the CO conversion, CO_2 yield and chain-growth probabilities for the fixed-bed, supercritical and slurry phase reactors as 33.0, 30.2 and 27.9; 8.65, 7.52 and 9.15; and 0.84, 0.83 and 0.80, respectively. The authors considered these differences to be significant and attribute the lower CO_2 yield for the supercritical operation as being due to the increased removal of water from the reactor. The reported chain growth probabilities appear high for an iron catalyst that contains such a low level of potassium. These data should be viewed as suggestive at best.

Fujimoto et al. (43) report that the addition of a small amount of heavy 1-olefin in a supercritical-phase or liquid-phase F.-T. reaction medium greatly enhanced the selectivity of wax products, with increased CO conversion and suppressed methane selectivity. A cobalt-silica catalyst that contained La was used. The authors reported that the addition of 1-tetradecene or 1-hexadecene significantly decreased the hydrocarbon production for carbon-number products lower than that of the added alkene, and increased significantly the production rate of the carbon-number products with higher carbon numbers that the added alkene (Figure 25). The impact shown in Figure 25 is astounding. When alkenes were not added the production rate of the products above carbon number 15 decreased with increasing carbon number; this is expected and observed in normal F.-T. synthesis. However, when the alkene is added,

the hydrocarbon production with carbon-numbers above that of the alkene become essentially constant; i.e., independent of carbon number. It appears that this requires the added alkene to initiate chain growth that differs from that of the F.-T. reaction. If the only impact of the alkene was to initiate additional growing chains, the product distribution above the carbon number of the added alkene should remain the same; i.e., the rate of production of all carbon-number products should increase but should still be produced in the same ratio as they were when no alkene was added. The data obtained when 1-heptene, in contrast to 1-tetradecene or 1-hexadecene was added, is in better agreement with the expectation.

Lang et al. (44) utilized a precipitated iron catalyst in a fixed-bed reactor and found that the catalyst activity and lumped hydrocarbon product distribution under the supercritical conditions were similar to those obtained during reaction at the baseline (non-supercritical) conditions. This is in contrast to the views expressed above. They did report slightly higher selectivities for the 1-alkenes during supercritical operation (Figure 26). They indicate that this suggests that the F.-T. reaction is not diffusionally limited under their reaction conditions. The higher alkene production during supercritical operation was due to higher diffusivities and desorption rates of the high molecular weight olefins relative to those under normal F.-T. conditions.

4. References

1. B. Jager, AIChE Mtg., Houston, 1997.
2. B. Jager and R. Espinoza, *Catal. Today*, **23** (1995) 17.
3. R. Srinivasan, L. Xu, R. L. Spicer, F. L. Tungate and B. H. Davis, *Fuel Sci. Tech. Int.*, **14** (1996) 1337.
4. T. Kuntze, K. Hedden and A. Jess, *Erdöl Erdgas Kohle*, **111** (1995) 67.
5. "Report on the Petroleum and Synthetic Oil Industry of Germany,: Ministry of Fuel and Power, His Majesty's Stationery Office, London, 1946, pp 96-100.
6. C. B. Benham, M. S. Bohn, and D. L. Yakobson, U.S. Patent 5,324,335, June 28, 1994.
7. "Synthesis of Liquid Fuels From Coal," (Bijiang Zhang, Ed.), Science and Technology Publishing Corp., Shanxi Province, China, 1993.
8. L. Koenig, et al., *Bet. Bunsenges. Phys. Chem.*, **91** (1987) 116.
9. B. Cornils, W. A. Herrmann and M. Rash, *Angew. Chem., Int. Ed. Engl.*, **33** (1994) 2144.
10. B. H. Davis, "Gulf-Badger - Review, April, 1977.
11. B. H. Davis, Statoil Report, June, 1997.
12. E. Iglesia, S. C. Reyes, R. J. Madon and S. L. Soled, *Advan. Catal.*, **39** (1993) 321.
13. B. H. Weil and J. C. Lane, "Synthetic Petroleum from the Synthine Process, Remsen Press, Chem. Pub. Co., Inc., New York, 1948, p 67.
14. P. J. van Berge and R. C. Everson in "Natural Gas Conversion IV," (M. de Pontes, et al., Eds.), Elsevier, Amsterdam, pp. 207-212.

15. H. Kölbel and M. Ralek, *Catal. Rev.-Sci. Eng.*, **21** (1980) 225.

16. J. M. Fox, III and S. S. Tam, *Topics in Catal.*, **2** (1995) 285.

17. J. R. Inga and B. I. Morsi, 13th Ann. Int. Pittsburgh Coal Conf., 1996, pp. 924-929.

18. J. C. W. Kuo, DOE/PC/60019-9, October, 1985.

19. M. L. Poutsma, ORNL-5635, February, 1980.

20. T. J. Donnelly, C. N. Satterfield and I. C. Yates, *Energy & Fuels*, **2** (1977) 313.

21. J. Eilers, S. A. Posthuma and S. T. Sie, *Catal. Lettr.*, **7** (1990) 253.

22. B. H. Davis, *ACS Div. Fuel Chem.*, **37** (1992) 172.

23. Y. Yang, S. Pen and B. Zhong, *Catal. Lettr.*, **16** (1992) 351.

24. V. K. Jones, L. R. Neubauer and C. H. Bartholomew, *J. Phys. Chem.*, **90** (1986) 3832.

25. T. Mitsudo, H. Boku, S. Murachi, A. Ishihara and Y. Watanabe, *Chem. Lettr.*, (1985) 1463.

26. R. Snel, *Catal. Lettr.*, **1** (1988) 327.

27. D. Fraenkel and B. C. Gates, *J. Am. Chem. Soc.*, **102** (1980) 2478.

28. D. Fraenkel and B. C. Gates, U,S. 4,294,725; assigned to U. Delaware.

29. D. Balleret-Tkatchenko and I. Tkatchenko, *J. Mol. Catal.*, **13** (1981) 1.

30. L. F. Nazar, G. A. Ozin, F. Hugues, J. Odber and D. Rancourt, *J. Mol. Catal.*, **21** (1983) 313.

31. H. H. Nijs, P. A. Jacobs and J. B. Utterhoeven, *J. Chem. Soc., Chem. Commun*., (1979) 1095.

32. H. H. Nijs, P. A. Jacobs and J. B. Utterhoeven, *J. Chem. Soc., Chem. Commun*., (1979) 180.

33. I. R. Leith, *J. Chem. Soc., Chem. Commun.*, (1983), 93.

34. R. K. Unger and M. C. Baird, *J. Chem. Soc., Chem. Commun.*, (1986), 643.

35. D. Vanhove, P. Makambo and M. Blanchard, *J. Chem. Soc., Chem. Commun.*, (1979), 605.

36. M. A. Agee, AIChE Meeting, Houston, March 1997.

37. M. A. Agee, ACS Meeting, Div. Fuel Chem. Preprints, April 1997.

38. M. D. Schlessinger, J. H. Crowell, M. Leva and H. H. Storch, *Eng. Process Dev.*, **43** (1951) 1474.

39. R. M. Koros, U.S. Patent 5,384,336, January 24, 1995.

40. Int. Pub. No. WO 90/07377, 12 July 1990; Int. Pub. No. WO 96/06683, 7 March, 1996; U.K. Appl. GB2,299,767A, 16 October, 1996; U.K. Patent Appl. GB2,281,224A, 1 March 1995; Int. Pub. No. WO 94/16807, 4 August 1994.

41. V.U.S. Rao, G. J. Stiegel, A. C. Bose, G. J. Cinquegrane and R. D. Srivastava, *ACS Div. Fuel Chem.*, **37** (1992) 184.

42. K. Yokota, Y. Hanakata and K. Fujimoto in "Natural Gas Conversion," (A. Holmen et al., Eds.), Elsevier, Amsterdam, (1991), pp. 289-295.

43. K. Fujimoto, L. Fan and K. Yoshii, *Topics in Catal.*, **2** (1995) 259.

44. X. Lang, A. Akgerman and D. B. Bukur, *Ind. Eng. Chem. Res.*, **34** (1995) 72.

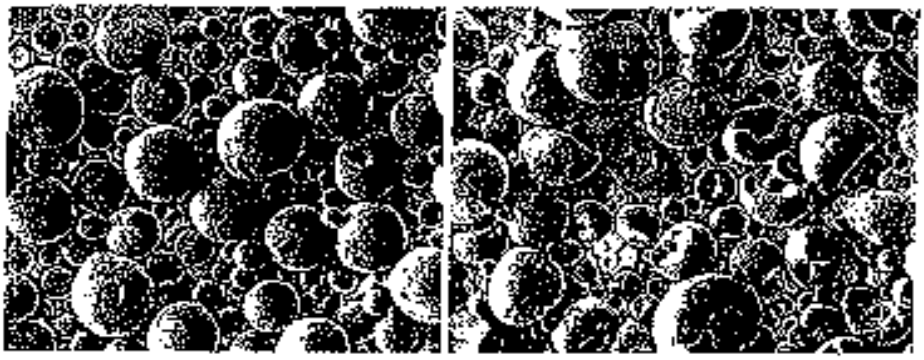

Figure 1. SEM pictures of spray-dried iron catalyst: (a) Typical Sasol spray-dried catalyst; (b) catalyst with dimpled particles (from ref. 2).

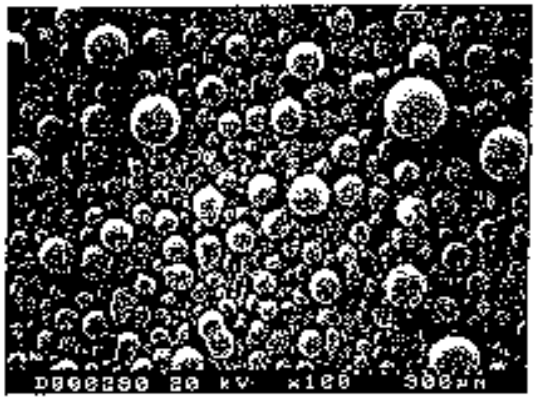

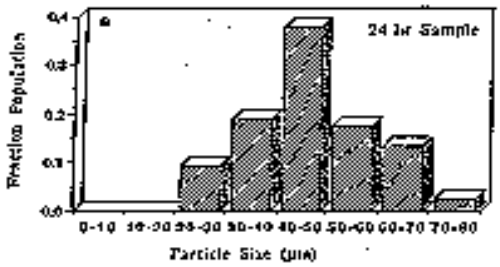

Figure 2. Scanning electron micrograph from the UCI sample after carbiding and fraction of population versus particle size (from ref. 10).

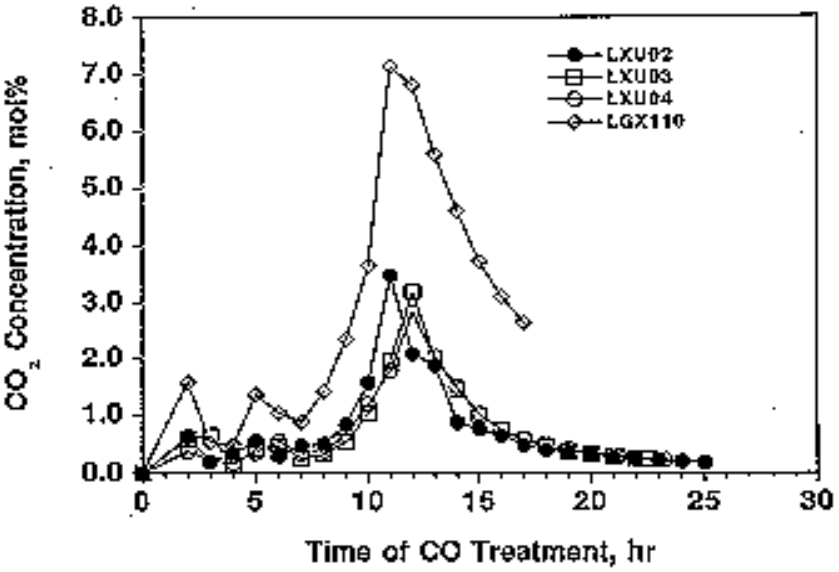

Figure 3. Generation of carbon dioxide, a measure of activation of an iron catalyst with carbon monoxide in the CAER autoclave (LEX 110) and slurry bubble column (LXU runs) reactor.

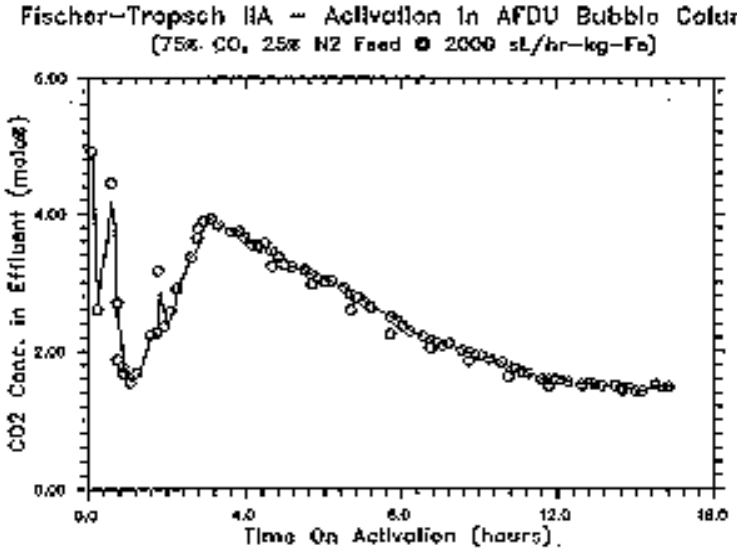

Figure 4. Activation of the iron catalyst prepared by United Catalysts, Inc. in the La Porte Run II.

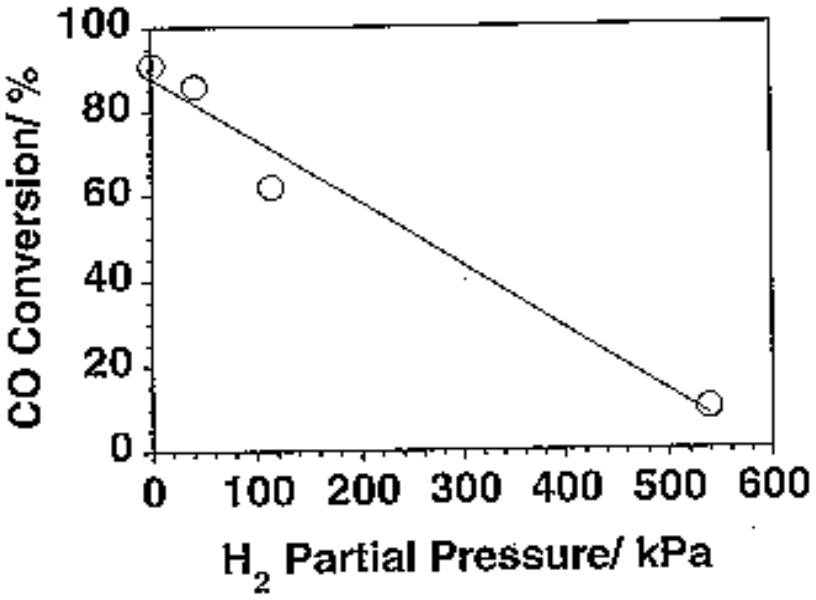

Figure 5. Catalyst activity (CO conversion) following activation at reaction conditions in a syngas containing an increasing amount of hydrogen.

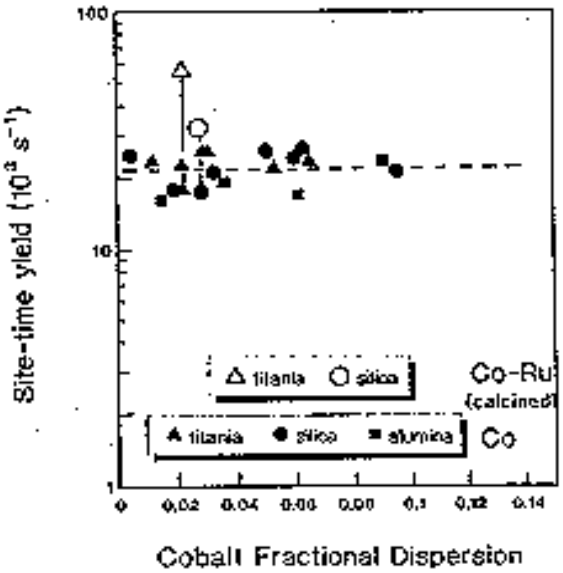

Figure 6. Site-time yield of products during F.-T. synthesis with various cobalt catalysts (from ref. 12).

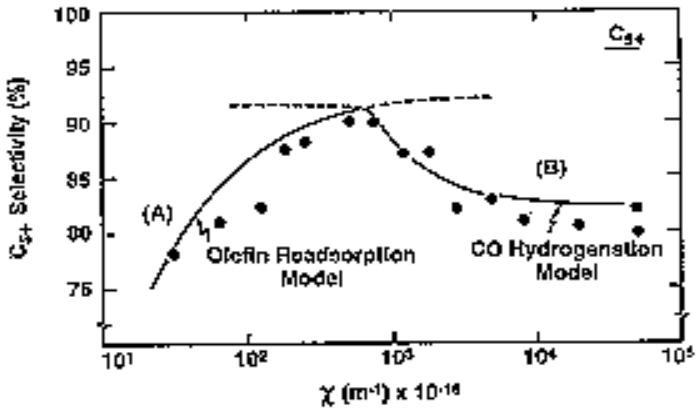

Figure 7. The effect of catalyst structural properties (χ) and site density on the C_{5+} selectivity (from ref. 12).

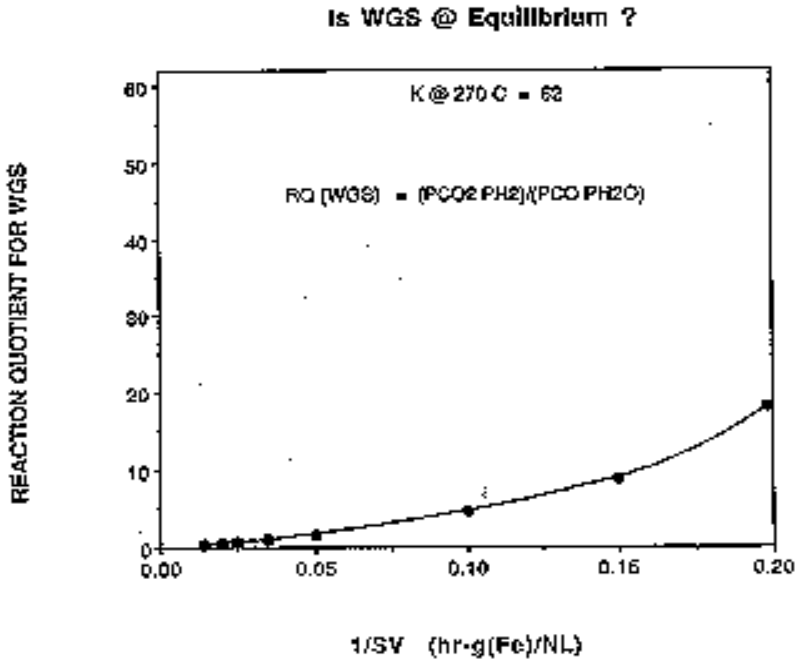

Figure 8. The extent of the water-gas-shift reaction as a function of the carbon monoxide conversion using an iron catalyst.

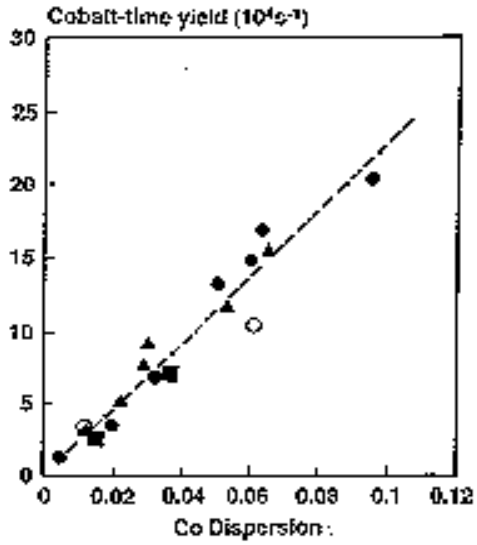

Figure 9. Effect of cobalt dispersion and support on Fischer-Tropsch synthesis rates using a cobalt catalyst (from reference 12).

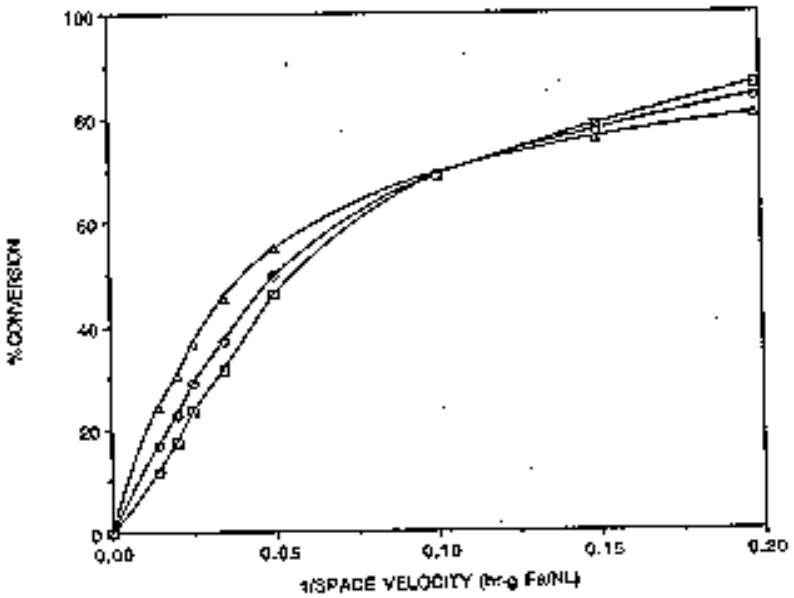

Figure 10. Conversion of hydrogen (△), carbon monoxide (□) and H_2 + CO (○) during Fischer-Tropsch synthesis with an iron catalyst.

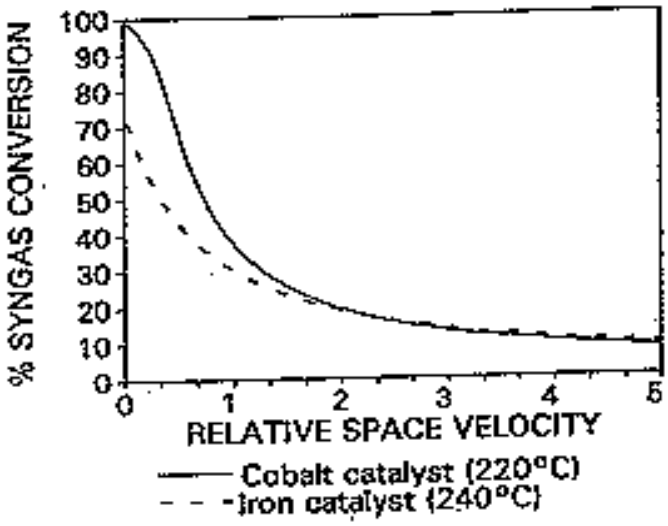

Figure 11. Activity comparison between an iron and cobalt catalyst at 20 atmosphere (from reference 14).

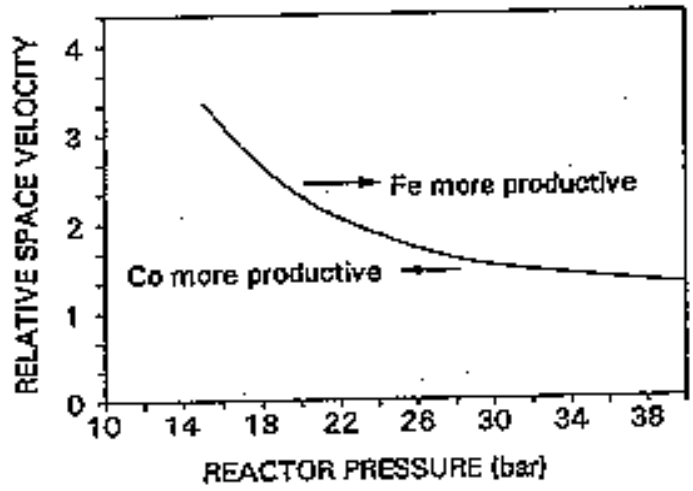

Figure 12. Productivity comparison between an iron catalyst (240°C) and a cobalt catalyst (220°C) (from reference 14).

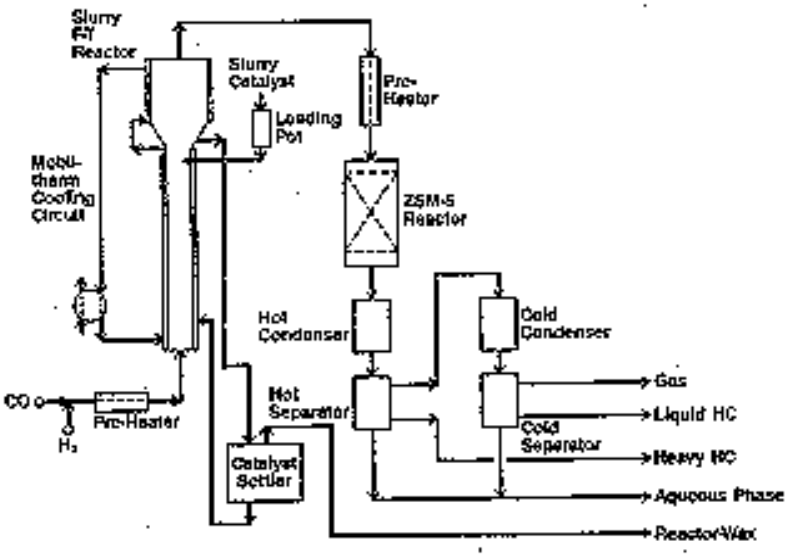

Figure 13. Simplified flow diagram of the Mobil Oil two-stage plant for synthesis gas conversion (from reference 18).

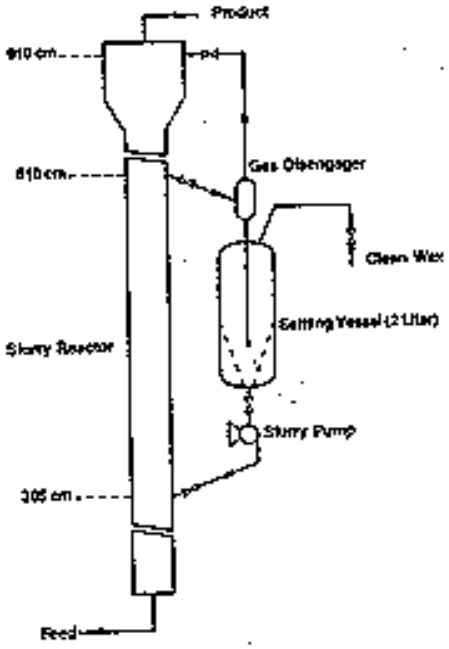

Figure 14. Schematic diagram of the continuous settling system for catalyst/wax separation (from reference 19).

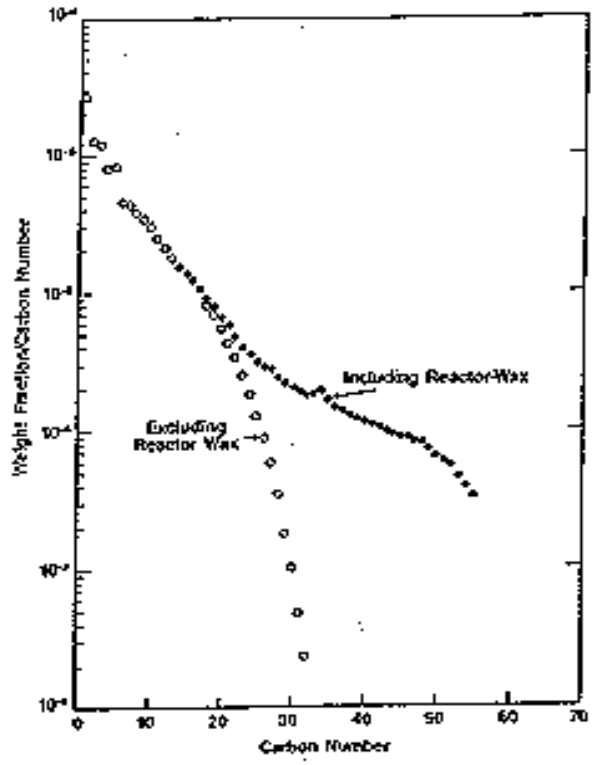

Figure 15. Schulz-Flory distribution for the first stage Fischer-Tropsch products obtained by Mobil Oil at a reactor wax yield of 46 wt.% (from reference 16).

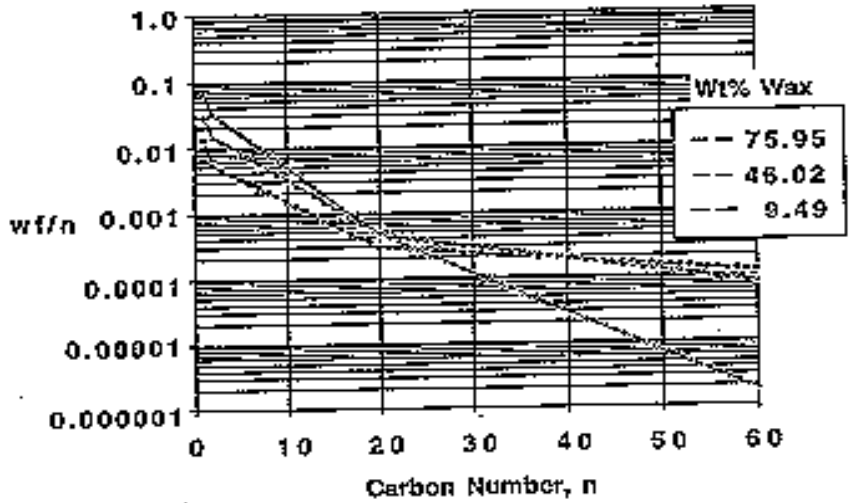

Figure 16. Schulz-Flory distribution based on Mobil Oil data at low, intermediate and high alpha synthesis conditions (from reference 16).

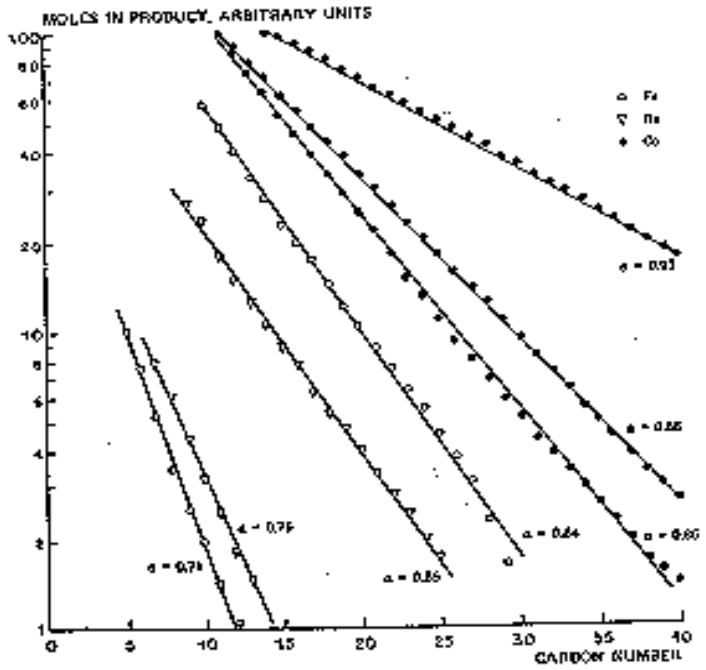

Figure 17. Typical carbon number distribution reported by Shell for their Fischer-Tropsch data (from reference 21).

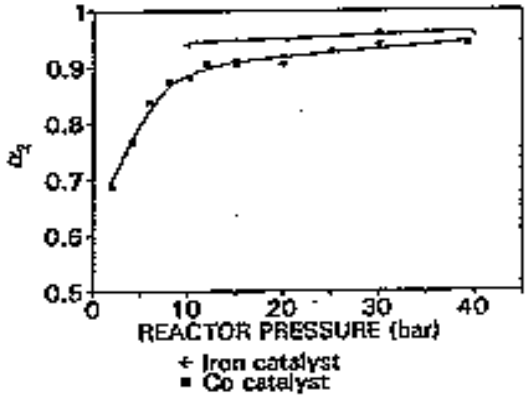

Figure 18. Chain growth probability α_2 as a function of reactor pressure at a constant superficial velocity (from reference 14).

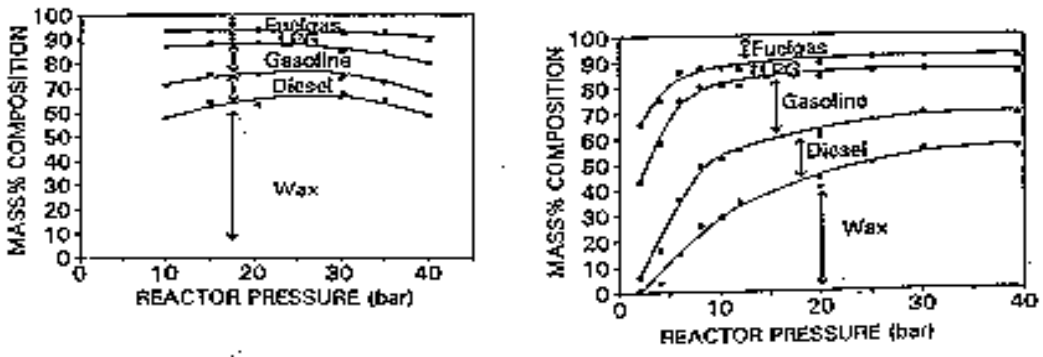

Figure 19. Mass% product distribution as a function of reactor pressure at constant superficial velocity for (left) iron slurry phase catalyst and (right) a cobalt catalyst (from reference 14).

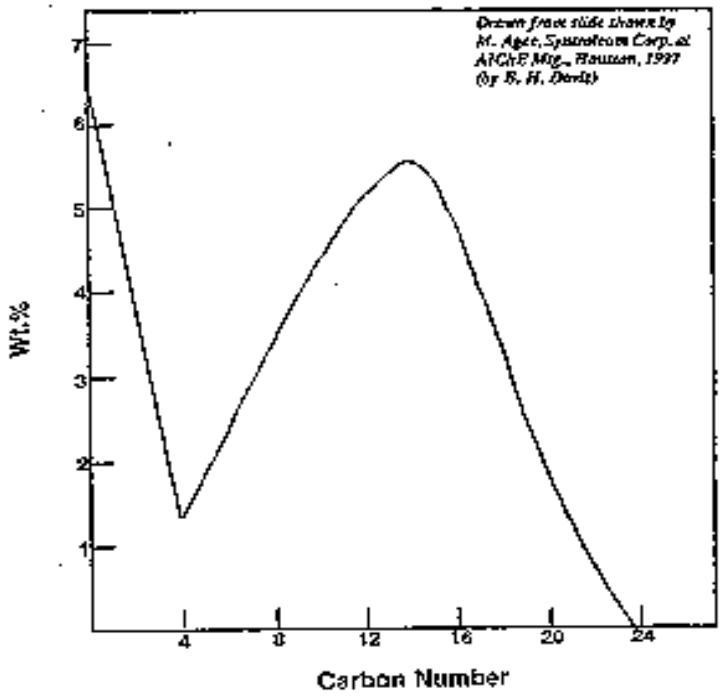

Figure 20. Plot showing selectivity data for Syntroleum "chain-limiting" catalyst (drawn from talk given by M. Agee at AIChE Meeting, Houston, 1997).

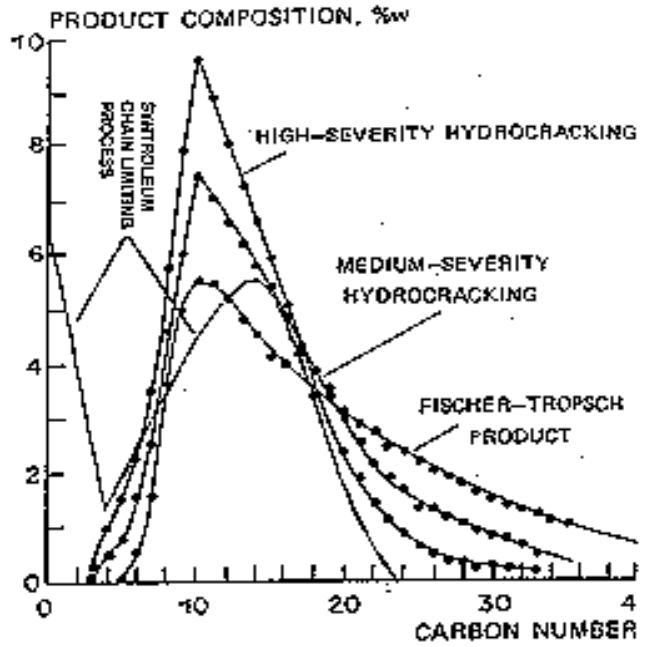

Figure 21. Data from figure 20 superimposed upon hydrocracking data presented by Shell (from reference 21).

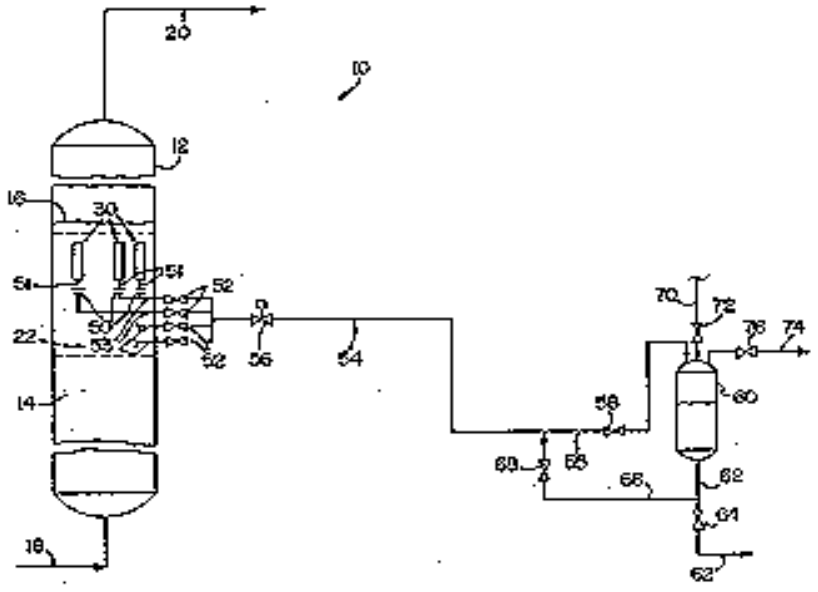

Figure 22. Schematic of reactor and filtration apparatus patented by Sasol.

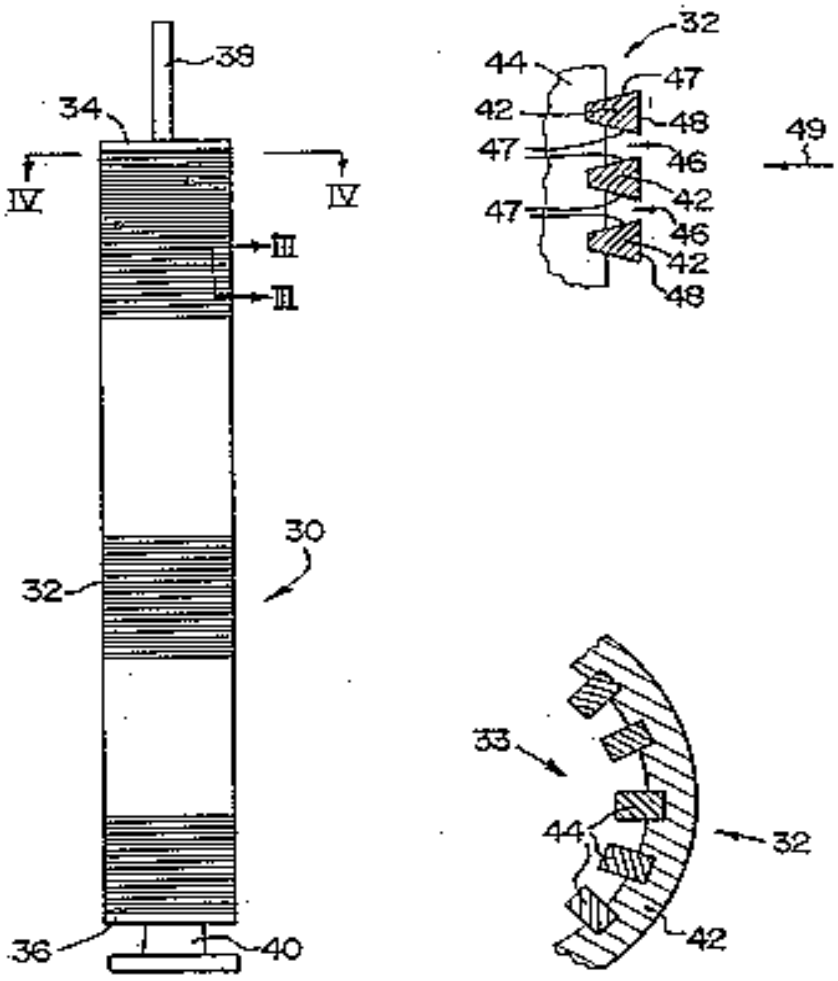

Figure 23. Expanded scale drawing of Sasol wax/catalyst separation device.

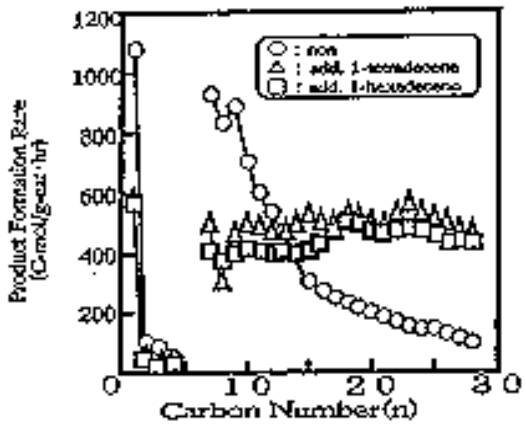

Figure 25. Product distribution in the olefin-added supercritical-phase F.-T. reaction with a cobalt catalyst: (○) no olefin added; (△), 1-tetradecene added; (□) 1-hexadecene added (from reference 42).

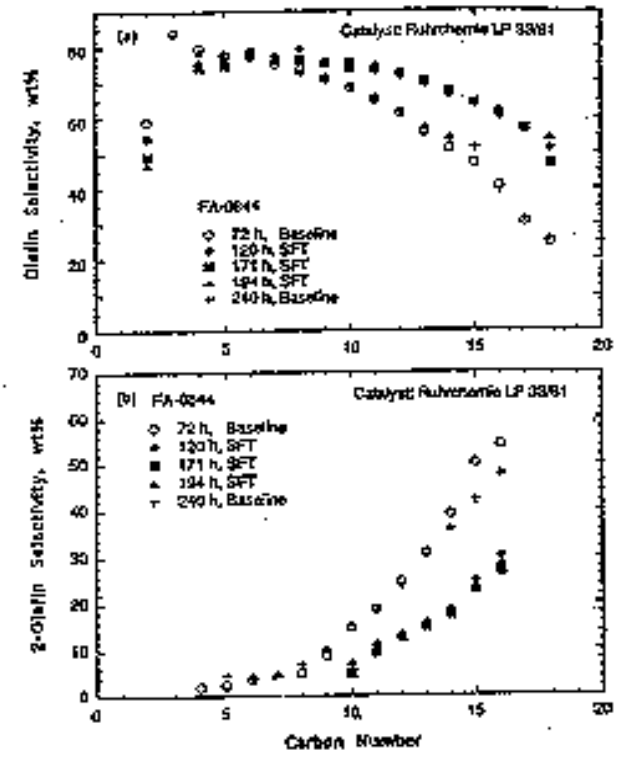

Figure 26. Effect of supercritical Ft Synthesis on α-olefin (a) and 2-olefin (b) selectivity using an iron catalyst (from reference 44).

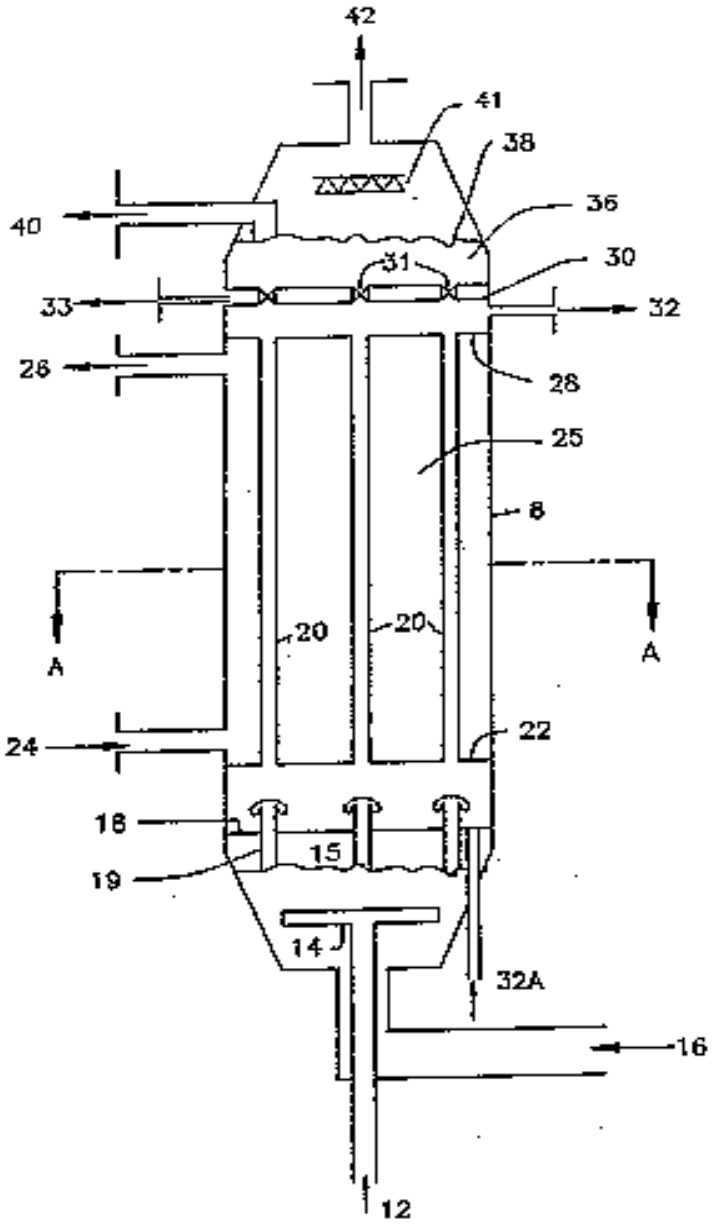

Figure 24. Schematic of reactor and filtration apparatus patented by Exxon (from reference 29).

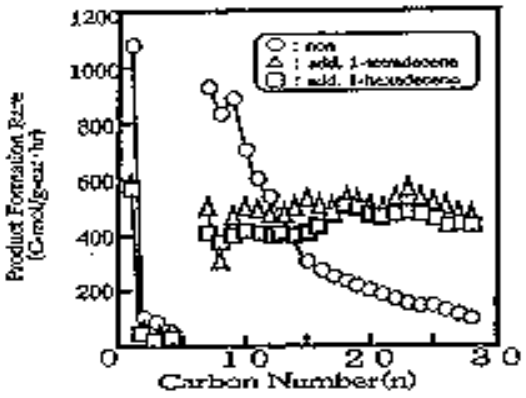

Figure 25. Product distribution in the olefin-added supercritical-phase F.-T. reaction with a cobalt catalyst: (○) no olefin added; (△), 1-tetradecene added; (□) 1-hexadecene added (from reference 42).

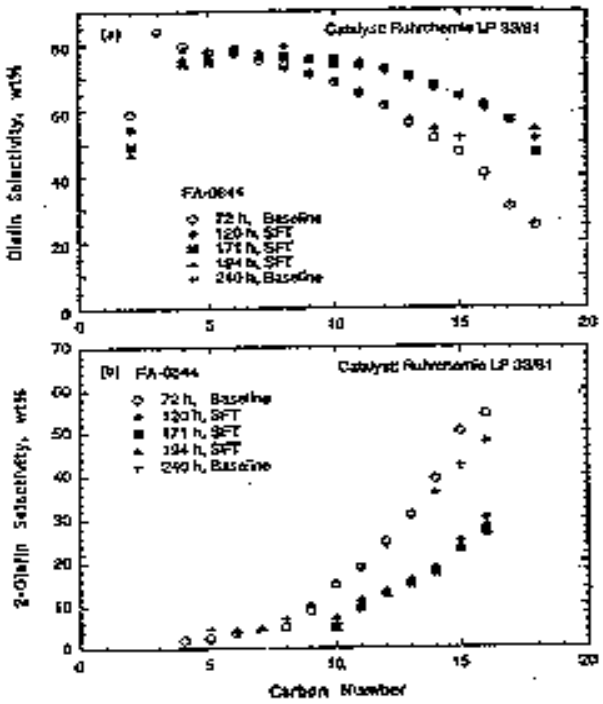

Figure 26. Effect of supercritical Ft Synthesis on α-olefin (a) and 2-olefin (b) selectivity using an iron catalyst (from reference 44).

3.3.4.8 Fischer-Tropsch Data Calculations

The FTS data and calculations can be broken into several major groups, these being the run and sample conditions, feed and product stream data, conversions, rates, selectivity's, product distributions, and finally alpha values. All the data is stored in raw form in a Microsoft Access database. Any conversions, scaling, and further manipulation of the data is done entirely by SQL query of the database system, with the single exception of the curve fitting for the calculation of alpha values. This curve fitting of is primarily done with the SAS system of Statistical Software. The system has a Microsoft Visual Basic 5.0 front end for data entry with reporting by Crystal Reports Professional Version 6.

Run and Sample Conditions:

The run conditions which are of interest here initial values which will be used for the first and subsequent samples feed gas flow rate (slph) and composition, and the weight of the catalyst (g) and the Active metal (Fe or Co) and its weight percent. Also the date and time of the start of synthesis is recorded.

The sample conditions of interest are the date and time of the sample along with the feed gas (slph) along with its composition, the product gas flow (slph) and the weight of any liquid stream sample which were taken these being the water, light oil, heavy oil, and the wax (rewax) phase all in grams.

Feed and Product Stream Data:

Gas analysis is done on a Carle Gas Analyzer (AGC) which provides the mol percent of Hydrogen, Carbon Monoxide, Carbon Dioxide, Nitrogen, Methane, Ethane, Ethene, Propane, Propene, n-Butane, i-Butane, 1-Butene, iso-Butene, 2-trans-Butene,

2-cis-Butene. This GC is calibrated with a standard gas. The area counts of the olefin and paraffin's of the carbon numbers from 5 to 10 are provided by the HP 5790 GC. The mol percents of the C5's through C10 will be calculated by multiplying the area count by a response factor. This factor is the sum of the AGC C4 mol percents divided by the sum of the area counts of the C4's from the HP 5790 GC. In summary, the database stores mol percents from the AGC and area counts from the HP 5790 GC. The conversion from area counts to mol percents is done on the fly using SQL queries. Additionally, The SQL will normalize these values after correcting for the vapor pressure of water at 1 atmosphere and 28^{O} C (assumed typical conditions for the laboratory). This results in all gas components being in normalized mol percents.

For the liquid product streams all data is based on the weight percent. Water phase data is from the HP 5790 GC. Both oil phases are combined and analyzed on the HP 5890 GC. Finally the wax (rewax) is analyzed on a High Temperature HP 5890. If the startup wax is one with a very high molecular weight this data must be corrected as the startup wax may not come off the column. For these cases, an internal standard is used to determine the correction factor need to account for this missing mass. This prevents the inflation of the product weight fractions due to the detector not seeing the startup wax which depending on the time on stream may be as high as eighty percent of the wax phase.

Conversions (%)

H_2 and CO Conversions	100 ((component mols in) - (component mols out)) / (component mols in)
(H2 + CO) Conversion	((CO in) (CO Conv.) + (H_2 in) (H_2 Conv.)) / ((H_2 in) + (CO in))

Conversion Rates (Conv. % / g Catalyst)

H_2, CO, Conversion Rates	((Component Conversion) / (weight catalyst {g})) / 100 (Percent Composition of Active Metal)
(H_2 + CO) Conversion Rate	(H2 Conversion Rate) + (CO Conversion Rate)

Rates (mol/h)

CO Rate	(CO Feed {mol/h}) (CO Conversion)
CO_2 Rate	(Gas Product {slph}) (CO_2 {mol %}) / (22.414 {mol/sl}) / 100
FT Rate	(CO Rate) - (CO_2 Rate)
C1-C4 Component Rate	(Gas Product {slph}) (Component {mol %}) / (22.414 {mol/sl}) / 100
C5 Plus Rate	(CO Rate) - (C1 Rate) - (C2 Rate) - (C3 Rate) - (C2 Rate) - (C1 Rate) - (CO_2 Rate)
C5 Plus HC Rate	(C5 Plus Rate) (14.027 {FW of CH_2}) / (Weight Catalyst {g})

Selectivity (Carbon Basis)

C1-C4 Component Selectivity	(Component Rate) / (CO Rate) 100 (Carbon Number)
C5 Plus Selectivity	(CO Selectivity) - (C1 Sel.) - (C2 Sel.) - (C3 Sel.) - (C4 Sel.) - (CO2 Sel.)

Product Distribution (mol fraction by carbon number)

Mol Fraction	For each carbon number C1 to C100 the sum of mol fractions in the gas, oil, wax, and water phases

Olefin / Paraffin Selectivity (per Carbon Number)

Total Alkenes	(1-alkene) + (cis-2-alkene) + (trans-2-alkenes) {all in mols per hour}
Paraffin Ratio	(paraffin {mol/h}) / (total alkenes {mol/h})
Olefin Ratio	(1-olefin {mol/h}) / (total olefins {mol/h})

Mass Balance

Product Gas Effective Molecular Weight	Sum of each of gas components: (Mol Fraction) (Formula Weight)
Water Vapor {g/h}	Product gas is assumed to be saturated at 28^{O} C and 1 atm.
Gas Prod {g/h}	(Gas Prod {slph}) (22.414 {mol/sl}) / (Effective MW {g/mol}) (Water Vapor {g/h})
Gas Feed {g/h}	(Gas Feed {slph}) (22.414 {mol/sl}) (28.01055 {FW of CO}) (CO Fraction) + (2.01594 {FW H_2}) (H_2 Fraction))
Sum Liquid Product {g/h}	(water {g/h}) + (oil {g/h}) + (wax {g/h})
Mass Balance {g/h}	(Gas Feed {g/h}) - (Gas Product {g/h}) - (Sum Liquid products {g/h})
Mass Closure	(Mass Balance {g/h}) / (Gas Feed {g/h})

Alpha Values

Alpha values are primally fitted using the SAS Statistical Software. For a two alpha fit the data is fitted to $m(n) = x(1-a_1)a_1^{(n-1)} + (1-x)(1-a_2)a_2^{(n-1)}$. Where m(n) is the mol fraction at carbon number n, x is the contribution by alpha 1, a_1 is alpha 1, and a_2 is alpha 2. For a single alpha fit: $m(n) = (1-a_1)a_1^{(n-1)}$. Where m(n) is the mol fraction at carbon number n, and a_1 is the single alpha. For the fitting of data from literature where mol fractions have been reported for ranges of carbon numbers for

example C1, C2-C4, C5-C10, C11-C20, and C20+ the internally written Alpha Fitter program was used.

SAS Program for Two Alpha Fit. (with sample data)

```
data a;
      input n y @@;
      cards;
1     0.047791693
2     0.040550869
3     0.035011413
4     0.020920487
5     0.013481663
6     0.010034115
7     0.007725418
8     0.006470921
9     0.005212527
10    0.004101158
11    0.00354337
12    0.002954146
13    0.002458323
14    0.002064626
15    0.001683087
16    0.001356415
17    0.001032646
```

18	0.000740856
19	0.000473017
20	0.000308679
21	0.000161864
22	0.000104361
23	6.27247E-05
24	3.94504E-05
25	2.37152E-05
26	1.61292E-05
27	9.86008E-06
28	6.6132E-06
29	4.34716E-06
30	3.20788E-06
31	2.25648E-06
32	1.7739E-06
33	1.06203E-06
34	8.12232E-07
35	5.66768E-07
36	4.37296E-07
37	3.16018E-07
38	2.50974E-07
39	1.51806E-07
40	1.51413E-07

41	1.21662E-07
42	7.46026E-08
43	6.56068E-08
44	6.40149E-08
45	5.68956E-08
46	5.62721E-08
47	4.98441E-08
48	4.98263E-08
49	4.41901E-08
50	4.37938E-08
51	3.82308E-08
52	3.87464E-08
53	3.29638E-08
54	3.37511E-08
55	2.86092E-08
56	2.9315E-08
57	2.43014E-08
58	2.45553E-08
59	1.97984E-08
60	1.96771E-08
61	1.44268E-08
62	1.56809E-08
63	1.16661E-08

```
64      1.25362E-08
65      9.49108E-09
66      1.1636E-08
67      8.09836E-09
68      7.88887E-09
69      4.77353E-09
70      5.51335E-09
71      2.848E-09
72      3.63534E-09
73      1.38808E-09
74      2.21318E-09
75      8.31286E-10
76      5.83877E-10
77      4.22772E-10
;

data r;
        set a;
        n = n;
        y = log(y);

proc nlin data=r method=dud best=10 smethod=golden;
```

```
        parms a1 = 0.5 to .99 by .1
              a2 = 0.5 to .99 by .1
              x  = 0.01 to .99 by .1;

        bounds 0.01<a1<=0.99;
        bounds 0.01<a2<=0.99;
        bounds 0.01<x<0.99;

        z =  x*(1-a1)*a1**(n-1) + (1-x)*(1-a2)*a2**(n-1);
        model y = log(z);

        output out=b p=yhat r=yresid;

data c;
        set b;
        y    = exp(y);
        yhat = exp(yhat);

proc plot data=b;
        plot y*n='a' yhat*n='p' / overlay vpos=25;
        plot yresid*n / vref=0 vpos=25;
```

```
proc univariate plot normal data=b;
        var yresid;

proc capability data=b gout=gseg graphics;

        var yresid;
        histogram yresid / normal;



run;
quit;
```

Program for Single Alpha Fit (with sample data):

```
data a;
        input n y @@;
        cards;
1       0.047791693
2       0.040550869
3       0.035011413
4       0.020920487
5       0.013481663
```

6	0.010034115
7	0.007725418
8	0.006470921
9	0.005212527
10	0.004101158
11	0.00354337
12	0.002954146
13	0.002458323
14	0.002064626
15	0.001683087
16	0.001356415
17	0.001032646
18	0.000740856
19	0.000473017
20	0.000308679
21	0.000161864
22	0.000104361
23	6.27247E-05
24	3.94504E-05
25	2.37152E-05
26	1.61292E-05
27	9.86008E-06
28	6.6132E-06

29	4.34716E-06
30	3.20788E-06
31	2.25648E-06
32	1.7739E-06
33	1.06203E-06
34	8.12232E-07
35	5.66768E-07
36	4.37296E-07
37	3.16018E-07
38	2.50974E-07
39	1.51806E-07
40	1.51413E-07
41	1.21662E-07
42	7.46026E-08
43	6.56068E-08
44	6.40149E-08
45	5.68956E-08
46	5.62721E-08
47	4.98441E-08
48	4.98263E-08
49	4.41901E-08
50	4.37938E-08
51	3.82308E-08

52	3.87464E-08
53	3.29638E-08
54	3.37511E-08
55	2.86092E-08
56	2.9315E-08
57	2.43014E-08
58	2.45553E-08
59	1.97984E-08
60	1.96771E-08
61	1.44268E-08
62	1.56809E-08
63	1.16661E-08
64	1.25362E-08
65	9.49108E-09
66	1.1636E-08
67	8.09836E-09
68	7.88887E-09
69	4.77353E-09
70	5.51335E-09
71	2.848E-09
72	3.63534E-09
73	1.38808E-09
74	2.21318E-09

```
75      8.31286E-10
76      5.83877E-10
77      4.22772E-10
;

data r;
        set a;
        n = n;
        y = log(y);

proc nlin data=r method=dud best=10 smethod=golden;

        parms a1 = 0.1 to .99 by 0.01;

        bounds 0.1<a1<=0.99;

        z =  (1-a1)*a1**(n-1);
        model y = log(z);

        output out=b p=yhat r=yresid;

data c;
        set b;
```

```
        y    = exp(y);
        yhat = exp(yhat);

proc plot data=b;
        plot y*n='a' yhat*n='p' / overlay vpos=25;
        plot yresid*n / vref=0 vpos=25;



proc univariate plot normal data=b;
        var yresid;

proc capability data=b gout=gseg graphics;

        var yresid;
        histogram yresid / normal;



run;
quit;
```